# Smoothness Criteria for WIM Scale Approaches

FINAL REPORT

Steven M. Karamihas and Thomas D. Gillespie, Ph.D.
The University of Michigan Transportation Research Institute

Report 2002-37
September 2002

**Technical Report Documentation Page**

| 1. Report No. | 2. Government Accession No. | 3. Recipient's Catalog No. |
|---|---|---|
| UMTRI-2002-37 | | |

| 4. Title and Subtitle | . Report Date |
|---|---|
| Smoothness Criteria for WIM Scale Approaches | September 2002 |
| | . Performing Organization Code: 43277 |
| 7. Author(s): S. M. Karamihas and T. D. Gillespie | . Performing Organization Report No.: UMTRI-2002-37 |
| 9. Performing Organization Name and Address: The University of Michigan Transportation Research Institute, 2901 Baxter Road, Ann Arbor, Michigan 48109 | 10. Work Unit No. (TRAIS) |
| | 1. Contract or Grant No. |
| 12. Sponsoring Agency Name and Address: Federal Highway Administration, Turner-Fairbank Highway Research Center, 6300 Georgetown Pike, HRDI-13, McLean, VA 22101-2296 | 3. Type of Report and Period Covered: Final Report, Mar. 2001 – Jul. 2002 |
| | 4. Sponsoring Agency Code |

15. Supplementary Notes

16. Abstract

This document reports on the development of smoothness criteria for weigh-in-motion (WIM) scale approaches. The criteria are meant to screen sites for excessive truck dynamic loading that exacerbates WIM scale error beyond levels recommended by the American Society of Testing and Materials (ASTM).

WIM scale error was related to pavement profile characteristics using a large simulation study of the response of virtual trucks over measured profiles. A distribution error was compiled over the truck population for steer axle, tandem axle, and total vehicle weight at each site. The error distributions were summarized by their 95th percentile absolute error levels. The error levels assigned to each site were then used as a correlation standard for the proposed roughness indices and for the selection of corresponding threshold values. Instead of a single index, two versions of the Butterworth filter were selected for use in the specifications. One addresses "Short Range" roughness and the other "Long Range" roughness. The Short and Long Range WIM error indices were then statistically related to WIM scale error to set the threshold values.

| 17. Key Words | 18. Distribution Statement |
|---|---|
| Road roughness, longitudinal profile, profile analysis, weight-in-motion (WIM), vehicle dynamics simulation, truck dynamic loading | No restrictions. This document is available to the public through the National Technical Information Service, Springfield, Virginia 22161. |

| 19. Security Classif. (of this report) | 0. Security Classif. (of this page) | 21. No. of Pages | 2. Price |
|---|---|---|---|
| Unclassified | Unclassified | 1 | |

## TABLE OF CONTENTS

## ACKNOWLEDGMENTS

The author of this report would like to acknowledge the contributions of Tom Gillespie and Chris Winkler, who helped develop the virtual fleet of vehicles for this study; David Cebon, for a very enlightening discussion of spectral analyses and other profile index options; Gonzalo Rada, Barbara Ostrom and Amy Simpson for technical assistance throughout the project; and Miriam Pitz and John Rush, for timely delivery on some difficult data requests.

## INTRODUCTION

This document reports on the development of smoothness criteria for weigh-in-motion (WIM) scale approaches. The criteria are meant to screen sites for excessive truck dynamic loading that exacerbates WIM scale error beyond levels recommended by the American Society of Testing and Materials (ASTM), listed in Table 1. (*1*) The tolerance values are set for 95 percent probability of conformity.

**Table 1. ASTM Error Tolerances.**

| Weighing Case | Error Tolerance |
|---|---|
| Single Axle | ± 20 % |
| Tandem Axle | ± 15 % |
| Gross Weight | ± 10 % |

The criteria developed in this project will be used in four applications: (1) acceptance of potential WIM sites, (2) location of the optimal scale position within a new site, (3) periodic verification of existing WIM sites, and (4) diagnosis of WIM sites that exhibit unacceptable error. These criteria classify sites as acceptable, unacceptable without major reconstruction, or unacceptable without some correction. Originally, these criteria targeted long-wavelength roughness relevant to truck body motion. As the work progressed, the project expanded to cover assessment of truck dynamic loading from axle motion also.

The scope of this study was limited to analysis of five-axle tractor-semitrailers operating on Long-Term Pavement Performance (LTPP) Study sites. Five-axle tractor semitrailers are by far the most common type of heavy truck expected to pass over the WIM scales. LTPP sites were analyzed because a vast amount of profile data were collected on them and a tremendous database of auxiliary information about them is available. Although several WIM scale verification tests were performed at pilot sites concurrently with this study, the report is limited to the simulation study.

In the simulation study described below, the assumptions were made that no roughness existed because of the presence of the scale, and that the scale itself measures the dynamic load applied to it accurately. Neither assumption is true, and testing will be needed to investigate them.

The development of WIM scale error criteria was carried out by searching for a profile-based index that predicts simulated WIM scale error, and selection of a corresponding threshold value. The index was developed in the following steps:

1. Select a set of profiles for placement of simulated WIM scales.
2. Compile a fleet of heavy trucks to represent the U.S. traffic fleet.
3. Simulate the fleet of heavy trucks over the WIM scales.
4. Associate a simulated aggregate WIM error level with each profile at the scale location.
5. Create a simple index, computed from profile, that predicts the error level.

6. Set a threshold value for the index that ensures adherence to ASTM error limits.

The simulated heavy truck fleet was confined to the pitch plane. Thus, the models accepted only one profile at a time. This means that the simulations do not consider vehicle roll motion. In most cases, this is sufficient to capture the relevant vehicle motions for wheel load analysis. The aggregate WIM error levels were compiled by examining the distribution of WIM scale percentage error over the simulated truck fleet. The WIM error index options were evaluated by correlating them to aggregate WIM error over the selected sites.

Two indices were needed to ensure that the background roughness near the scale was acceptable as well as localized roughness very close to the scale.

Descriptions of most of the details of this study appear in Appendices. The main report provides an overview of the steps taken in the study, recommends a set of WIM scale error criteria, and lists some issues for future study.

## WIM SCALE ERROR SIMULATION

WIM scale error was related to profile characteristics using a large simulation study of the response of 3,696 virtual five-axle tractor-semitrailers over 63 measured profiles. A distribution error was compiled over the truck population for steer axle, tandem axle, and total vehicle weight at each site. The error distributions were summarized by their 95th percentile absolute error levels. The error levels assigned to each site were used as a correlation standard for proposed roughness indices.

### Simulated Truck Population

A "virtual fleet" of five-axle tractor semitrailers was constructed to represent the diverse population of heavy trucks. This approach was first attempted by Cole for the study of the spatial distribution of truck loads. (*2*) Overall, 616 combinations of suspension, tire, loading scheme, and layout options appear in this fleet. These combinations represent typical combinations found in practice. Overall, the fleet includes 9 types of tractor, 18 types of trailer, and 6 loading schemes. Each vehicle was given an appropriate set of standard truck tires, but a small subset of the vehicles was fitted with wide-based single tires. Appendix C provides all of the details about this set of vehicles.

Preliminary simulations were done that covered a much larger number of parameter combinations (> 50,000) on a limited number of profiles to study the effect of each parameter on the predicted statistical performance of a weigh scale. Certain vehicle properties emerged as having a major influence on the results. These were drive axle and trailer axle suspension force-deflection characteristics, suspension damping, gross vehicle weight, and speed. Care was taken to cover a reasonable range of these properties and include some diversity in them.

Although suspension damping was found to be important, little information was available to describe typical values found in practice. For this reason, all 616 combinations of other parameters were simulated with high damping, representing new shock absorbers, and low damping, representing worn shock absorbers. In reality, a much more continuous variation exists. Another "factorial" applied to the base set of vehicles was speed. Each

vehicle was simulated at 72.4 kph (45 mph), 88.5 kph (55 mph), and 104.6 kph (65 mph). This raised the total number of simulation runs for each site to 3,696.

## Measured Profiles

A matrix of road profile measurements was assembled for input to the truck simulation models. The composite WIM scale error at a single location within each of these profiles served as the correlation standard for all proposed indices. Thus, care was taken to compile a set of profiles of diverse construction type and diverse roughness. In addition, an attempt was made to distribute the roughness of the sites evenly over the range of interest. All of the profiles were extracted from the LTPP database. The criteria used to select specific profiles are described in detail in Appendix A, as is a complete listing of the profile measurements that were chosen.

The profiles cover four construction types: (1) asphalt concrete, (2) jointed plain concrete, (3) jointed reinforced concrete, and (4) asphalt overlay on concrete. The profiles for these surface types were all sites from LTPP General Pavement Studies 1, 3, 4, and 7, respectively. For each surface type a set profiles was chosen that have overall International Roughness Index (IRI) values near multiples of 0.158 m/km (10 in/mi) over as large a range as possible. Only one profile was used to cover each target value. Table 2 summarizes the matrix. The overall range is 0.48-3.86 m/km (30-245 in/mi), but profiles could not be found to cover that range for all surface types. In particular, very rough sites with an overlay and very smooth jointed reinforced sites were rare. Other selection criteria for these profiles included geographical diversity, the absence of significant localized roughness, and screening for measurement errors.

**Table 2. Profile Matrix Summary.**

| Surface Type | Roughness Range (m/km) | Number of Profiles |
|---|---|---|
| Jointed Plain Concrete | 0.78-3.43 | 18 |
| Jointed Reinforced Concrete | 1.09-3.17 | 14 |
| Asphalt Concrete | 0.50-3.86 | 20 |
| Asphalt Overlay on Concrete | 0.48-2.06 | 11 |

1 m/km = 63.36 in/mi

## Simulation

Overall, 232,848 simulation runs were performed using a pitch-plane vehicle model. (The model is described in Appendix B.) These runs simulated each vehicle in the virtual fleet on each profile. Only one scale location was examined per profile, so five scale readings were produced per run. Figure 1 illustrates the procedure for obtaining one set of scale readings. In a simulation run a set of vehicle properties and a measured road profile are provided to the simulation model. It produces time histories of wheel load for all five axles. The wheel load is extracted from the instant in each time history when it is over the scale, denoted by a small circle in the figure. The scale reading for each axle occurred at a different time, because each axle reached the scale successively later. The WIM scale readings are compared to the static wheel loads for the corresponding truck and used to generate individual weighing error values for: (1) steer axle load, (2) tractor tandem axle load, (3) trailer tandem axle load, and (4) total vehicle weight.

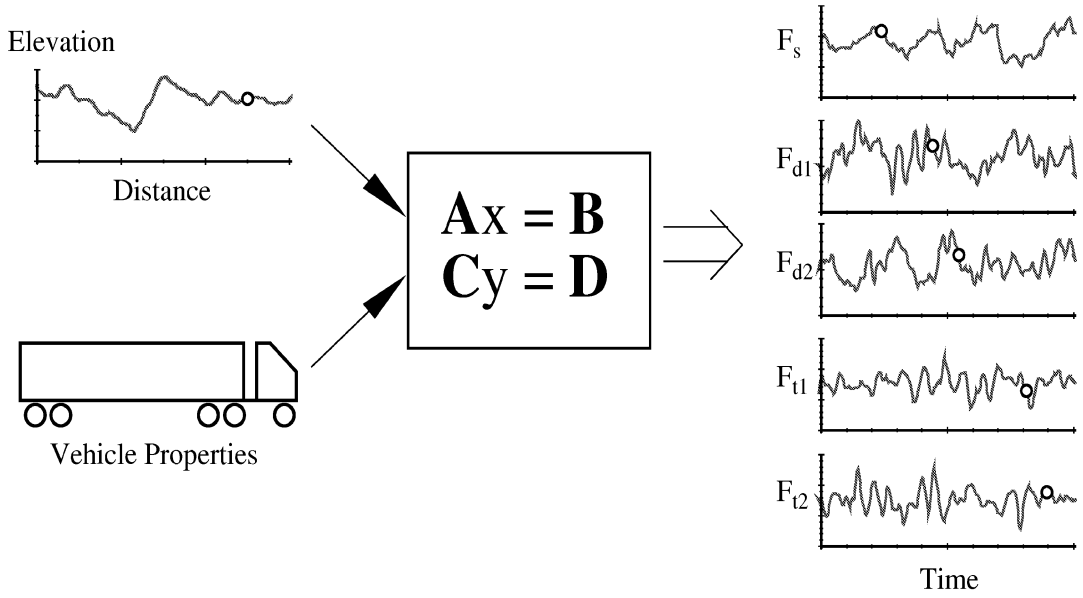


**Figure 1. Single simulation run.**

The distributions of steer axle, tandem axle, and total vehicle weighing error were compiled over the entire set of 3,696 vehicles on each simulated weigh scale. In turn, the distributions were summarized by 95th percentile absolute error. Figure 2 shows a sample error distribution. It contains 7,392 values because it includes two tandem axles per simulated vehicle pass. The 95th percentile error for this distribution is 19.8 percent. In this case, all of the instances of error above the 95th percentile level occurred when the weight was underestimated. On most sites, all of the extreme values occurred for error in only one direction, but a few sites showed extreme errors in both directions. A noteworthy feature of the distribution in figure 2 is that a bias exists for the site. A bias occurs because response of the simulated vehicle fleet to the roughness upstream of the scale is (somewhat) spatially repeatable. (*3*) Significant bias appeared in many of the distributions. (A complete set of statistics is provided in Appendix D.)

The ASTM error tolerances for weigh scale performance call for 95 percent confidence that: (1) steer axle load will be measured within 20 percent, (2) tandem axle load will be measured within 15 percent, and (3) gross vehicle load will be measured within 10 percent. The 95th percentile error levels for each type of weight were meant to serve as a correlation standard for testing proposed profile-based indices. Candidate indices would be sought that predict all three error levels. The existence of three sets of values with three separate error limits, covering steer, tandem, and total vehicle load complicated the analysis. Fortunately, no site violated the steer axle load limit without also violating the tandem axle load limit. In addition, a very strong relationship existed between tandem axle weight error and total vehicle weight error. This was no surprise, since all of the vehicles in this simulation study are five-axle tractor semitrailers, and a major percentage of the gross vehicle weight is carried by the tandem axles.

Figure 3 compares tandem axle and gross vehicle weighing error over the 63 sites. Tandem axle and total vehicle weight error levels increase together such that the two error limits are usually violated on the same sites. In fact, only two sites adhered to the gross weight error limits while violating the tandem error limit, and only one site adhered to the

tandem axle weight limit while failing the gross weight error limit. For this reason, most of the index development was performed by optimizing prediction of tandem axle weight error.

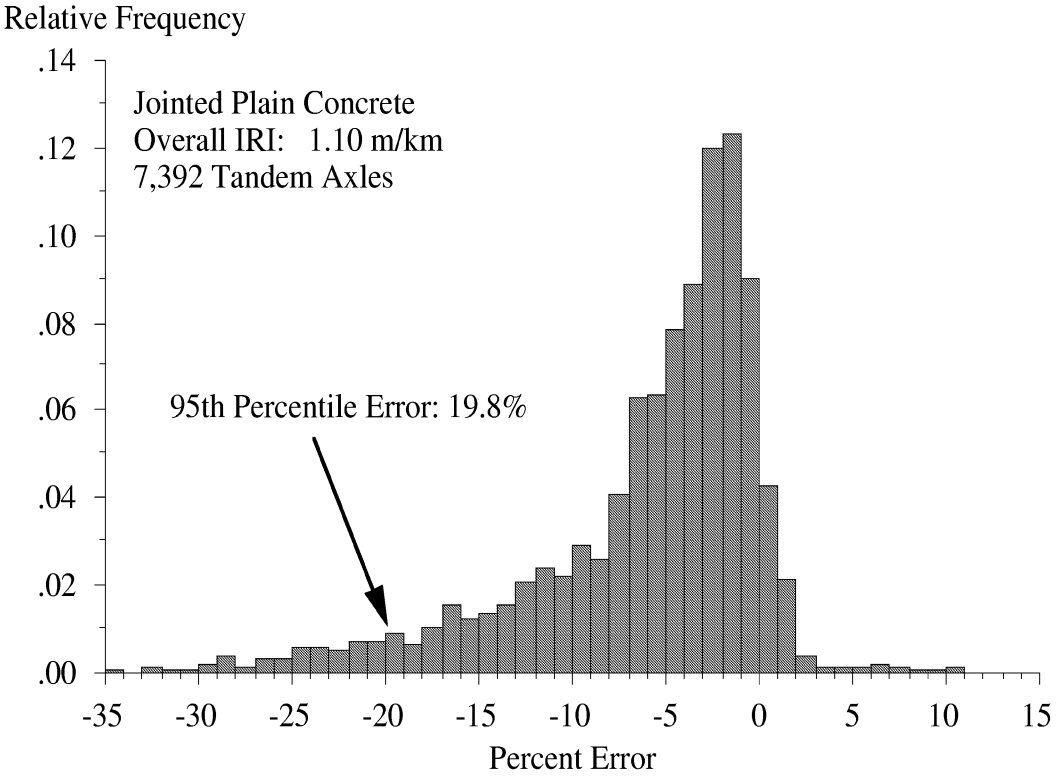


**Figure 2. Sample distribution of tandem axle weighing error.**

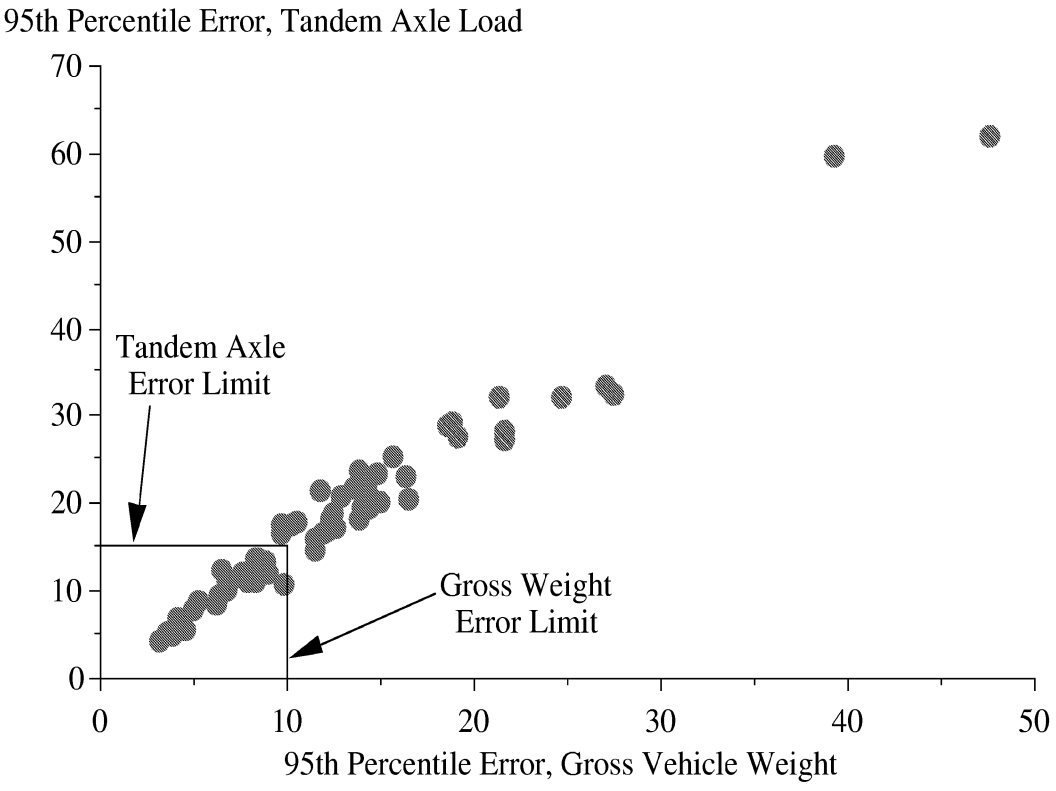


**Figure 3. Comparison of total vehicle load and tandem axle load error.**

The road profiles chosen for this study purposely covered their range of roughness uniformly. Unfortunately, the distribution of 95th percentile WIM scale error was not uniform. In particular, two of the values (shown in figure 3) were extreme compared to the others. A correlation standard for roughness index development should include a set of values that are uniformly distributed. Thus, the two extreme values shown in figure 3 were ignored in the index development. (High correlation would have been much easier to obtain with these values included, but less meaningful.) This will prevent them from imposing disproportionate influence on the level of correlation to proposed roughness indices.

## INDEX DEVELOPMENT

Development of smoothness criteria for WIM scale approaches required the formulation of a profile-base index that, when applied to the measured profile at a site, could predict WIM error level. For this study, the correct value of WIM error level for each profile (and scale location) was assembled from simulation results using a virtual truck fleet. Development of the criteria was a matter of finding the index options that related best to scale error. Two broad classes of index were used for this purpose.

First, PSD analyses were performed to learn what range of wavelengths was most relevant to predicting scale error. The analyses were combined with spatial profile weighting to learn what range of pavement near the scales affected their performance most. When a promising waveband was identified using PSD analysis, a band-pass filter with similar sensitivity was developed into a candidate index. Second, band-pass filters were tested as options for the final index. Two types of band-pass filter were considered: (1) a quarter-car model and (2) a four-pole Butterworth filter represented in state space. Index options were explored for all of these types of filter by optimizing:

- The filter wave-number sensitivity: This was optimized by manipulating the filter coefficients. For the quarter-car filter, the vehicle properties were treated as simple tuning parameters. For the Butterworth filter, the long- and short-wavelength cutoff values were varied. Both filters included a moving average for smoothing and conversion of the profile to slope.
- The spatial weighting function: This determines the range of pavement that affects the scale. Three types of weighting function were examined: (1) box, (2) Hanning (a cosine function), and (3) quadratic. The endpoints of each type of weighting function were manipulated to adjust the range of pavement that contributed to the index value.
- The accumulator: Once the profile was filtered and weighted, a final index value was calculated by performing some type of averaging over the resulting signal. Root-mean-square (RMS), root-mean-quad (RMQ), and average rectified (AR) accumulation were all examined. (An average rectified value is calculated by taking the absolute value of every point in a signal, then averaging the resulting values.)

The IRI and Ride Number were also examined. Technical details about these index components are provided briefly in Appendix E, and described in detail in another report.

(*4*) Every combination of these index components was explored. Some of the best combinations and their correlation level to WIM scale error are listed in Appendix F.

## WIM APPROACH INDEX

The search for an optimal index produced some predictable results. First, no spatial weighting function emerged as superior to the others. A "box" weighting function was chosen, because it allows a profile to be quickly searched for viable locations. This is demonstrated below. Second, no accumulation type emerged as superior to the others. This is partly because profile measurements were chosen that did not have rough localized features near the scale. That prevented the exponent level used in the summing of roughness from influencing the comparison between sites. Third, roughness near the scale was important. Two ranges of pavement stood out as influencing scale error.

1. "Short Range" roughness, covering the range of pavement that included about 3 meters preceding the scale, the scale itself, and about 0.3 meters beyond it, and
2. "Long Range" roughness, covering the range of pavement that included about 25 meters preceding the scale, the scale itself, and about 3 meters beyond it.

Some index options were found to predict scale error well using an intermediate range, but it is thought that this is because they contain some influence from each. In the search for the best single index, optimal versions of just about every index type appeared with spatial weighting functions that approximately covered the two ranges listed above.

Instead of making a choice between them, two of the best versions of the Butterworth filter were selected for development of WIM site criteria. Table 3 lists their essential characteristics. The "Long Range" criterion is a limit on average rectified Butterworth filter response over the range of pavement listed in the table, using a box-type spatial weighting function. A negative value for the start of the range indicates distance preceding the scale. The filter cutoff values represent wavelengths at which the filter response gain is attenuated by 30 percent. The "Short Range" criterion is also a limit on average rectified Butterworth filter response over the range of pavement listed in the table, and also uses a box-type spatial weighting function. It simply covers a shorter range of pavement and uses different filter cutoff values.

**Table 3. WIM Scale Error Index Details.**

| Criterion | Pavement Range | | Filter Cutoff Values | | Index Limit |
|---|---|---|---|---|---|
| | Start (m) | End (m) | Short (m) | Long (m) | (m/km) |
| Long Range | -25.8 | 3.20 | 1.1 | 11.4 | 0.789 |
| Short Range | -2.74 | 0.46 | 1.6 | 16.5 | 0.789 |

1 m/km = 63.36 in/mi

The Short and Long Range WIM error indices implied by table 3 were statistically related to WIM scale error, but a high level of scatter was found. This is demonstrated in figure 4, which compares the Long Range Index to simulated WIM scale error for tandem axles. For this reason, the index limit was set rather conservatively, as shown. This was done to prevent unacceptable error on pavement where the index under-predicted dynamic

load variation. Similar assessment was done using the Short Range Index, and comparison to gross vehicle weight error. (See Appendix F.)

This level of scatter is rather high for a simulation study, but the aim is to predict the response of a diverse set of vehicles at a particular point. Overall dynamic loading measures, such as RMS dynamic load, were predicted with a much lower level of scatter.

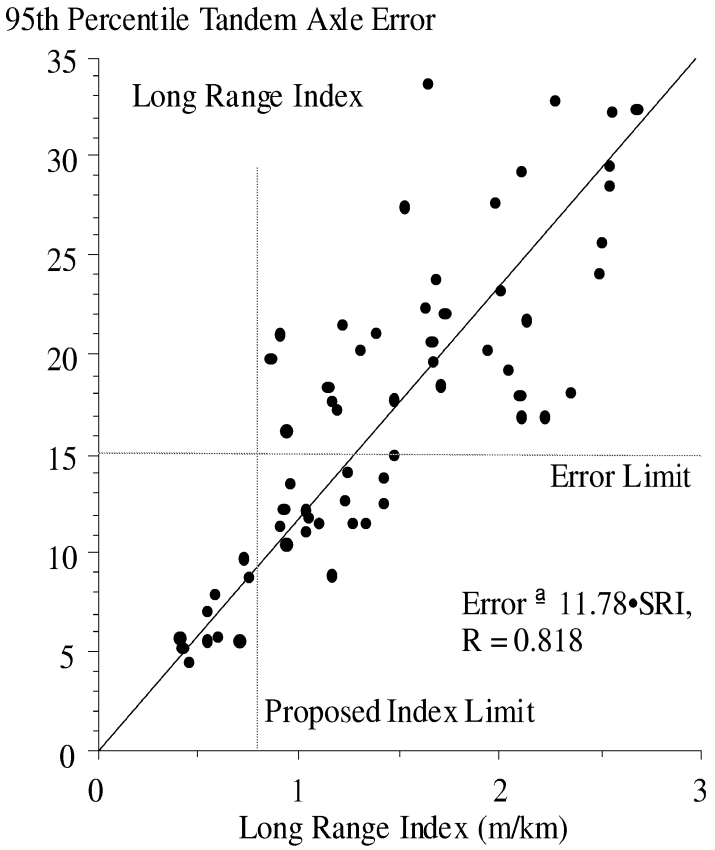


**Figure 4. Long range WIM error index vs. tandem weighing error.**

When the two recommended criteria are used together, the limits placed on them should ensure acceptable levels of WIM error. Each criterion is implemented by passing the entire profile into the Butterworth filter. The source code and subroutine calls needed for this are listed in Appendix G. The index values are accumulated by averaging them over the proper range of pavement. It is very important not to apply the spatial weighting function before the filter. Some of the filter response included in the spatial weighting function boundaries are caused by roughness preceding the range.

Although these criteria were developed as if the WIM scale location on a given pavement is known, they do not have to be used that way. At a potential WIM site, the "roughness profile" approach can be used to scan the site for the best scale location. (*5*) Figure 5 illustrates this for the Short Range Index. The figure shows the value of the Index for every possible scale location along a site. This process is started by filtering the entire profile, then taking the absolute value of every point. The index for a single scale location is calculated by averaging the signal over the appropriate range. The plot simply shows how this result varies with potential scale location. The calculation is very efficient because of the box-type weighting function and the use of average rectified accumulation. Once the

value at a given location is known, the value for the next possible scale location is calculated by subtracting the influence of the trailing point and adding the influence of the leading point. (This is really just a moving average. The efficiency is gained because the entire average does not have to be calculated over and over again.) These calculations can be done fast enough for real-time reporting in the field.

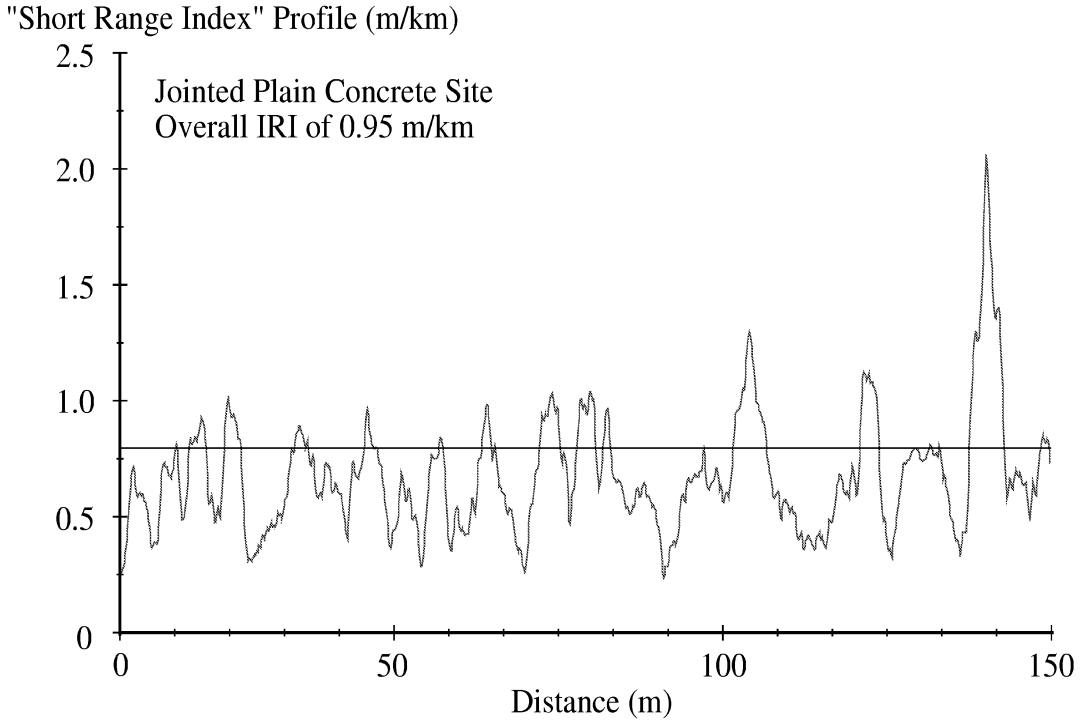


**Figure 5. Scan for acceptable short range roughness.**

Figure 5 illustrates this process for a jointed plain concrete site with an overall IRI of 0.95 m/km (60 in/mi). A WIM scale could be placed on this site, but localized segments appear within it that fail the Short Range criterion. With this plot, and a companion plot for the long-range criterion, a viable scale location can be found by seeking a location with a Long Range Index and Short Range Index below 0.79 m/km (50 in/mi). Note also that even though individual values of the Short Range Index only cover 3.20 meters (10.5 feet) of pavement, longer wavelength roughness does elevate the background level in figure 5.

## RECOMMENDATIONS

This report recommends two criteria for roughness limits at WIM scale approaches. This first covers a short range near the scale and the second covers a longer range leading up to the scale. These criteria are applied to only one profile at a time, and both the left and right wheel path profiles must pass simultaneously for a site to be deemed acceptable. They are recommended for four applications: (1) acceptance of potential WIM sites, (2) location of the optimal scale position within a new site, (3) periodic verification of existing WIM sites, and (4) diagnosis of WIM sites that exhibit unacceptable error. At potential sites, a search of the roughness profile for the best scale location is recommended. To facilitate this, profile measurements for potential WIM sites should cover a much longer segment of pavement than conventional LTPP profile measurements.

A further application of the roughness profile method is to identify candidates for corrective action. Certainly, if the Short Range Index criterion is violated, corrective action is indicated. On the other hand, grinding is not likely to be a practical so near to the scale. It is recommended that any short segment that would fail the Short Range criterion up to 26 meters (85 feet) upstream of the scale be considered a candidate for corrective action. If the Long Range Index is above the recommended tolerance, it is only considered correctable if hot spots appear in the Short Range Index roughness profile.

## FUTURE STUDY

The criteria recommended in this report are expected to identify unacceptable roughness at WIM scale approaches. The index threshold values were set rather conservatively because not all of the variation in WIM scale error within the simulation study was accounted for by the indices. The following recommendations for future study are offered.

- A small set of profiles that failed the old short-wavelength criterion (i.e. the plate test) should be analyzed to make sure that the Short Range Index recommended above captures these cases. The relevance of the old test should be tested by subjecting some profiles of sites that failed to the simulation of the virtual truck fleet used in this study.
- The three-sensor WIM system recommended by Cebon was simulated in conjunction with a single-sensor system. (*6*) Threshold values for roughness could be set much more liberally with a three-sensor system in place. The additional cost of a three-sensor system should be weighed against the cost of obtaining an acceptable roughness level by correcting the pavement. The additional cost of moving the site should also be weighed against the cost of installing two more scales on an existing site.
- The profiles used in this study were not measured at WIM scale approaches. Further, no profiles were included that contain localized roughness. Concentrated roughness ahead of the scale could affect WIM error, even if it is well outside of the range covered by the Long Range Index. Profiles from WIM installations should be studied carefully to screen them for unique roughness characteristics that may not have been covered in the simulation study. Profiles that include WIM scales should also be evaluated with the criteria recommended in this report as a means of estimating the increase in estimated WIM error that may occur in a new WIM site because of the scale.
- The simulation models used in this study did not include direct treatment of tire envelopment. Instead, the anti-aliasing filters applied to the profiles serve as a surrogate envelopment model. A better representation of tire envelopment may be needed to simulate truck response over narrow, concave profile features such as wide expansion joints. This may be especially important if the roughness at a WIM scale is included in the profile.
- The virtual vehicle population constructed for this study was as representative as the researchers could make it, and is considered sufficient for its intended purpose.

Nevertheless, representing the vehicle population is a difficult task, and improvements are always possible. The study could be expanded to take a limited look at vehicles other than five-axle tractor semitrailers.

- It should be recognized that logistics, local industry, deviation from prevailing weight laws, and a host of other factors may cause the truck population at a specific scale to be much less diverse than the overall population. This study showed that bias, in which a scale measures systematically high or low over the population, is a significant part of WIM scale error. (For example, 25 of the 63 simulated sites passed the ASTM criterion for tandem axle error, but 7 of them exhibited a bias level of over 2 percent, and 1 of them exhibited a bias of over 4 percent.) A uniform truck population at a given scale would exacerbate this problem.
- Jointed plain concrete (JPC) pavements have exhibited significant changes in roughness throughout the day under certain conditions. (*7*) If WIM scales are installed with JPC upstream, care should be take to measure the profile several times throughout a daily cycle when the weather is expected to exacerbate slab curl. If any type of jointed concrete is expected to prevail as the standard pavement type for WIM approaches, their interaction with truck loading should be examined. This could be particularly important if the standard site design includes consistent placement of joints in the same location near the scale.

## REFERENCES


1. American Society of Testing and Materials, Annual Book of ASTM Standards, Volume 4.03, Road and Paving Materials; Vehicle-Pavement Systems, Philadelphia, 1999.
2. Cole, D. J. and Cebon, D., "Spatial Repeatability of Dynamic Tyre Forces Generated by Heavy Vehicles." Journal of Automotive Engineering Proc. I.Mech.E, Vol 206 (1992).
3. Cole, D. J., et. al., "Spatial Repeatability of Measured Dynamic Tyre Forces." Automotive Engineering, I.Mech.E., Vol. 210, No. D3 (1996) pp. 185-197.
4. Sayers, M. W. and Karamihas, S. M., "Interpretation of Road Roughness Profile Data." Federal Highway Administration Report FHWA/RD-96/101 (1996) 177 p.
5. Sayers, M.W., "Profiles of Roughness." Transportation Research Record 1260, (1990) pp. 106-111.
6. Cebon, D. and Winkler, C. B., "A Study of Road Damage Due to Dynamic Wheel Loads Using a Load Measuring Mat." Strategic Highway Research Program, National Research Council, Report SHRP-ID/UFR-91-518 (1991) 152 p.
7. Karamihas, S. M., et. al. "Diurnal Changes in Profile of Eleven Jointed PCC Pavements." 7th International Conference on Concrete Pavements. Proceedings. Volume 1, (2001) pp. 69-80.

# Appendix A: Road Profiles

A matrix of road profile measurements was compiled to support statistical comparisons between simulated weigh-in-motion (WIM) scale performance and alternative summary roughness indices. The matrix consists of profile measurements from the Long-Term Pavement Performance Study Database, and covers a broad range of roughness level and surface type. Several thousand vehicle simulations were performed over each profile; and several thousand roughness indices were proposed for predicting scale performance.

The matrix covers four pavement construction types: asphalt concrete, jointed plain concrete, jointed reinforced concrete, and asphalt overlay on concrete. These profiles were measured on sites from General Pavement Studies 1, 3, 4, and 7, respectively. For each construction type, profiles were assembled that span as large a range of International Roughness Index (IRI) as possible, with uniform representation over the range. To accomplish this, target roughness levels in multiples of 0.16 m/km (10 in/mi) were covered from 0.47 m/km (30 in/mi) to 3.47 m/km (220 in/mi). Thus, the matrix consists of up to 20 profile measurements for each construction type. Profile data were selected using the following criteria:

- Only profiles from the left wheel path were considered.
- Profiles were selected with IRI values near multiples of 0.16 m/km (10 in/mi).
- Profiles were avoided if Evans found them to have measurement errors. (*1*)
- Sites were avoided if the progression of IRI values over time could not be justified by the reported construction and maintenance history. (*2, 3*)
- No more than one profile was used from a given site.

Tables A.1 through A.4 list the measurements that were selected. Note that data were not always available to cover the entire roughness range. In some cases, several measurements of a given surface type and roughness level were available that fit the criteria listed above. The following additional criteria were then used to choose between them:

- Sites without concentrated roughness were favored. This was done by attempting to avoid profiles that contained a 10-meter (33-foot) long segment with an IRI value greater than double the value for the entire section.
- Profiles were favored from groups of repeat measurements with IRI values that have a low standard deviation.
- Profiles were favored that showed good subjective visual agreement with other repeat measurements. Agreement was confirmed objectively by cross-correlating IRI filter output. (*4*)
- Sites were selected to be as geographically diverse as possible.

All of the profile measurements selected for the study covered a length of 152.4 meters (500 feet). Note that measurements of longer segments of road would have been

preferable, because a greater variety of scale locations could be investigated within each profile. (More than half of a 152.4 meter segment is needed for leading up to and away from the proposed scale so that the simulation is valid.) All of the measurements were also collected at a sample interval of 25.4 mm (1 inch), averaged with a 304.8-mm (12-inch) baselength, and decimated to an interval of 152.4 mm (6 inches). The averaging serves as a crude approximation of tire enveloping, but a better model may be needed for narrow concave features that are "bridged" by a passing tire. This may be especially important for evaluating roughness near the scale. A shorter sample interval would also provide greater insight into the source of localized roughness. For example, only severe concrete faulting can be detected after the decimation to a 152.4-mm (6-inch) interval, but low and moderate levels of faulting can be estimated using profiles with a 25.4-mm (1-inch) interval. (Joints are also easier to locate.) To accommodate these considerations, profile measurements at existing and proposed WIM sites are now made over a total length of 320 meters (1050 feet) and recorded at a sample interval of 25 mm (1 inch).

No special attempt was made to select jointed plain concrete sites of specific slab length. Many of the selected profiles show evidence of warping or curling, and a few of them showed evidence of faulting. A majority of the jointed reinforced concrete sites also included periodic roughness that corresponds to slab length. Some of these sites also possessed roughness near the joints. The profiles of asphalt concrete contained a greater portion of roughness in the long-wavelength (> 6 m) range than did the jointed concrete. Asphalt overlay of concrete covered the smallest range of roughness, because few sites that could be confirmed as having an overlay were very rough. In addition, none of the selected profiles had yet to reflect any periodic roughness from the underlying slabs.

**Table A.1. Jointed Reinforced Concrete.**

| Target IRI (m/km) | State Code | State | Section Number | Date | Repeat Num. | Actual IRI (m/km) |
|---|---|---|---|---|---|---|
| 1.10 | 29 | Missouri | 5473 | 21-May-94 | 4 | 1.092 |
| 1.26 | 18 | Indiana | 5538 | 05-Apr-90 | 1 | 1.270 |
| 1.42 | 42 | Pennsylvania | 1606 | 11-Jan-96 | 2 | 1.419 |
| 1.58 | 26 | Michigan | 4015 | 05-Jul-94 | 6 | 1.583 |
| 1.74 | 34 | New Jersey | 4042 | 26-Jun-95 | 3 | 1.743 |
| 1.89 | 22 | Louisiana | 4001 | 02-Jun-95 | 1 | 1.890 |
| 2.05 | 39 | Ohio | 4031 | 04-Nov-91 | 1 | 2.048 |
| 2.21 | 27 | Minnesota | 4040 | 27-Jun-95 | 2 | 2.214 |
| 2.37 | 17 | Illinois | 5217 | 15-Jun-91 | 3 | 2.403 |
| 2.53 | 21 | Kentucky | 4025 | 12-Jan-91 | 4 | 2.522 |
| 2.68 | 54 | West Virginia | 4004 | 03-Dec-92 | 2 | 2.673 |
| 2.84 | 1 | Alabama | 4084 | 07-May-90 | 3 | 2.842 |
| 3.00 | 5 | Arkansas | 4023 | 13-Aug-91 | 2 | 3.012 |
| 3.16 | 48 | Texas | 4152 | 08-Apr-91 | 3 | 3.166 |

1 m/km = 63.36 in/mi

**Table A.2. Asphalt Concrete.**

| Target IRI (m/km) | State Code | State | Section Number | Date | Repeat Num. | Actual IRI (m/km) |
|---|---|---|---|---|---|---|
| 0.47 | 4 | Arizona | 1006 | 21-Jan-92 | 5 | 0.495 |
| 0.63 | 33 | New Hampshire | 1001 | 21-Jul-92 | 1 | 0.630 |
| 0.79 | 32 | Nevada | 1020 | 09-Aug-89 | 9 | 0.793 |
| 0.95 | 53 | Washington | 1006 | 14-Aug-94 | 3 | 0.947 |
| 1.10 | 36 | New York | 1011 | 05-Jun-90 | 1 | 1.115 |
| 1.26 | 25 | Massachusetts | 1003 | 31-Aug-92 | 5 | 1.269 |
| 1.42 | 21 | Kentucky | 1014 | 02-Feb-93 | 1 | 1.424 |
| 1.58 | 53 | Washington | 1002 | 29-Sep-92 | 8 | 1.585 |
| 1.74 | 16 | Idaho | 9032 | 08-Jul-97 | 4 | 1.732 |
| 1.89 | 8 | Colorado | 1047 | 29-Oct-91 | 3 | 1.877 |
| 2.05 | 51 | Virginia | 1023 | 07-Oct-95 | 7 | 2.028 |
| 2.21 | 47 | Tennessee | 3104 | 15-May-92 | 1 | 2.223 |
| 2.37 | 12 | Florida | 4153 | 06-Sep-94 | 1 | 2.380 |
| 2.53 | 2 | Alaska | 1004 | 04-Jun-90 | 7 | 2.503 |
| 2.68 | 45 | South Carolina | 1025 | 30-Apr-92 | 3 | 2.685 |
| 2.84 | 23 | Maine | 1001 | 04-Oct-90 | 7 | 2.837 |
| 3.00 | 20 | Kansas | 1005 | 24-Apr-96 | 5 | 3.013 |
| 3.16 | 12 | Florida | 4136 | 05-Jul-90 | 7 | 3.200 |
| 3.31 | 48 | Texas | 1178 | 02-Jun-93 | 5 | 3.295 |
| 3.47+ | 81 | Alberta | 1804 | 11-Sep-92 | 3 | 3.860 |

1 m/km = 63.36 in/mi

**Table A.3. Overlay on Concrete.**

| Target IRI (m/km) | State Code | State | Section Number | Date | Repeat Num. | Actual IRI (m/km) |
|---|---|---|---|---|---|---|
| 0.47 | 28 | Mississippi | 3099 | 21-Jan-94 | 5 | 0.480 |
| 0.63 | 48 | Texas | 3629 | 31-Jan-95 | 5 | 0.637 |
| 0.79 | 23 | Maine | 7023 | 28-Sep-92 | 2 | 0.788 |
| 0.95 | 31 | Nebraska | 7040 | 29-Nov-93 | 2 | 0.948 |
| 1.10 | 29 | Missouri | 7073 | 14-Feb-92 | 7 | 1.106 |
| 1.26 | 28 | Mississippi | 3097 | 17-Feb-92 | 5 | 1.265 |
| 1.42 | 17 | Illinois | 5151 | 10-Mar-94 | 5 | 1.426 |
| 1.58 | 46 | South Dakota | 7049 | 11-Aug-91 | 9 | 1.584 |
| 1.74 | 40 | Oklahoma | 7024 | 26-Aug-91 | 3 | 1.719 |
| 1.89 | 31 | Nebraska | 7005 | 17-Aug-91 | 3 | 1.890 |
| 2.05 | 54 | West Virginia | 7008 | 29-Apr-92 | 1 | 2.057 |

1 m/km = 63.36 in/mi

**Table A.4. Jointed Plain Concrete.**

| Target IRI (m/km) | State Code | State | Section Number | Date | Repeat Num. | Actual IRI (m/km) |
|---|---|---|---|---|---|---|
| 0.79 | 6 | California | 3042 | 01-May-91 | 2 | 0.784 |
| 0.95 | 38 | North Dakota | 3006 | 21-Jul-94 | 1 | 0.949 |
| 1.10 | 40 | Oklahoma | 4157 | 16-Sep-93 | 1 | 1.077 |
| 1.26 | 5 | Arkansas | 3011 | 27-Sep-94 | 1 | 1.259 |
| 1.42 | 13 | Georgia | 3016 | 12-Dec-95 | 2 | 1.413 |
| 1.58 | 49 | Utah | 7085 | 31-Jul-95 | 5 | 1.588 |
| 1.74 | 16 | Idaho | 3017 | 11-Sep-94 | 2 | 1.739 |
| 1.89 | 19 | Iowa | 3009 | 16-Sep-94 | 2 | 1.908 |
| 2.05 | 37 | North Carolina | 3816 | 20-Dec-95 | 1 | 2.040 |
| 2.21 | 48 | Texas | 3589 | 13-Dec-94 | 6 | 2.212 |
| 2.37 | 50 | Vermont | 1682 | 23-Oct-89 | 1 | 2.363 |
| 2.53 | 12 | Florida | 4138 | 29-Jun-90 | 5 | 2.520 |
| 2.68 | 23 | Maine | 3013 | 17-Aug-95 | 6 | 2.680 |
| 2.84 | 56 | Wyoming | 3027 | 20-Jul-94 | 5 | 2.825 |
| 3.00 | 46 | South Dakota | 3012 | 28-Nov-90 | 2 | 2.993 |
| 3.16 | 55 | Wisconsin | 3014 | 17-Apr-93 | 5 | 3.167 |
| 3.31 | 1 | Alabama | 3028 | 16-Feb-94 | 3 | 3.302 |
| 3.47 | 39 | Ohio | 3013 | 26-Sep-89 | 5 | 3.429 |

1 m/km = 63.36 in/mi

## REFERENCES


1. Evans, L. D. and Eltahan, A., "LTPP Profile Variability." Federal Highway Administration Report FHWA-RD-00-113 (2000) 178 p.
2. Datapave, Release 3.0, <http://www.tfhrc.gov/pavement/ltpp/datapave.htm>
3. Perera, R. W., et. al., "Investigation of the Development of Pavement Roughness." Federal Highway Administration Report FHWA-RD-97-147 (1998) 244 p.
4. Sayers, M. W. and Karamihas, S. M., "Interpretation of Road Roughness Profile Data." *Federal Highway Administration Report FHWA/RD-96/101* (1996) 177 p.

# Appendix B: Simulation Models

This appendix provides a description of the simulation models used to predict the vertical wheel loads imposed on the pavement by virtual trucks running on measured profiles. This study was limited to five-axle tractor semitrailers, dubbed "3S2" vehicles, with common suspension configurations. The study was also confined to rigid body models of behavior in the pitch plane.† These models are defined by the inertial elements (parts with mass), compliant elements (tires and suspensions), rigid connections between parts (the hitch), and specific kinematics and compliance needed to capture relevant suspension behavior. Two multi-body models were needed for this study. One model was needed for four-spring and air-suspended vehicles, and another was needed for the less common walking-beam suspension. These models require a modest list of specific parameters to describe individual trucks. Thus, while only two models were needed for the study, thousands of parameter combinations were used to represent the broad range of vehicles operating on U.S. highways.

Three-dimensional models have also been suggested for the purpose of predicting vertical wheel loads. In a validation of two- and three-dimensional rigid-body models for predicting wheel loads, Cole reported that behavior of 3S2 vehicles with well-damped suspensions could be predicted with a two-dimensional model under typical operating conditions. (*1*) Cole also concluded that a three-dimensional model is needed when unsprung mass roll modes contribute significantly to vertical wheel loads. This was verified in a study that calibrated a three-dimensional model of a 3S2 vehicle to hydraulic shaker response. (*2*) In this study, it was found that unsprung mass roll motion, called "axle tramp", is most likely to be important on asphalt pavement. A three-dimensional model would provide broader coverage of the vehicle vibration behavior that might affect vertical wheel loads. However, it would require a much more substantial list of parameters to describe each truck, many of which are not as readily available as those needed for two-dimensional models.

Two-dimensional (pitch-plane) rigid-body models are the most common type used for predicting vertical wheel loads imposed by 3S2 vehicles. (*3, 4*) In most instances they have been found to be sufficient for prediction of vehicle wheel loads. (*5*) For this study, the equations of motion for the simulation models used were written using the AUTOSIM™ software package. AUTOSIM **auto**matically generates efficient **sim**ulation programs for mechanical systems composed of multiple rigid bodies. *(6, 7)* In AUTOSIM, an engineer describes the vehicle system in terms of the rigid bodies, the manner in which they are connected, compliant elements (linear or non-linear) within the system, and disturbance inputs. AUTOSIM formulates the equations of motion symbolically, and then writes a file containing the source code for a FORTRAN or C program that can numerically integrate the equations of motion. When the program is compiled and executed, it produces ready-to-

† The pitch plane is essentially the side view, so these models assume that the vehicle is two-dimensional and has height and length but no width, and that it rides in a single wheel path.

plot data files of time histories of output variables of interest, such as wheel loads. AUTOSIM has been used to generate models for similar studies in the past. (*3, 8*) As such, it contains specialized modeling options needed to properly represent vehicle dynamic behavior such as truck suspension system friction and tandem axle load sharing. (*9, 10*)

The assumptions made in modeling 3S2 vehicles for this study are described here. Much of the material used in the description is paraphrased from existing literature. (*2, 3, 11*) Some improvements to the models should be considered for use in future studies. In particular, a better representation of tire envelopment may be needed to simulate truck response over narrow, concave profile features such as wide expansion joints. This may be especially important if the roughness at a weigh-in-motion scale is included in the profile.

## BODIES/DEGREES-OF-FREEDOM

The pitch-plane model, illustrated in figure 1, includes two sprung masses (the tractor and semitrailer) and five unsprung masses (one for each axle). The tractor sprung mass translates vertically and longitudinally, and rotates in pitch. The trailer is attached to the tractor at the hitch point with a pin joint. The pin joint allows the semitrailer to rotate in pitch relative to the tractor. This gives the sprung masses a total of four kinematic degrees of freedom. (One of these degrees of freedom appears in a constraint equation needed to set the initial vehicle speed.) Each unsprung mass translates vertically relative to the sprung mass it supports. This adds another five degrees of freedom to the system. Two other degrees of freedom exist for the purpose of predicting the load sharing properties of the two tandem suspensions, as described below.

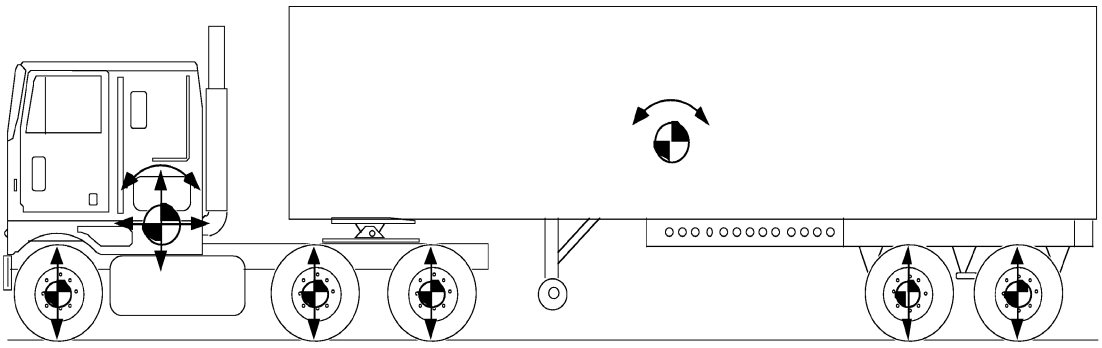

**Figure 1. Degrees of freedom.**

The treatment of the various masses as rigid bodies ignores structural vibrations of the individual components. While these may be significant to vibrations present on the body of the vehicle (the ride behavior), in general they have little influence on the loads experienced under the wheels.

## SUSPENSION SPRINGS

A key system that must be modeled properly in order to accurately predict truck wheel loads is the suspension spring, particularly leaf springs. Truck leaf springs exhibit a high magnitude of friction in their operation which produces complex force-displacement

characteristics. Figure 2 shows the force-displacement characteristic for a typical truck leaf spring measured experimentally in the Suspension Parameter Measurement Facility at UMTRI. (*12*) Friction in the system causes the force-deflection characteristic to have separate boundaries upon loading and unloading. As a consequence the force-displacement behavior follows the complex intermediate curves for the small displacements typical of ride motions. Modeling this behavior is essential to duplicating the appropriate stiffness and damping properties in the suspension.

An analytical model, documented elsewhere, is used to represent this behavior. (*9*) The model is based on representing the upper and lower boundaries of the force-deflection characteristic with a set of interconnected line segments, as shown in figure 3. When the springs are exercised over the small displacements in the mid-region of the plot, which are typical of ride motions, they approach the outer boundaries exponentially. (See figure 2.) The acuteness of the approach to the outer boundary is characterized by a "beta" parameter, which is given in units of displacement.

This type of behavior has been observed in air spring suspensions also, but the suspension stiffness (implied by the force-deflection boundaries), friction level, and beta parameter values are usually quite different than those observed in leaf spring suspensions. Air suspensions also require a unique set of suspension properties for each nominal loading case, because the air bag pressure depends on the nominal load.

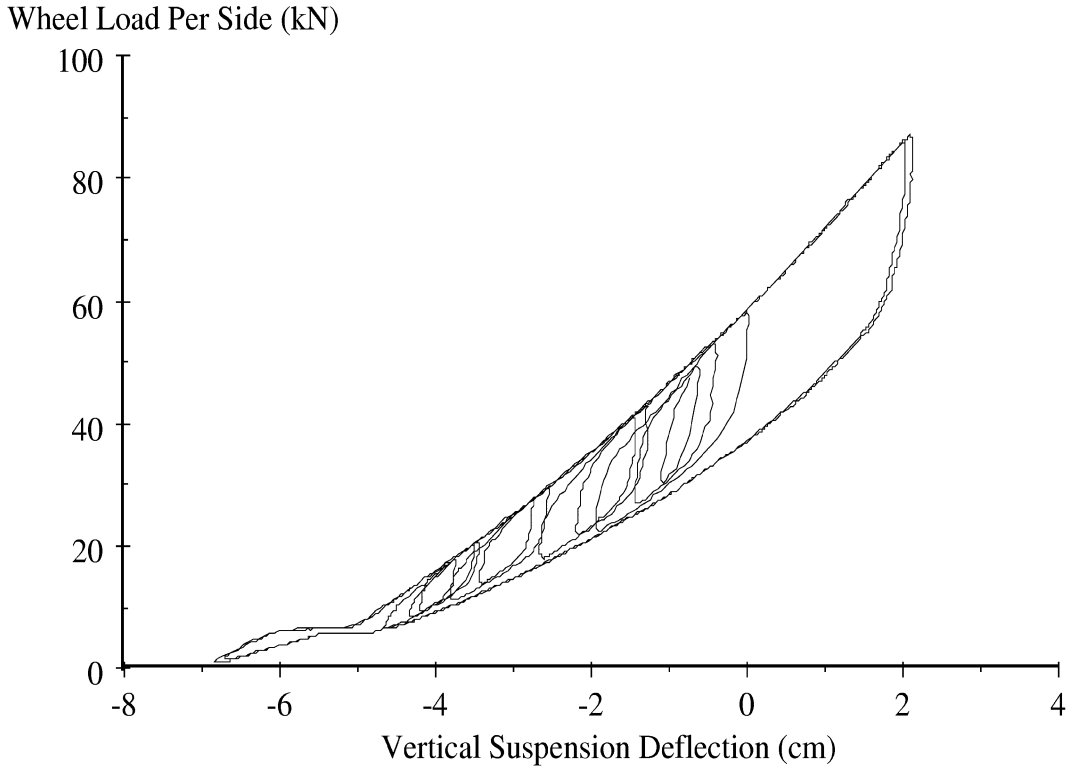


**Figure 2. Sample truck suspension force-deflection measurement.**

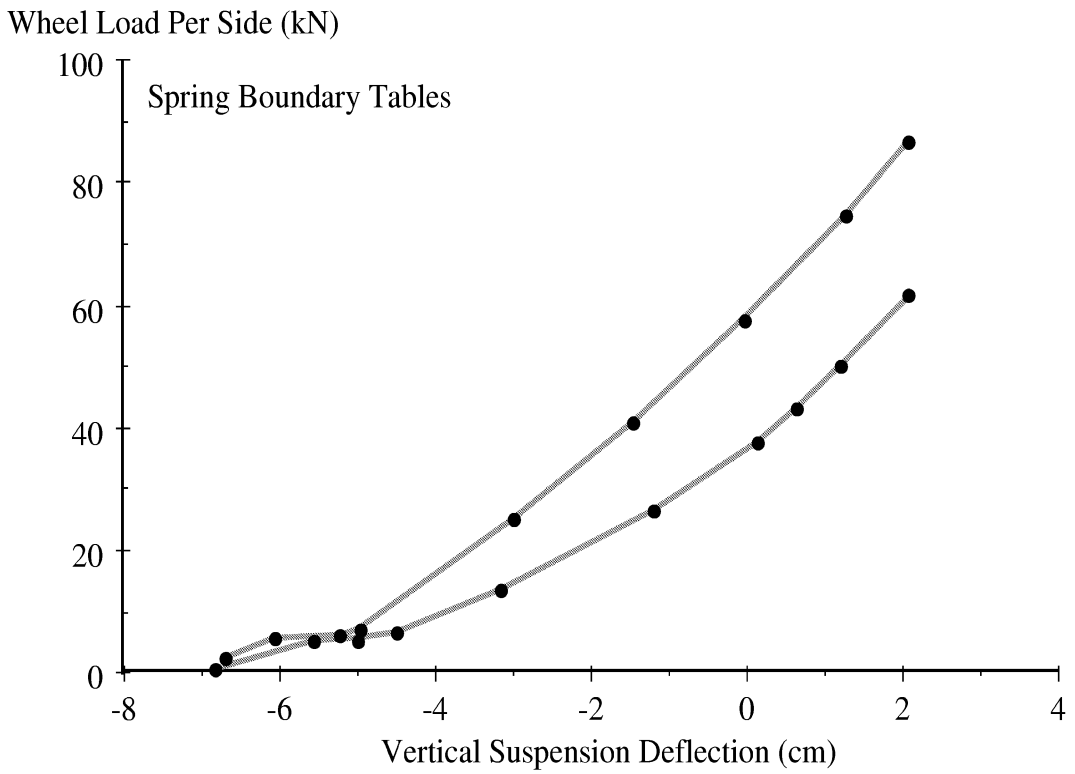


**Figure 3. Sample spring boundary tables.**

## SUSPENSION DAMPING

Much of the damping in truck suspensions is derived from friction, which is represented in the model as described above. The models also include linear viscous shock absorbers acting between each unsprung mass and its host sprung mass.

## TANDEM SUSPENSION LOAD SHARING

Four-spring tandem suspensions incorporate complaint elements, such as leaf springs, and linkages to equalize the load between the two axles. A schematic is shown in figure 4, with degrees of freedom for the suspension indicated with arrows. Unsprung mass is concentrated below each spring, and may translate vertically. An equalizer beam connects the ends of the two springs and is free to rotate. Many tandem suspensions are functionally equivalent to the model shown in the figure, in which the load on both axles is equalized by a balance of forces in the springs, accomplished by an equalizer beam.

The four-spring suspension has three degrees of freedom, shown using heavy arrows in figure 4. Including the inertial properties of the equalizer link would result in dynamic equations of motion that are "stiff" and require an order of magnitude more computation to predict vehicle motions. However, the inertial effects of the link are insignificant in comparison to the loading forces, such that a quasi-static solution method can be used to account for the load-equalization and the frictional behavior of the link.

Air spring suspensions do not possess a dynamic load sharing mechanism. They are represented with the same mechanical model as the four-spring suspension, but the load equalizer is frozen in place. (This is done by assigning a very high friction value to resist its motion.)

The degrees of freedom for the walking beam suspension are shown in figure 5. Since they are different from the four-spring suspension, an alternative rigid-body model is required. The walking-beam suspension only has one spring (per side). The spring is connected to a rigid beam with two degrees of freedom (vertical and pitch). In this model, unsprung mass is also concentrated in the position of the two wheels, but they are rigidly linked by a massless beam.

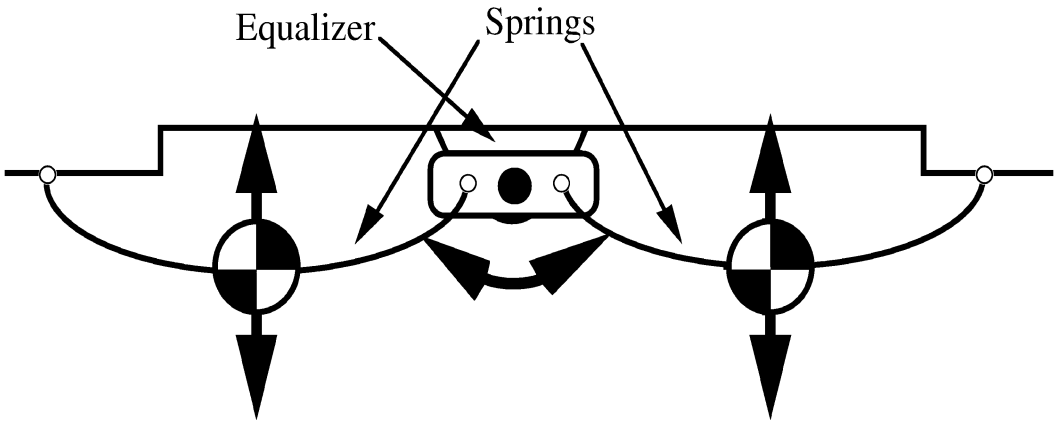


**Figure 4. Four-spring suspension schematic.**

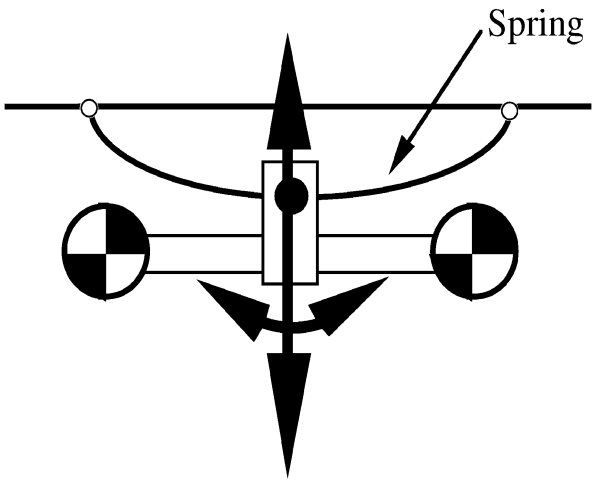


**Figure 5. Walking-beam suspension schematic.**

## TIRES

Tires are normally modeled as springs and dampers in parallel connecting the axles to the ground. The tire springs and dampers are simple linear elements while in contact with the ground. Should the tire leave the ground, the tire force goes to zero (the model does not allow the ground to pull back on the tire).

## PROFILE

The road surface is described by a series of road elevation values spaced at fixed intervals along the road. The road surface is assumed to be straight (constant slope) between these points. The elevation in the tire contact patch is averaged over the length of contact to reflect the envelopment properties of the tires. (*13*) This was done partly because the majority of profiles available for the study were already averaged with a baselength of 304.8 mm (12 inches) and decimated to a sample interval of 152.4 mm (6 inches). Profiles at new weigh in motion sites are now stored at a sample interval of 25 mm (about 1 inch). This should allow future models to include tire envelopment with "bridging" that allows a gap to exist under tire contact patch over narrow concave road features.

## REFERENCES


1. Cole, D. J., and Cebon, D., "Validation of an Articulated Vehicle Simulation." Vehicle system Dynamics, Vol. 21, No. 4 (1992) pp. 197-224.
2. Karamihas, S. M., et. al., "Axle Tramp Contribution to the Dynamic Wheel Loads of a Heavy Truck." Proceedings, 4th International Symposium on Heavy Vehicle Weights and Dimensions, Ann Arbor, Michigan. Ed. C. B. Winkler. (1995) pp. 425-434.
3. Gillespie, T.D., et al., "Effects of Heavy Vehicle Characteristics on Pavement Response and Performance." National Cooperative Highway Research Program Report 353 (1993) 126 p.
4. Streit, D. A., et al., "Road Simulator Study of Heavy-Vehicle Wheel Forces." Federal Highway Administration Report FHWA-RD-98-019 (1998) 272 p.
5. Cebon, D., "Handbook of Vehicle-Road Interaction." Swets & Zeitlinger B.V., Lisse, the Netherlands (1999) pp. 106-107.
6. Sayers, M.W., "Symbolic Computer Language for Multibody Systems." Journal of Guidance, Control, and Dynamics Vol 14, No. 6 (1991) pp. 1153-1163.
7. Sayers, M.W., "Symbolic Vector/Dyadic Multibody Formalism for Tree-Topology Systems." Journal of Guidance, Control, and Dynamics Vol 14, No. 6 (1991) pp. 1240-1250.
8. Gillespie, T. D., and Karamihas, S. M., "The Feasibility of Multi-Sensor Weighing for Increased Accuracy of WIM." International Journal of Vehicle Design: Heavy Vehicle Systems, Vol. 3, Nos. 1-4 (1996) pp. 149-164.
9. Fancher, P.F., et al., "Measurement and Representation of the Mechanical Properties of Truck Leaf springs." Society of Automotive Engineers Paper 800905 (1980) 16 p.
10. Sayers, M. W. and Gillespie, T. D., "Dynamic Pavement Wheel Loading for Trucks with Tandem Suspensions." Proceedings, Symposium on the Dynamics of Vehicles on Roads and Tracks, Lisse, Swets and Zeitlinger (1984) pp. 517-533.

11. Gillespie, T. D., and Karamihas, S. M., "Characterizing the Road Damaging Dynamics of Truck Tandem Suspensions." Society of Automotive Engineers Paper No. 932994 (1993) 8 p.

12. Winkler, C. B. and Hagan, M., "A Test Facility for Measurement of Heavy Vehicle Suspension Parameters." Transactions of the Society of Automotive Engineers, Vol. 89, Paper No. 800906 (1980) 29 p.

13. Gillespie, T.D., et al., "Calibration of Response-Type Road Roughness Measuring Systems." National Cooperative Highway Research Program Report 228 (1980) 81 p.

# Appendix C: Truck Simulation Fleet

This appendix describes the mix of five-axle tractor semitrailer properties covered in the "simulation fleet" for the development of roughness criteria at weigh-in-motion (WIM) scale approaches. Overall, 616 combinations of suspension, tire, loading scheme, and layout options appear in this fleet. These combinations do not represent a simple factorial matrix of possible parameter values. Rather, they are a set of typical trailers, towed by a set of typical tractors, loaded in typical ways. Some combinations of tractor, trailer, and loading are somewhat unusual, so they were excluded. In addition, certain tractor and trailer options are much more common than others, so they were combined with a greater number of loading and tire options.

Preliminary simulations were done that covered a much larger number of parameter combinations (> 50,000) on a limited number of profiles to study the effect of each parameter on the predicted statistical performance of a weigh scale. When these parameter values varied over a typical range, certain parameters emerged as having a major influence on the results. These were drive axle and trailer axle suspension force-deflection characteristics, suspension damping, gross vehicle weight, and speed. (This should be no surprise.) Care was taken to cover a reasonable range of these properties and include some diversity in them. Other parameters influenced the statistical performance of a simulated weigh scale very little. This was true of parameter values that simply do not vary much in practice, and of parameters that vary somewhat but do not have much impact on truck wheel loads. In these cases, variations in the parameter values were not allowed to increase the number of trucks in the virtual fleet. Often, a single standard value was chosen for the parameter.

Overall, the fleet includes 9 types of tractors, 18 types of trailers, and 6 loading schemes. Each vehicle was given an appropriate set of standard truck tires, but a small subset of the vehicles was fitted with wide-based single tires.

## TRACTORS

Nine tractors were examined in this simulation study. In some cases, direct measurements (done prior to this study) were made of all of the parameters needed to describe a given tractor. Other sample tractors were "built" by combining parameter measurements of several common tractors and estimates of parameter values from past experience. Tables C.1 and C.2 list the essential mix of properties used to define the tractors. These tables do not provide all of the parameters needed to describe the tractors to the simulation models. Rather, they describe the parameters needed to distinguish the tractors in the baseline set from each other. Other parameters are discussed below. In particular, multiple cases of suspension damping and tire mix were also included in the simulation study.

**Table C.1. Tractor Suspensions.**

| Tractor | Steer Axle Suspension | Drive Axle Suspension | | Unsprung Wt. (kN) | |
|---|---|---|---|---|---|
| | | Style | Spring | Steer | Drive |
| 1 | Taper Leaf (2) | Trailing Arm (1LO) | Air | 5.34 | 10.23 |
| 2 | Taper Leaf (2) | Trailing Arm (1LU) | Air | 5.34 | 10.23 |
| 3 | Taper Leaf (2) | Trailing Arm (2LU) | Air | 5.34 | 10.23 |
| 4 | Taper Leaf (2) | Trailing Arm (2LU) | Air | 5.34 | 10.23 |
| 5 | Taper Leaf (2) | Trailing Arm (2LU) | Air | 5.34 | 10.23 |
| 6 | Taper Leaf (3) | 4-Spring | Taper Leaf (3) | 5.93 | 11.01 |
| 7 | Taper Leaf (3) | 4-Spring | Taper Leaf (1) | 5.93 | 10.81 |
| 8 | 2-Stage (6, 5) | 4-Spring | Flat Leaf (11) | 6.56 | 11.56 |
| 9 | Flat Leaf (9) | Walking Beam | Flat Leaf (9) | 5.34 | 10.90 |

**Table C.2. Tractor Wheelbase and Weight Distribution.**

| Tractor | Wheelbase (m) | Weight (kN) | Sprung Mass C.G. aft of Steer Axle (m) | Sprung Mass Pitch Moment of Inertia (kg-m$^2$) | Tandem Spread (m) |
|---|---|---|---|---|---|
| 1 | 3.91 | 63.70 | 0.91 | 7,462 | 1.30 |
| 2 | 5.64 | 61.65 | 1.12 | 12,748 | 1.30 |
| 3 | 4.57 | 62.76 | 1.04 | 9,937 | 1.30 |
| 4 | 4.83 | 76.48 | 1.19 | 14,805 | 1.30 |
| 5 | 4.19 | 55.61 | 1.09 | 7,614 | 1.30 |
| 6 | 4.80 | 86.38 | 1.24 | 18,657 | 1.30 |
| 7 | 4.70 | 67.25 | 1.60 | 14,066 | 1.30 |
| 8 | 5.69 | 80.96 | 1.55 | 13,633 | 1.30 |
| 9 | 4.06 | 62.36 | 0.79 | 6,458 | 1.37 |

### Wheelbase

Tractor wheelbase is a relatively easy value to measure and estimate. When a specific model of vehicle was represented, the proper value was used. In other cases, a typical value was entered. (*1*) The line-up of tractors was also designed to span a broad range. In practice, the range from 3.66 to 6.10 m (144 to 240 inches) covers the vast majority of three-axle tractors.

### Weight Distribution

Tractor weight, longitudinal center of mass, and pitch moment of inertia values were direct measurements or estimates from past experience. (*2-4*) In some cases, a value of pitch moment of inertia was estimated using a scaling equation that considers tractor weight, wheelbase, and body type. (*2, 5*) The sprung mass center of gravity location is not an input parameter to the model, but it is needed to calculate the static axle loads.

## Suspensions

All of the suspensions assigned to these tractors were represented by parameters measured on real vehicles in the UMTRI Suspension Parameter Measurement Facility. (*6*) They were chosen from a database of over 150 heavy truck suspensions that were tested at UMTRI since 1984. Few of these data are published. (*4, 7, 8*) The suspensions listed in table C.1 comprise the set that was considered the most representative of the U.S. fleet. The suspensions are identified by style and spring type. This method of suspension classification has been used previously for describing characteristics that affect truck handling. (*8*)

### Steer Axle Suspension

Taper leaf springs are by far the most common type of steer axle suspension on three-axle tractors. (*1*) The stiffness and friction properties of taper leaf suspensions that appear on these vehicles are not very diverse. Nevertheless, each tractor was given a unique steer axle suspension. Flat leaf springs are more common on severe-service trucks, but they do also appear on highway tractors. One rather rigidly suspended tractor was given a flat leaf suspension on its steer axle.

Unless a direct measurement of unsprung weight was available, steer axle suspensions were assigned a value of 5.34 kN (1200 lbs).

### Drive Axle Suspension

Five of the nine drive axles are air suspended. Air suspensions make up a wide majority of new drive axle suspensions sold in North America. (*9*) Although the proportion of air suspensions among new suspension sales is greater than five of nine, leaf sprung suspensions are still well represented in the truck population, because truck equipment replacement is relatively slow. As such, some common four-spring leaf suspensions were included. A single walking-beam suspension was also included among the baseline set of tractors. This suspension is the least prevalent of the group. (*10*) As such, it is combined with smallest number of trailer and loading options.

Note that air suspension force-deflection behavior changes with nominal suspension loading. (*5*) Therefore, a separate set of suspension properties was entered for each nominal load condition. In such cases where direct measurements of air suspension properties were not available for the appropriate nominal loading, measured properties from the nearest load condition were used.

All trailing arm drive axle air suspensions were assigned a value of 10.23 kN (2300 lbs) for unsprung weight. This value is based on several measured weights. All leaf spring suspensions were assigned the proper measured value. Very few of these values were published previously. (*2, 4, 11*)

Values of tandem spread were fixed at 1.30 m (51 inches) for all drive axle suspensions, except the walking-beam type, which had a tandem spread of 1.37 m (54 inches).

## TRAILERS

Sixteen trailers were examined in this simulation study. In a few cases, direct measurements (done prior to this study) were made of all of the parameters needed to describe a given trailer. However, most of the trailers were "built" by combining parameter measurements of several common trailers and estimates of parameter values from past experience. The trailers cover various combinations of seven tandem axle suspension types with four basic trailer types.

### Trailer Suspension

Table C.3 lists the trailer suspensions covered in this study. All of the suspensions assigned to these trailers were represented by parameters measured on real vehicles in the UMTRI Suspension Parameter Measurement Facility. (*6*) They were chosen from a database of over 150 heavy truck suspensions that were tested at UMTRI since 1984. The suspensions listed in table C.3 comprise the set that was considered the most representative of the U.S. fleet. The suspensions are identified by style and spring type. This method of suspension classification has been used previously for describing characteristics that affect truck handling. (*8*)

Four of the seven trailer suspensions have air springs; the other three have leaf springs. Air suspensions make up a wide majority of new trailer axle suspensions sold in North America. (*9*) Although the proportion of air suspensions among new suspension sales is greater than four of seven, leaf sprung suspensions are still well represented in the truck population, because truck equipment replacement is relatively slow. As such, some common four-spring leaf suspensions were included.

Note that air suspension force-deflection behavior changes with nominal suspension loading. (*5*) Therefore, a separate set of suspension properties was entered for each nominal load condition. In such cases where direct measurements air suspension properties were not available for the appropriate nominal loading, measured properties from the nearest load condition were used.

All trailer axle suspensions were assigned a value that corresponds to a value measured from the same suspension type. All suspensions were given a tandem spread of 1.22 m (48 inches).

**Table C.3. Trailer Suspensions.**

| Suspension | Suspension Style | Spring Type | Unsprung Weight (kN) |
|---|---|---|---|
| 1 | Trailing Arm (WT) | Air | 6.67 |
| 2 | Trailing Arm (WU) | Air | 6.67 |
| 3 | Trailing Arm (1LO) | Air | 8.36 |
| 4 | Trailing Arm (1LO) | Air | 8.36 |
| 5 | 4-Spring | Taper Leaf (1) | 7.29 |
| 6 | 4-Spring | Taper Leaf (3) | 8.01 |
| 7 | 4-Spring | Flat Leaf | 8.54 |

### Trailer Type

Trailer size and body type only affect two parameters called for by the simulation models: (1) wheelbase and (2) loaded trailer sprung mass pitch moment of inertia. Subtle changes in pitch moment of inertia of the laden vehicle are characteristic of a given body length for the same total loading and wheelbase. These do not affect the pitch moment of inertia significantly, and small changes in pitch moment of inertia were found to have little affect on the statistical results in preliminary simulations. For this reason, only four very broad categories of trailer type were included in the simulations:

1. 14.63-meter (48-foot) trailers: This is the most common trailer length. (*10)* It is included in the simulations to cover several types of 14.63-meter (48-foot) trailers, such as a conventional van box, a flatbed, etc. This trailer size was included with all of the trailer suspension options.

2. 16.15-meter (53-foot) trailers: Several states currently allow 16.15-meter (53-foot) trailers. (*12*) These trailers are often used to carry freight with density so low that even a full trailer is under the legal weight limit. (*13, 14*) To avoid problems maneuvering these trailers, many states regulate their wheelbase to be no longer than 12.50 meters (41 feet). (*10, 12)* This value was chosen as the standard wheelbase for the study. Since this trailer size has only been allowed in recent years, it almost always appears with air suspensions. Therefore, it is only included in the simulations with air suspensions 1, 2, and 3.

3. 12.80-meter (42-foot) tanker: This is a common overall tanker length. The basic properties of this vehicle were derived from a common gasoline tanker. (*15*) The tanker is not as common as a 14.63-meter (48-foot) trailer. It is also not likely to have a very harsh suspension. Therefore, it is only fitted with suspensions 1, 2, 4, and 5.

4. 12.80-meter (42-foot) heavy trailers: This option represents trailers that carry very dense freight, such as dirt, stone, or dry industrial scrap materials. Dense freight of this type does not require a long trailer to reach the legal load limit. (*14*) It is not nearly as prevalent as the 14.63-meter (48-foot) trailer. This type of trailer also has no need for a soft suspension. It is only fitted with suspensions 6 and 7.

Table C.4 lists the four trailer sizes. The sprung mass distribution properties are also listed. The sprung mass pitch moment of inertia is listed because the total trailer pitch moment of inertia depends on the unsprung mass, and those values will change with suspension type. As described below, the laden trailer mass distribution depends heavily on the load.

**Table C.4. Unladen Trailer Size and Mass Distribution.**

| Trailer Type | Wheelbase (m) | Sprung Mass (kN) | Sprung Mass Pitch Moment of Inertia (kg-m$^2$) |
|---|---|---|---|
| 14.63-meter | 12.19 | 50.26 | 113,548 |
| 16.15-meter | 12.50 | 57.78 | 173,525 |
| 12.80-meter, Tanker | 10.06 | 33.80 | 73,829 |
| 12.80-meter, Heavy | 9.75 | 44.39 | 85,937 |

### Combinations

The options listed in tables C.3 and C.4 were combined to make up a total of sixteen trailers. These tables do not include all of the parameters needed to describe the trailers to the simulation models. Rather, they include the parameters needed to distinguish the trailers from each other. Other parametric variations on them are also considered, such as loading, tire mix, and suspension damping.

## TIRES

Although tires can be very diverse in their construction and dynamic properties, they are represented to the simulation models by only three basic properties: vertical stiffness, weight, and enveloping behavior.

### Weight

Tire weight is accounted for as a portion of the unsprung weight listed for each axle. Only three tire types were considered in this study: (1) 275/80R22.5, (2) 11R24.5, and (3) 425/65R22.5. The first two types correspond to the unsprung weight values listed in tables C.1 and C.3. Whenever the wide-based tire is used on a drive or trailer axle, the unsprung weight for that axle is decreased by 0.89 kN (200 lbs).

### Enveloping

Tire enveloping is modeled with a simple moving average filter. (*16*) For isolated disturbances near the scale, this may not be appropriate. The moving average is also not capable of allowing the tire to bridge over narrow, concave disturbances in a measured road profile. Nevertheless, it was used because most of the profile data that were available for the study were already processed in this manner.

### Stiffness

Tire stiffness depends on tire construction, load, and inflation pressure. Often, tires with the same designation operated at the same load and inflation pressure will vary somewhat in their stiffness properties. (*17*) Comparison of several published measurements of truck tire vertical stiffness, data provided by tire manufacturers, and measurements made on the UMTRI Flatbed Tire Testing Machine showed that this variation is typically on the order of 5 percent. (*18, 19*) Variation in tire stiffness with load was also found to be small enough to ignore. Thus, each tire type was assigned a standard stiffness value for rated load and inflation pressure, as shown in table C.5. The value listed for tire damping rate is a standard value intended to set the damping ratio at 2 percent of critical. (*16*)

At a given nominal loading, tire stiffness is also affected by inflation pressure. Several roadside surveys of truck tire inflation pressure, summarized by Johansen (*20*), were conducted in the U.S. from 1984 to 1990. Most of these surveys reported the number of tires, the mean inflation pressure, the high and low inflation pressure values, and separate statistics for bias and radial ply tires. Unfortunately, the custom for reporting survey results

did not include a plot of the distribution or a listing of the standard deviation. The reader is therefore left to guess at the typical level of variation. One exception was a study in Texas (*21*), which reported average values for radial tires on the axles of 3S2 vehicles ranging from 668-689 kPa (97-100 psi), and standard deviations from 90-103 kPa (13-15 psi). In the practical operating range, tire stiffness is roughly proportional to the square root of inflation pressure. (*18, 19*) Thus, the standard deviations reported in Texas correspond to less than 8 percent variation in tire stiffness. (In turn, this very roughly translates to a 4 percent variation in axle hop natural frequency.) Preliminary simulations on a limited number of profiles showed little affect on the results of a variation in tire stiffness of 10 percent. Thus, tire inflation pressure variations were not covered in the simulation study.

**Table C.5. Standard Tire Stiffness Values**

| Tire | Vertical Stiffness (N/mm) | Damping Rate (N-s/mm) |
|---|---|---|
| 275/80R22.5 | 805.5 | 1.05 |
| 11R24.5 | 823.1 | 1.05 |
| 465/65R22.5 | 1,164.5 | 1.26 |

### Tire Mix

Each tractor was assigned a set of tires based on the standard tires commonly delivered with that make and model. All air-sprung trailers were given 275/80R22.5 tires and all leaf sprung trailers were given 11R24.5 tires. Naturally, dual tires appear on the tractor drive and trailer axles.

Wide-based single tires are not nearly as common as standard dual tires. They are used to decrease tare weight by some fleet owners. They also offer extra lateral separation, which allows tanker bodies to ride lower. One leaf-sprung tanker trailer and one air-sprung 14.63-meter (48-foot) trailer with wide-based single tires were added to the line-up. Any vehicle with wide-based single tires on the trailer was also given wide-based tires on the drive axle.

## LOADING

Six common loading schemes were chosen for this simulation study. They are discussed here. Each section heading provides a nickname for the loading case. Each loading implies an appropriate value of payload weight and sprung mass pitch moment of inertia for a given combination of tractor and trailer. Table C.6 lists the range of these values (for all tractors) for each trailer and loading scheme.

### Loaded to the Legal Limit (Limit)

The most common gross vehicle weight (GVW) limit for 3S2 vehicle is 355.84 kN (80,000 lbs). (*10, 12*) The corresponding axle weight limits are 53.38 kN (12,000 lbs) for the steer axle and 151.23 kN (34,000 lbs) for the drive and trailer tandem axles. In this loading scheme, cargo was added to each sample vehicle to bring the total vehicle weight and individual axle loads to the legal limit.

Each tractor and trailer combination had a known tare weight. (See tables C.3 through C.5.) To achieve the desired total vehicle weight, the needed cargo weight was added to the trailer sprung mass. The hitch location and cargo center of gravity were adjusted to achieve the desired individual axle loads. In the calculation of trailer sprung mass pitch moment of inertia it was assumed that the load was distributed evenly along the trailer. Since each vehicle required a different payload weight and position, a slightly different value of trailer sprung mass pitch moment of inertia was needed for each tractor and trailer combination. Table C.6 provides the range for each trailer size.

### Loaded to the Legal Limit with Concentrated Load (Concentrated)

This loading scheme is the same as the "legal" case, with the exception that the load is concentrated over the axles. This represents very dense freight, such as coils of sheet metal, stacks of bricks, etc. These products are heavy enough to load a 3S2 vehicle to the legal limit, but require very little volume. The most common practice for loading these products is to place them on a flatbed trailer, and place half the cargo over the drive axles and half the cargo over the trailer axles. Compared to the evenly-distributed loading described above, this loading scheme amounts to a parametric variation on sprung mass pitch moment of inertia. In the simulation models, the calculation of pitch moment of inertia are done with the load concentrated at locations that are separated by 95 percent of the wheelbase.

### Empty

Empty vehicles make up a significant portion of the trucks measured at WIM scales. (*22, 23*) In this loading scheme, each tractor and trailer were simply combined with no payload. The hitch location needed to achieve the proper axle loading for the legal-limit case was maintained for the empty case. This was thought to be appropriate, because drivers are not likely to change the hitch location after a vehicle is unloaded.

### Overloaded

Measurements of overloaded truck weights are difficult to obtain. Drivers who know they are overloaded usually avoid truck weigh scales. Nevertheless, anecdotal evidence exists that vehicles do exceed legal weight limits, occasionally by a broad margin. A GVW of 422.56 kN (95,000 lbs) was chosen as the standard value for overloaded vehicles in this study because several types of cargo exist that could achieve this overload level in a conventional 14.63-meter (48-foot) box-type trailer. (*14*) The overload was achieved by adding 66.72 kN (15,000 lbs) to the cargo in the legal limit case, but placing its center of gravity in the same location and distributing it the same way. (This is equivalent to increasing the density of the cargo by the amount needed to achieve the desired total weight.) This resulted in a variety of individual axle loads ranging from 54.62 kN (12,280 lbs) to 60.36 kN (13,570 lbs) for steer axles and 177.96 kN (40,010 lbs) to 186.10 kN (41,840 lbs) for tandem axles.

### Intermediate Uniform Loading (Intermediate)

In-situ truck weight measurement in the U.S. often shows a bi-modal distribution of 3S2 GVW. (*22-24*) A bulge often appears near 142.34 kN (32,000 lbs) that represents empty vehicles, and a second bulge appears from 302.46 kN (68,000 lbs) to 338.05 kN (76,000 lbs) that represents the most common cases of loaded vehicles. An intermediate loading case of 320.26 kN (72,000 lbs) was chosen for this study.

This loading was achieved by removing 35.58 kN (8,000 lbs) of cargo from the legal limit case, but placing its center of gravity in the same location and distributing the load the same way. (This is equivalent to decreasing the density of the cargo by the amount needed to achieve the desired total weight.) This resulted in a variety of individual axle loads ranging from 49.64 kN (11,160 lbs) to 52.71 kN (11,850 lbs) for steer axles and 132.64 kN (29,820 lbs) to 137.00 kN (30,800 lbs) for tandem axles.

**Table C.6. Laden Trailer Mass Distribution.**

| Loading Scheme | Trailer Type | Wheelbase (m) | Payload Weight (kN) | Sprung Mass Pitch Moment of Inertia (kg-m$^2$) |
|---|---|---|---|---|
| Legal | 14.63-m | 12.19 | 221.2–257.5 | 469,209–531,381 |
| Legal | 16.15-m | 12.50 | 217.7–251.8 | 587,052–665,018 |
| Legal | 12.80-m, Tanker | 10.06 | 232.3–267.0 | 346,552–390,273 |
| Legal | 12.80-m, Heavy | 9.75 | 225.5–257.3 | 346,065–390,563 |
| Concentrated | 14.63-m | 12.19 | 221.2–257.5 | 890,889–1,020,918 |
| Concentrated | 12.80-m, Tanker | 10.06 | 232.3–267.0 | 633,391–718,810 |
| Empty | 14.63-m | 12.19 | 0 | 113,548 |
| Empty | 16.15-m | 12.50 | 0 | 173,525 |
| Empty | 12.80-m, Tanker | 10.06 | 0 | 73,829 |
| Empty | 12.80-m, Heavy | 9.75 | 0 | 85,937 |
| Overloaded | 14.63-m | 12.19 | 287.9–324.2 | 571,344–633,895 |
| Overloaded | 12.80-m, Heavy | 9.75 | 292.2–324.0 | 417,687–462,455 |
| Intermediate | 14.63-m | 12.19 | 185.6–221.9 | 414,522–476,433 |
| Intermediate | 16.15-m | 12.50 | 182.1–216.3 | 524,497–601,818 |
| Intermediate | 12.80-m, Tanker | 10.06 | 196.7–231.4 | 307,155–350,771 |
| Forward | 14.63-m | 12.19 | 110.6–128.7 | 158,123–163,717 |
| Forward | 16.15-m | 12.50 | 108.8–125.9 | 220,358–228,090 |
| Forward | 12.80-m, Tanker | 10.06 | 116.1–133.5 | 105,640–110,606 |

### Forward-Biased Loading (Forward)

Many trucks make several stops to unload and remove a portion of the cargo at each stop. The cargo is usually unloaded from the rear of the trailer. Other vehicles that travel with a partially-empty trailer place the load as far forward as possible. A forward-biased loading scheme was added to cover this case.

This loading was achieved by removing the rear half of the cargo from the legal limit case. This shifted the cargo center of mass forward significantly, and decreased the cargo pitch moment of inertia. In this loading arrangement, the steer axle loads range from 45.50 kN (10,230 lbs) to 52.26 kN (11,750 lbs). The drive axle loads range from 115.38 kN

(25,940 lbs) to 122.72 kN (27,590 lbs), and the trailer axle loads range from 58.89 kN (13,240 lbs) to 74.28 kN (16,700 lbs).

## COMBINATIONS

The nine tractors, eighteen trailers (including the two trailers with wide-based tires), and six loading cases were all combined to make up a virtual truck "fleet". However, not every possible combination was included, because certain combinations are not likely to appear in practice. (That is why some entries are missing from table C.6.) For example, tankers are rarely towed by tractors with a walking-beam drive axle suspension, because walking-beam suspensions are harsh.

Table C.7 shows the tractor and trailer combinations that were included, and the number of loading cases covered by each combination. Any blank cell represents a combination that was not included at all.

**Table C.7. Tractor and Trailer Combinations.**

| Trailer | | | | Tractor Number | | | | | | | | |
|---|---|---|---|---|---|---|---|---|---|---|---|---|
| Num. | Type | Susp. | Tires† | 1 | 2 | 3 | 4 | 5 | 6 | 7 | 8 | 9 |
| 1 | 14.63-m | 1 | C | 6 | 6 | 6 | 6 | 5 | 6 | 6 | 3 | 4 |
| 2 | 14.63-m | 2 | C | 6 | 6 | 6 | 6 | 5 | 6 | 6 | 3 | 4 |
| 3 | 14.63-m | 2 | W | 4 | 4 | 4 | 4 | 4 | 4 | 4 | 2 | 3 |
| 4 | 14.63-m | 3 | C | 6 | 6 | 6 | 6 | 5 | 6 | 6 | 3 | 4 |
| 5 | 14.63-m | 4 | C | 6 | 6 | 6 | 6 | 5 | 6 | 6 | 3 | 4 |
| 6 | 14.63-m | 5 | C | 6 | 6 | 6 | 6 | 5 | 6 | 6 | 3 | 4 |
| 7 | 14.63-m | 6 | C | 6 | 6 | 6 | 6 | 5 | 6 | 6 | 3 | 4 |
| 8 | 14.63-m | 7 | C | 6 | 6 | 6 | 6 | 5 | 6 | 6 | 3 | 4 |
| 9 | 16.15-m | 1 | C | 4 | 4 | 4 | 3 | 4 | 4 | 3 | 1 | |
| 10 | 16.15-m | 2 | C | 4 | 4 | 4 | 3 | 4 | 4 | 3 | 1 | |
| 11 | 16.15-m | 3 | C | 4 | 4 | 4 | 3 | 4 | 4 | 3 | 1 | |
| 12 | 12.80-m, Tanker | 1 | C | 4 | 4 | 4 | 4 | 3 | 4 | 4 | | |
| 13 | 12.80-m, Tanker | 2 | C | 3 | 3 | 3 | 3 | 3 | 3 | 3 | | |
| 14 | 12.80-m, Tanker | 4 | C | 4 | 4 | 4 | 4 | 3 | 4 | 4 | | |
| 15 | 12.80-m, Tanker | 4 | W | 3 | 3 | 3 | 3 | 3 | 3 | 3 | | |
| 16 | 12.80-m, Tanker | 5 | C | 4 | 4 | 4 | 4 | 4 | 4 | 4 | | |
| 17 | 12.80-m, Heavy | 6 | C | 3 | | 3 | 3 | 3 | 3 | 3 | | 3 |
| 18 | 12.80-m, Heavy | 7 | C | 3 | | 3 | 3 | 3 | 3 | 3 | | 3 |

† C - Conventional W - Wide-Based

Several rules for combining tractors, trailers, and loading schemes were used to eliminate unusual combinations:

- Tankers (#12-16) were not carried by the tractor with a walking-beam drive axle suspension (#9) or the other harsh leaf-sprung suspension (#8).
- No tankers were operated with an overload.
- Only one tanker (#16) was operated with a forward-biased load.
- Only two of the tankers (#12, #14) were operated with concentrated loading.

- No 12.80-meter (42-foot) heavy-duty trailers (#17, #18) were operated at the intermediate loading, with forward loading, or with concentrated loading.
- No 12.80-meter (42-foot) heavy-duty trailers (#17, #18) were carried by long-wheelbase (sleeper) tractors (#2, #8)
- No 16.15-meter (53-foot) trailers (#9-11) were towed by the tractor with a walking-beam drive axle (#9).
- No 16.15-meter (53-foot) (#9-11) trailers were overloaded or operated with concentrated loads.
- No 16.15-meter (53-foot) trailers were run empty with tractors #4, #7, and #8.
- Only the most common tractors (#1-7) were operated with a forward-biased load.
- Only two-thirds of the tractors towed trailers with concentrated loading, eliminating #5, #8, and #9.
- The most unusual tractor (#8) was not operated with intermediate loading.
- Trailers with wide-based single tires (#3, #15) were not operated with an overload or concentrated loading.

Tables C.8 through C.13 show the coverage of tractor and trailer combinations for each loading case. There are 616 vehicle and loading combinations overall.

- The vehicles are distributed by loading case as follows: 136 are empty, 84 have forward-biased loading, 120 have intermediate loading, 145 are legally loaded, 54 have concentrated loading, and 77 are overloaded.
- The vehicles are distributed by trailer size as follows: 369 have 14.63-meter (48-foot) trailers, 81 have 16.15-meter (53-foot) trailers, 124 have tanker trailers, and 42 have heavy freight trailers.
- The vehicles are distributed by tractor drive axle suspension type as follows: 392 have air suspensions, 187 have four-spring suspensions, and 37 have a walking-beam suspension.
- Wide-based single tires appear on 54 of the vehicles.

**Table C.8. Empty vehicle combinations.**

| Trailer | | | | Tractor Number | | | | | | | | |
|---|---|---|---|---|---|---|---|---|---|---|---|---|
| Num. | Type | Susp. | Tires | 1 | 2 | 3 | 4 | 5 | 6 | 7 | 8 | 9 |
| 1 | 14.63-m | 1 | C | ■ | ■ | ■ | ■ | ■ | ■ | ■ | ■ | ■ |
| 2 | 14.63-m | 2 | C | ■ | ■ | ■ | ■ | ■ | ■ | ■ | ■ | ■ |
| 3 | 14.63-m | 2 | W | ■ | ■ | ■ | ■ | ■ | ■ | ■ | ■ | ■ |
| 4 | 14.63-m | 3 | C | ■ | ■ | ■ | ■ | ■ | ■ | ■ | ■ | ■ |
| 5 | 14.63-m | 4 | C | ■ | ■ | ■ | ■ | ■ | ■ | ■ | ■ | ■ |
| 6 | 14.63-m | 5 | C | ■ | ■ | ■ | ■ | ■ | ■ | ■ | ■ | ■ |
| 7 | 14.63-m | 6 | C | ■ | ■ | ■ | ■ | ■ | ■ | ■ | ■ | ■ |
| 8 | 14.63-m | 7 | C | ■ | ■ | ■ | ■ | ■ | ■ | ■ | ■ | ■ |
| 9 | 16.15-m | 1 | C | ■ | ■ | ■ | | ■ | ■ | | | |
| 10 | 16.15-m | 2 | C | ■ | ■ | ■ | | ■ | ■ | | | |
| 11 | 16.15-m | 3 | C | ■ | ■ | ■ | | ■ | ■ | | | |
| 12 | 12.80-m, Tanker | 1 | C | ■ | ■ | ■ | ■ | ■ | ■ | ■ | | |
| 13 | 12.80-m, Tanker | 2 | C | ■ | ■ | ■ | ■ | ■ | ■ | ■ | | |
| 14 | 12.80-m, Tanker | 4 | C | ■ | ■ | ■ | ■ | ■ | ■ | ■ | | |
| 15 | 12.80-m, Tanker | 4 | W | ■ | ■ | ■ | ■ | ■ | ■ | ■ | | |
| 16 | 12.80-m, Tanker | 5 | C | ■ | ■ | ■ | ■ | ■ | ■ | ■ | | |
| 17 | 12.80-m, Heavy | 6 | C | ■ | | ■ | ■ | ■ | ■ | ■ | | ■ |
| 18 | 12.80-m, Heavy | 7 | C | ■ | | ■ | ■ | ■ | ■ | ■ | | ■ |

**Table C.9. Vehicle combinations with forward-biased loading.**

| Trailer | | | | Tractor Number | | | | | | | | |
|---|---|---|---|---|---|---|---|---|---|---|---|---|
| Num. | Type | Susp. | Tires | 1 | 2 | 3 | 4 | 5 | 6 | 7 | 8 | 9 |
| 1 | 14.63-m | 1 | C | ■ | ■ | ■ | ■ | ■ | ■ | ■ | | |
| 2 | 14.63-m | 2 | C | ■ | ■ | ■ | ■ | ■ | ■ | ■ | | |
| 3 | 14.63-m | 2 | W | ■ | ■ | ■ | ■ | ■ | ■ | ■ | | |
| 4 | 14.63-m | 3 | C | ■ | ■ | ■ | ■ | ■ | ■ | ■ | | |
| 5 | 14.63-m | 4 | C | ■ | ■ | ■ | ■ | ■ | ■ | ■ | | |
| 6 | 14.63-m | 5 | C | ■ | ■ | ■ | ■ | ■ | ■ | ■ | | |
| 7 | 14.63-m | 6 | C | ■ | ■ | ■ | ■ | ■ | ■ | ■ | | |
| 8 | 14.63-m | 7 | C | ■ | ■ | ■ | ■ | ■ | ■ | ■ | | |
| 9 | 16.15-m | 1 | C | ■ | ■ | ■ | ■ | ■ | ■ | ■ | | |
| 10 | 16.15-m | 2 | C | ■ | ■ | ■ | ■ | ■ | ■ | ■ | | |
| 11 | 16.15-m | 3 | C | ■ | ■ | ■ | ■ | ■ | ■ | ■ | | |
| 12 | 12.80-m, Tanker | 1 | C | | | | | | | | | |
| 13 | 12.80-m, Tanker | 2 | C | | | | | | | | | |
| 14 | 12.80-m, Tanker | 4 | C | | | | | | | | | |
| 15 | 12.80-m, Tanker | 4 | W | | | | | | | | | |
| 16 | 12.80-m, Tanker | 5 | C | ■ | ■ | ■ | ■ | ■ | ■ | ■ | | |
| 17 | 12.80-m, Heavy | 6 | C | | | | | | | | | |
| 18 | 12.80-m, Heavy | 7 | C | | | | | | | | | |

**Table C.10. Vehicle combinations with intermediate loading.**

| Trailer | | | | Tractor Number | | | | | | | | |
|---|---|---|---|---|---|---|---|---|---|---|---|---|
| Num. | Type | Susp. | Tires | 1 | 2 | 3 | 4 | 5 | 6 | 7 | 8 | 9 |
| 1 | 14.63-m | 1 | C | | | | | | | | | |
| 2 | 14.63-m | 2 | C | | | | | | | | | |
| 3 | 14.63-m | 2 | W | | | | | | | | | |
| 4 | 14.63-m | 3 | C | | | | | | | | | |
| 5 | 14.63-m | 4 | C | | | | | | | | | |
| 6 | 14.63-m | 5 | C | | | | | | | | | |
| 7 | 14.63-m | 6 | C | | | | | | | | | |
| 8 | 14.63-m | 7 | C | | | | | | | | | |
| 9 | 16.15-m | 1 | C | | | | | | | | | |
| 10 | 16.15-m | 2 | C | | | | | | | | | |
| 11 | 16.15-m | 3 | C | | | | | | | | | |
| 12 | 12.80-m, Tanker | 1 | C | | | | | | | | | |
| 13 | 12.80-m, Tanker | 2 | C | | | | | | | | | |
| 14 | 12.80-m, Tanker | 4 | C | | | | | | | | | |
| 15 | 12.80-m, Tanker | 4 | W | | | | | | | | | |
| 16 | 12.80-m, Tanker | 5 | C | | | | | | | | | |
| 17 | 12.80-m, Heavy | 6 | C | | | | | | | | | |
| 18 | 12.80-m, Heavy | 7 | C | | | | | | | | | |

**Table C.11. Vehicle combinations loaded to the legal limit.**

| Trailer | | | | Tractor Number | | | | | | | | |
|---|---|---|---|---|---|---|---|---|---|---|---|---|
| Num. | Type | Susp. | Tires | 1 | 2 | 3 | 4 | 5 | 6 | 7 | 8 | 9 |
| 1 | 14.63-m | 1 | C | | | | | | | | | |
| 2 | 14.63-m | 2 | C | | | | | | | | | |
| 3 | 14.63-m | 2 | W | | | | | | | | | |
| 4 | 14.63-m | 3 | C | | | | | | | | | |
| 5 | 14.63-m | 4 | C | | | | | | | | | |
| 6 | 14.63-m | 5 | C | | | | | | | | | |
| 7 | 14.63-m | 6 | C | | | | | | | | | |
| 8 | 14.63-m | 7 | C | | | | | | | | | |
| 9 | 16.15-m | 1 | C | | | | | | | | | |
| 10 | 16.15-m | 2 | C | | | | | | | | | |
| 11 | 16.15-m | 3 | C | | | | | | | | | |
| 12 | 12.80-m, Tanker | 1 | C | | | | | | | | | |
| 13 | 12.80-m, Tanker | 2 | C | | | | | | | | | |
| 14 | 12.80-m, Tanker | 4 | C | | | | | | | | | |
| 15 | 12.80-m, Tanker | 4 | W | | | | | | | | | |
| 16 | 12.80-m, Tanker | 5 | C | | | | | | | | | |
| 17 | 12.80-m, Heavy | 6 | C | | | | | | | | | |
| 18 | 12.80-m, Heavy | 7 | C | | | | | | | | | |

**Table C.12. Vehicle combinations with concentrated loading.**

| Trailer | | | | Tractor Number | | | | | | | | |
|---|---|---|---|---|---|---|---|---|---|---|---|---|
| Num. | Type | Susp. | Tires | 1 | 2 | 3 | 4 | 5 | 6 | 7 | 8 | 9 |
| 1 | 14.63-m | 1 | C | ■ | ■ | ■ | ■ | | ■ | ■ | | |
| 2 | 14.63-m | 2 | C | ■ | ■ | ■ | ■ | | ■ | ■ | | |
| 3 | 14.63-m | 2 | W | | | | | | | | | |
| 4 | 14.63-m | 3 | C | ■ | ■ | ■ | ■ | | ■ | ■ | | |
| 5 | 14.63-m | 4 | C | ■ | ■ | ■ | ■ | | ■ | ■ | | |
| 6 | 14.63-m | 5 | C | ■ | ■ | ■ | ■ | | ■ | ■ | | |
| 7 | 14.63-m | 6 | C | ■ | ■ | ■ | ■ | | ■ | ■ | | |
| 8 | 14.63-m | 7 | C | ■ | ■ | ■ | ■ | | ■ | ■ | | |
| 9 | 16.15-m | 1 | C | | | | | | | | | |
| 10 | 16.15-m | 2 | C | | | | | | | | | |
| 11 | 16.15-m | 3 | C | | | | | | | | | |
| 12 | 12.80-m, Tanker | 1 | C | ■ | ■ | ■ | ■ | | ■ | ■ | | |
| 13 | 12.80-m, Tanker | 2 | C | | | | | | | | | |
| 14 | 12.80-m, Tanker | 4 | C | ■ | ■ | ■ | ■ | | ■ | ■ | | |
| 15 | 12.80-m, Tanker | 4 | W | | | | | | | | | |
| 16 | 12.80-m, Tanker | 5 | C | | | | | | | | | |
| 17 | 12.80-m, Heavy | 6 | C | | | | | | | | | |
| 18 | 12.80-m, Heavy | 7 | C | | | | | | | | | |

**Table C.12. Overloaded vehicle combinations.**

| Trailer | | | | Tractor Number | | | | | | | | |
|---|---|---|---|---|---|---|---|---|---|---|---|---|
| Num. | Type | Susp. | Tires | 1 | 2 | 3 | 4 | 5 | 6 | 7 | 8 | 9 |
| 1 | 14.63-m | 1 | C | ■ | ■ | ■ | ■ | ■ | ■ | ■ | ■ | ■ |
| 2 | 14.63-m | 2 | C | ■ | ■ | ■ | ■ | ■ | ■ | ■ | ■ | ■ |
| 3 | 14.63-m | 2 | W | | | | | | | | | |
| 4 | 14.63-m | 3 | C | ■ | ■ | ■ | ■ | ■ | ■ | ■ | ■ | ■ |
| 5 | 14.63-m | 4 | C | ■ | ■ | ■ | ■ | ■ | ■ | ■ | ■ | ■ |
| 6 | 14.63-m | 5 | C | ■ | ■ | ■ | ■ | ■ | ■ | ■ | ■ | ■ |
| 7 | 14.63-m | 6 | C | ■ | ■ | ■ | ■ | ■ | ■ | ■ | ■ | ■ |
| 8 | 14.63-m | 7 | C | ■ | ■ | ■ | ■ | ■ | ■ | ■ | ■ | ■ |
| 9 | 16.15-m | 1 | C | | | | | | | | | |
| 10 | 16.15-m | 2 | C | | | | | | | | | |
| 11 | 16.15-m | 3 | C | | | | | | | | | |
| 12 | 12.80-m, Tanker | 1 | C | | | | | | | | | |
| 13 | 12.80-m, Tanker | 2 | C | | | | | | | | | |
| 14 | 12.80-m, Tanker | 4 | C | | | | | | | | | |
| 15 | 12.80-m, Tanker | 4 | W | | | | | | | | | |
| 16 | 12.80-m, Tanker | 5 | C | | | | | | | | | |
| 17 | 12.80-m, Heavy | 6 | C | ■ | | ■ | ■ | ■ | ■ | ■ | | ■ |
| 18 | 12.80-m, Heavy | 7 | C | ■ | | ■ | ■ | ■ | ■ | ■ | | ■ |

## SUSPENSION DAMPING

Suspension shock absorber damping was found in preliminary vehicle simulations to have a significant impact on the dynamic loading experienced at the weight scales.

Unfortunately, little data on measured truck shock absorber force-velocity appear in the literature. The shock absorber damping coefficient values that were used represent the experience of the engineers at UMTRI. The relative contribution of the shock absorbers to overall suspension damping depends on the level of friction present in the suspension force-deflection characteristic. In general, the drive and trailer axle suspension exhibited damping ratio values of 15-20 percent under the crude characterization provided by simulating truck vibration after passing over a large step.

Since shock absorber damping was found to be so important to the results, all vehicles were simulated with two damping cases. The first case, with new shock absorbers, is covered by the 15-20 percent overall damping ratio. The second case is worn shock absorbers. This case is approximated by reducing the trailer axle damping coefficient values to 25 percent of their original values and the tractor shock absorber damping coefficient values to 50 percent of the original values. The tractor is not allowed to lose as much of its damping power as the trailer, because the driver is expected to complain if the damping gets too low.

This parametric variation serves to double the number of vehicles to 1,232. (It is reasonable to expect that vehicle units would not always wear out simultaneously, but the number of vehicles in the simulation study could not be allowed to grow too large.)

## SPEED

All vehicles were simulated at three speeds: 72.4, 88.5, and 104.6 kph (45, 55, and 65 mph).

## REFERENCES


1. "2001 Diesel Truck Index." Truck Index, Inc., Santa Ana, CA (2001) 300 p.
2. Fancher, P. S., et. al., "A Factbook of the Mechanical Properties of the Components for Single Unit and Articulated Heavy Trucks." National Highway Traffic Safety Administration Report DOT HS 807 125 (1986) 190 p.
3. Winkler, C. B., "Inertial Properties of Commercial Vehicles." University of Michigan Transportation Research Institute Report UMTRI-83-17, Volume 2 (1983) 25 p.
4. Winkler, C. B, et. al., "Parameter Measurements of a Highway Tractor Semitrailer." National Highway Traffic Safety Administration Vehicle Research and Test Center Report (1995) 159 p.
5. Segel, L., et. al., "Mechanics of Heavy-Duty Trucks and Truck Combinations." Engineering Summer Conferences, University of Michigan College of Engineering (2002).
6. Winkler, C. B. and Hagan, M., "A Test Facility for Measurement of Heavy Vehicle Suspension Parameters." Transactions of the Society of Automotive Engineers, Vol. 89, Paper No. 800906 (1980) 29 p.

7. Ervin, R., et. al., "Two Active Systems for Enhancing Dynamic Stability in Heavy Truck Operations." University of Michigan Transportation Research Institute Report UMTRI-98-39 (1998) 216 p.

8. Winkler, C. B., et. al., "Roll Stability Performance of Heavy Vehicle Suspensions." Transactions of the Society of Automotive Engineers, Vol. 101, Paper No. 922426 (1992) 9 p.

9. Hajek, J. J. and Selezneva, O. I., "Estimating Cumulative Traffic Loads, Final Report for Phase I." Federal Highway Administration Publication No. FHWA-RD-00-054 (2000) 202 p.

10. Fancher, P. S. and Gillespie, T. D., "Truck Operating Characteristics." National Cooperative Highway Research Program Synthesis 241 (1997) 66 p.

11. Karamihas, S. M. and Gillespie, T. D., "Characterizing Trucks for Dynamic Load Prediction." Heavy Vehicle systems, Vol. 1, No. 1 (1993) pp. 3-19.

12. "2002 Size & Weight Update." A Supplement to Transport Topics Magazine.

13. Ervin, R. D., "Influence of Size and Weight Variables on the Roll Stability of Heavy Duty Trucks." Society of Automotive Engineers Paper No. 831163 (1983).

14. Winkler, C. B., et. al., "Heavy Vehicle Size and Weight – Test Procedures for Minimum Safety Performance Standards." National Highway Traffic Safety Administration Report, DOT HS 807 855 (1992) 118 p.

15. Winkler, C. B., et. al., "The Dynamics of Tank-Vehicle Rollover and the Implications for Rollover-Protection Devices." University of Michigan Transportation Research Institute Report UMTRI-98-53 (1998) 187 p.

16. Gillespie, T. D., et. al., "Effect of Heavy Vehicle Characteristics on Pavement Response and Performance." National Cooperative Highway Research Program Report 353 (1993) 126 p.

17. Pottinger, M. G., et. al. "Force and Moment Properties of a Small Sample of Tire Specifications: Drive, Steer, and Trailer with Evolution from New to Naturally Worn-out to Retreaded considered." Society of Automotive Report No. SAE 982748. (1998) 13 P.

18. Pezo, R. F., et. al., "Truck Tire Pavement Contact Pressure Distribution Characteristics for the Bias Goodyear 18-22.5, the Radial Michelin 275/80R/24.5, the Radial Michelin 255/70R/22.5, and the Radial Goodyear 11R24.5 Tires" Center for Transportation Research at the University of Texas at Austin, Research Report 1190-2F (1989) 56 p.

19. Streit, D. A., et. al. "Road Simulator Study of Heavy-Vehicle Wheel Forces." Federal Highway Administration Report FHWA-RD-98-019 (1998) 272 p.

20. Johansen, J. M. and Senstad, P. K., "Effects of Tire Pressures on Flexible Pavement Structures - A Literature Survey." Norwegian Road Research Laboratory Publication No. 62 (1992) 100 p.

21. Roberts, R. L., et. al., "Effects of Tire Pressures on Flexible Pavements." Texas Transportation Institute Research Report 372-1F (1986) 245 p.

22. Ott, W. C. and Papagiannakis, A. T., "Weigh-in-Motion Data Quality Assurance Based on 3-S2 Steer Axle Load Analysis." Transportation Research Record 1536 (1996) pp. 12-18.

23. Schmoyer, R., et. al., "Analysis of Vehicle Classification and Truck Weight Data of the New England States." Oak Ridge National Laboratories Report (1998) 125 p.

24. Dahlin, C., "Proposed Method for Calibrating Weigh-in-Motion Systems and for monitoring that Calibration Over Time." Transportation Research Record 1364 (1992) pp. 161-168.

# Appendix D: Statistical Weigh Scale Performance

This appendix lists the statistical performance of 63 simulated weigh scales. It summarizes the output of 232,848 simulations of 3,696 "virtual" five-axle tractor-semitrailers over 63 measured road profiles. Each profile covered 152.4 meters (500 feet) of pavement, with a simulated weigh scale 120.0 meters (393.75 feet) from the start. Every combination of vehicle and road profile yielded simulated weigh scale readings for five axles. In turn, individual weighing error values were calculated for: (1) steer axle load, (2) tractor tandem axle load, (3) trailer tandem axle load, and (4) total vehicle weight. The distributions of steer axle, tandem axle, and total vehicle weighing error were compiled over the entire set of vehicles for each simulated weigh scale. In turn, the distributions were summarized by calculating the average error, root-mean-square error, and 95th percentile absolute error, as described below

## INDIVIDUAL SCALE READINGS

Each simulation run produced five axle-load† time histories. Extracting weigh scale readings required some simple post-processing steps. The instant that each axle reached the scale was determined, as illustrated in figure D.1. The figure shows a portion of the time history of steer, leading drive, and leading trailer axle load of a vehicle with a forward-biased payload traveling at 72.4 kph (45 mph) over a jointed plain concrete site.

The steer axle load reading is extracted from the instant in the time history that it traveled to the location of the scale, 120 meters (393.75 feet) into the site. At a simulated speed of 72.4 kph (45 mph), the proper instant is about 5.97 seconds into the run. The reading is 46.62 kN (10,480 lbs). The leading drive axle is 3.28 meters (129 inches) behind the steer axle, and reaches the scale about 0.164 seconds later. It produces a reading of 57.33 kN (12,888 lbs). The leading trailer axle is positioned 15.01 meters (591 inches) behind the steer axle, reaches the scale about 0.746 seconds after it, and produces a reading of 32.59 kN (7,328 lbs). Note that a scale reading for the trailing drive and trailing trailer axles, not shown in the figure, must also be extracted. These reach the scale a very short time (~0.06 seconds) after their leading counterparts. This process is a simple matter of reading instantaneous axle loads from the proper sample within each time history.

## TANDEM AXLE AND GROSS VEHICLE LOAD

This study called for an estimate of the error in the measurement steer axle load, total tandem axle load, and gross vehicle weight. Thus, individual scale readings were summed to produce total load applied to the scale by each tandem axle and the complete vehicle. Figure D.2 shows the load applied to a range of locations, including that of the simulated

† Note that the term "load" in this Appendix refers to the total force applied to the pavement by all of the tires of a given axle. The instantaneous value will be denoted simply as load, and the static value will be named explicitly as static load.

weigh scale, by the tandem axles of a vehicle. These values do not represent the instantaneous loads applied to the pavement by each tandem axle. Instead they represent the sum of the loads applied by the leading axle of a given tandem at a given location and the trailing axle applied in the same location a very short time afterward.

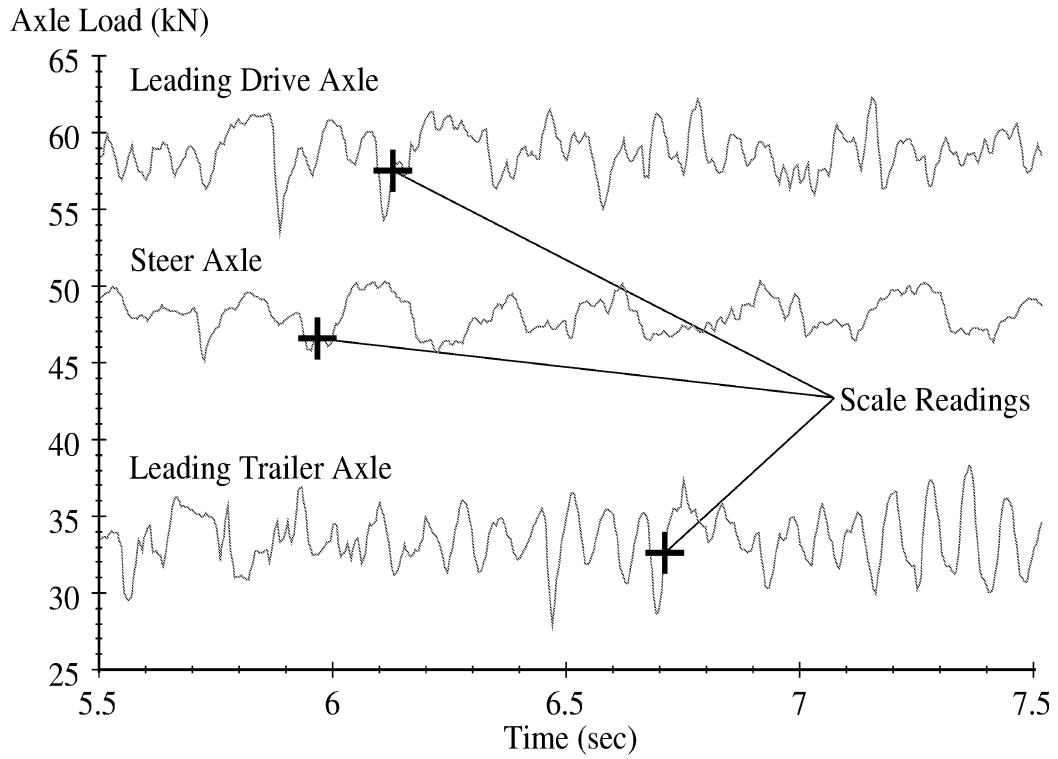


**Figure D.1. Sample axle load time histories.**

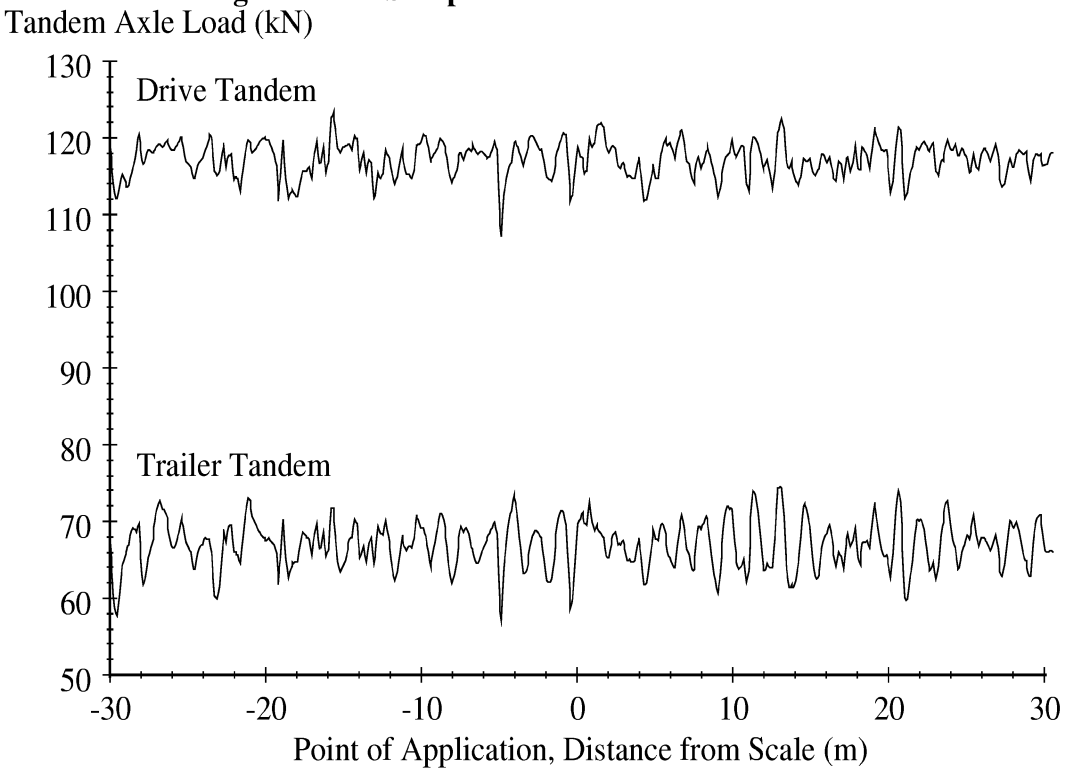


**Figure D.2. Sample applied tandem axle load.**

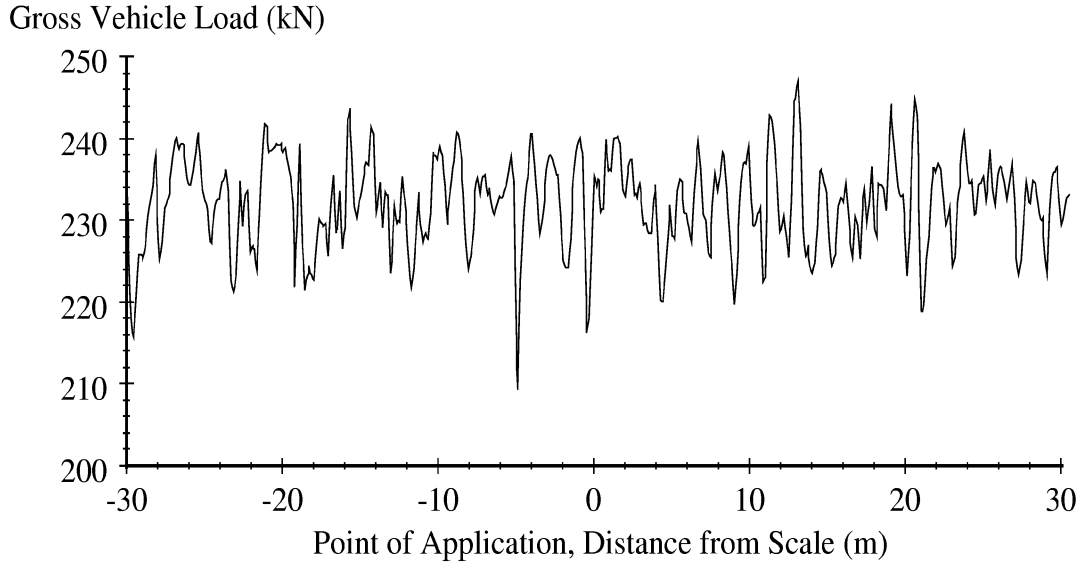


**Figure D.3. Sample applied gross vehicle load.**

The same process was applied to the total vehicle load. This is shown in figure D.3. The figure shows the total load applied by a vehicle at a range of locations. Only one scale location per profile was included in the statistical analysis for this study, so the only relevant value in the figure is the load applied at a distance of zero. Figure D.3 also illustrates the sensitivity of measured total vehicle weight to scale location. The figure was generated using a road profile from a jointed plain concrete site with an overall IRI value of about 1.10 m/km (70 in/mi).

## ERROR CALCULATION

Each vehicle pass yielded four scale measurements: a steer axle load, two tandem axle loads, and a gross vehicle load. The weighing error is calculated by comparing the measured load to the corresponding static load. Several possible strategies were considered for doing this:

- Absolute Error: Judging scale accuracy by absolute weighing error has the effect of assigning greatest importance to measurement of the heaviest loads. This is because absolute error usually increases with total weight for the same road profile and speed. This may be a desirable strategy if the scales are intended to facilitate enforcement of weight limits, where measurement of the heaviest axles is most important.
- Percentage Error: Judging scale accuracy by percentage error has the effect of assigning equal importance to the measurement of each vehicle, regardless of static load. This may be a desirable strategy if the scales are intended to study freight movement. This strategy is also appropriate if the scales are meant to study pavement performance qualities that are believed to suffer a penalty that is roughly proportional to the total load applied to the pavement.

- Weighted Aggregate Forces: This is a strategy for estimating pavement wear from axle load histories suggested by Cebon. (*1*) In this strategy, pavement wear is estimated by raising the value of axle load to an appropriate power. The most common example of this would be to raise the scale measurement to the fourth power and compare the result to the static load raised to the fourth power. Of course, this strategy is most appropriate if study of a specific type of pavement wear motivated the installation of the scales.

The weigh scales may exist for multiple purposes. Nevertheless, scale accuracy requirements are expressed in terms of percentage in the American Society for Testing and Materials Standard E-1318. (*2*) Therefore, percentage error was used in compiling distributions of weigh scale error for this study. A sample set of percentage error values for the individual vehicle and scale combination illustrated in figures D.1 through D.3 are provided in table D.1.

**Table D.1. Single Pass Error Values.**

| Measurement | Measured Load (kN) | Static Load (kN) | Percent Error |
|---|---|---|---|
| Steer Axle | 46.62 | 48.07 | -3.03 |
| Tractor Tandem Axle | 117.39 | 117.03 | 0.31 |
| Trailer Tandem Axle | 67.26 | 66.92 | 0.51 |
| Gross Vehicle | 231.26 | 232.03 | -0.33 |

## SITE STATISTICS

Each simulated weigh scale was covered by 3,696 vehicles. The effect of road roughness on scale performance is characterized by distributions of weighing error percentage for the steer axle, tandem axles, and total vehicle. Figure D.4 shows the distribution of steer axle weighing error for a scale on a section of jointed plain concrete pavement with an IRI of 1.10 m/km (70 in/mi). The mean error level in the distribution is -3.68 percent. A non-zero mean error implies a systematic bias in load measurement. A negative value indicates bias toward underestimating the load. A bias occurs because response of the simulated vehicle fleet to the roughness upstream of the scale is (somewhat) spatially repeatable. This could be a legitimate property of real truck traffic, or a consequence of the design of the virtual fleet used in this study. (See Appendix C.) The standard deviation of the distribution is 2.40 percent. The standard deviation represents the scatter, and characterizes the diversity of the truck fleet. The root-mean-square (RMS) error level for the distribution, which includes the influence of bias and scatter, is 4.39 percent.

The ASTM error tolerances for weigh scale performance call for 95 percent confidence that: (1) steer axle load will be measured within 20 percent, (2) tandem axle load will be measured within 15 percent, and (3) gross vehicle weight will be measured within 10 percent. If the error distributions were Gaussian, the mean and standard deviation values would be enough to define them, and to calculate the 95th percentile error level as illustrated by figures D.5 and D.6. They show the error distributions for tandem axle and gross vehicle load, respectively, for the same vehicle covered in figure D.4. These are

definitely not Gaussian, and show a subset of weight measurements with large downward bias.

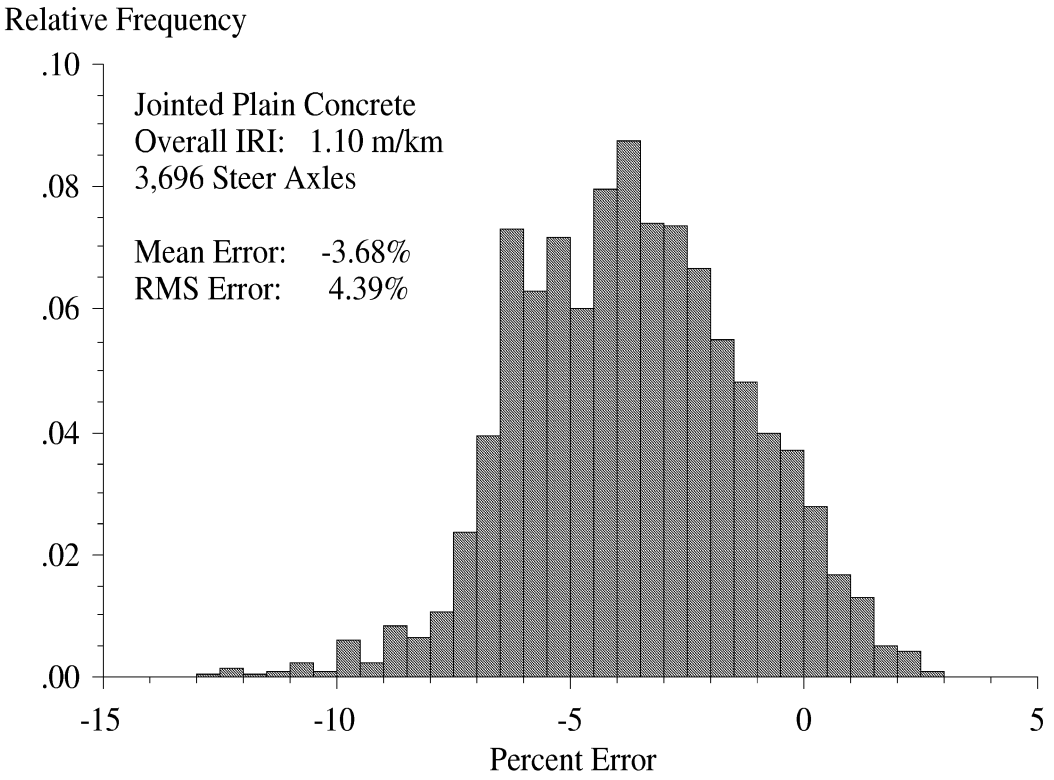


**Figure D.4. Distribution of steer axle weighing error.**

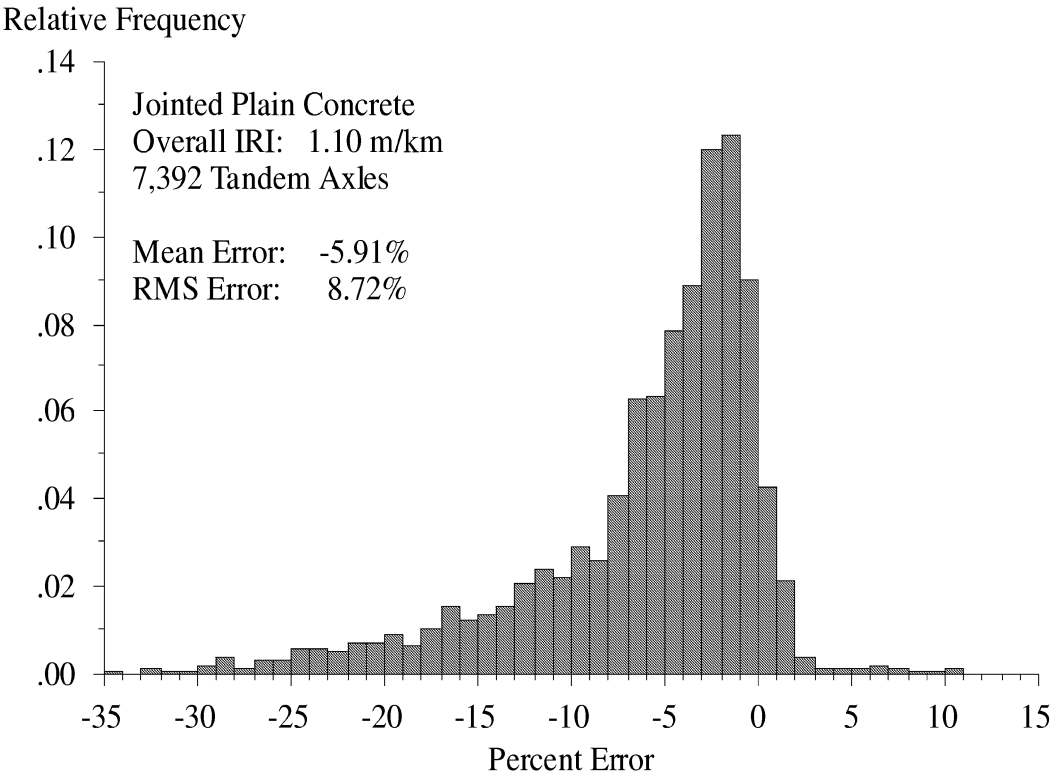


**Figure D.5. Distribution of tandem axle weighing error.**

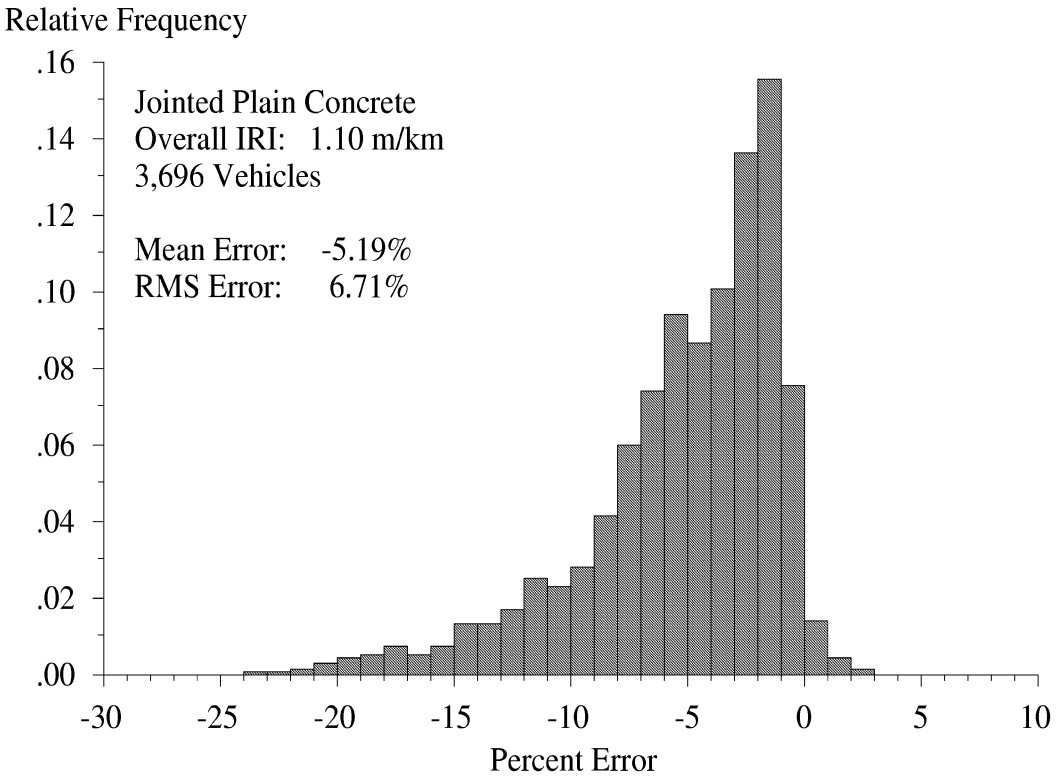


**Figure D.6. Distribution of total vehicle weighing error.**

A very large number of samples appear in the error distributions for each simulated scale: 3,696 for steer axle and total vehicle load and 7,392 for tandem axle load. Therefore, 95th percentile error level can be substituted for 95 percent confidence interval. Tables D.2 through D.5 list these values for every simulated scale. The 95th percentile absolute error level values were extracted directly from the distributions. In most cases, all of the extreme error values were biased in the same direction. The mean and RMS error levels are also listed in the tables to describe the bias and scatter at each scale.

**Table D.2. Weighing Error on Overlaid Sites.**

| Target IRI | Steer Axles | | | Tandem Axles | | | Gross Vehicle | | |
|---|---|---|---|---|---|---|---|---|---|
| (m/km) | Mean | RMS | 95% | Mean | RMS | 95% | Mean | RMS | 95% |
| 0.47 | -2.05 | 2.43 | 4.13 | -1.51 | 2.59 | 5.27 | -1.58 | 1.99 | 3.81 |
| 0.63 | 0.87 | 2.67 | 5.01 | 0.53 | 3.24 | 7.08 | 0.65 | 1.97 | 3.96 |
| 0.79 | 0.87 | 2.99 | 5.78 | 0.99 | 2.83 | 5.88 | 0.96 | 2.07 | 4.50 |
| 0.95 | 0.94 | 2.89 | 5.34 | 2.20 | 5.63 | 11.79 | 1.66 | 3.56 | 7.77 |
| 1.10 | -0.86 | 3.25 | 6.52 | -5.03 | 9.85 | 21.05 | -3.74 | 6.12 | 12.75 |
| 1.26 | -3.47 | 4.10 | 6.48 | -3.34 | 5.59 | 10.39 | -3.40 | 4.00 | 6.68 |
| 1.42 | 3.15 | 4.79 | 8.76 | 5.03 | 8.36 | 17.58 | 4.53 | 6.08 | 12.44 |
| 1.58 | -1.72 | 3.37 | 6.11 | -2.48 | 5.65 | 11.50 | -2.31 | 4.12 | 7.75 |
| 1.74 | -2.08 | 3.20 | 5.70 | -0.46 | 5.93 | 12.52 | -0.89 | 3.14 | 6.44 |
| 1.89 | -0.81 | 2.91 | 5.62 | -1.30 | 5.77 | 12.65 | -1.03 | 3.81 | 8.03 |
| 2.05 | 0.57 | 3.15 | 6.25 | 1.46 | 7.09 | 13.82 | 1.37 | 4.39 | 8.39 |

**Table D.3. Weighing Error on Jointed Plain Concrete Sites.**

| Target IRI | Steer Axles | | | Tandem Axles | | | Gross Vehicle | | |
|---|---|---|---|---|---|---|---|---|---|
| (m/km) | Mean | RMS | 95% | Mean | RMS | 95% | Mean | RMS | 95% |
| 0.79 | -2.27 | 3.52 | 6.90 | -1.30 | 4.10 | 8.72 | -1.57 | 2.78 | 6.06 |
| 0.95 | 0.16 | 2.35 | 4.98 | 2.06 | 4.53 | 9.75 | 1.60 | 3.00 | 6.22 |
| 1.10 | -3.68 | 4.39 | 7.26 | -5.91 | 8.72 | 19.80 | -5.19 | 6.71 | 13.94 |
| 1.26 | -2.93 | 4.01 | 7.41 | 0.62 | 6.61 | 13.51 | -0.43 | 4.11 | 8.71 |
| 1.42 | -1.16 | 3.22 | 6.39 | 0.49 | 4.31 | 8.92 | 0.05 | 2.49 | 5.17 |
| 1.58 | 4.02 | 4.59 | 7.47 | 5.69 | 8.11 | 18.32 | 5.26 | 6.57 | 13.81 |
| 1.74 | 4.12 | 4.51 | 7.43 | 5.87 | 9.76 | 20.29 | 5.16 | 6.96 | 14.34 |
| 1.89 | -6.01 | 7.88 | 13.32 | -5.44 | 10.45 | 21.20 | -5.54 | 7.84 | 14.34 |
| 2.05 | 0.84 | 3.93 | 7.82 | 1.05 | 5.44 | 11.49 | 1.16 | 3.26 | 6.76 |
| 2.21 | -5.97 | 7.15 | 12.12 | -0.45 | 8.86 | 17.97 | -1.66 | 4.84 | 9.64 |
| 2.37 | -4.22 | 5.87 | 11.58 | -5.84 | 8.99 | 19.69 | -5.37 | 6.72 | 14.27 |
| 2.53 | -10.95 | 11.61 | 17.91 | -15.01 | 17.63 | 32.41 | -14.18 | 15.34 | 24.55 |
| 2.68 | -5.84 | 6.81 | 12.13 | -4.54 | 8.62 | 16.95 | -5.11 | 6.74 | 11.87 |
| 2.84 | -1.97 | 4.76 | 10.00 | -3.90 | 10.71 | 21.81 | -3.42 | 6.30 | 11.67 |
| 3.00 | 0.79 | 2.94 | 6.13 | 6.69 | 11.55 | 25.65 | 5.09 | 7.37 | 15.51 |
| 3.16 | 4.55 | 7.72 | 13.99 | -3.37 | 9.57 | 18.13 | -1.66 | 5.27 | 10.35 |
| 3.31 | -0.50 | 3.79 | 8.17 | 2.40 | 8.14 | 16.92 | 1.75 | 4.77 | 9.62 |
| 3.47 | 5.07 | 7.77 | 14.31 | 8.21 | 12.17 | 23.26 | 7.67 | 9.25 | 16.23 |

**Table D.4. Weighing Error on Jointed Reinforced Concrete Sites.**

| Target IRI | Steer Axles | | | Tandem Axles | | | Gross Vehicle | | |
|---|---|---|---|---|---|---|---|---|---|
| (m/km) | Mean | RMS | 95% | Mean | RMS | 95% | Mean | RMS | 95% |
| 1.10 | 3.20 | 4.40 | 8.82 | -0.15 | 3.68 | 7.94 | 0.47 | 2.33 | 4.80 |
| 1.26 | 6.83 | 7.28 | 11.75 | 4.48 | 9.11 | 17.28 | 5.19 | 6.92 | 12.11 |
| 1.42 | -2.05 | 3.02 | 5.57 | -4.18 | 6.15 | 12.23 | -3.70 | 4.54 | 8.83 |
| 1.58 | -2.87 | 4.59 | 8.70 | -5.32 | 8.18 | 16.12 | -5.11 | 6.30 | 11.38 |
| 1.74 | 0.75 | 3.19 | 6.64 | -1.64 | 6.99 | 14.07 | -1.02 | 3.91 | 8.21 |
| 1.89 | 5.05 | 6.89 | 11.13 | -1.41 | 10.40 | 22.09 | 0.27 | 6.21 | 13.50 |
| 2.05 | -3.75 | 5.89 | 11.78 | 0.77 | 5.34 | 11.50 | -0.11 | 3.29 | 6.60 |
| 2.21 | 2.07 | 4.39 | 8.51 | 7.90 | 13.13 | 29.31 | 6.07 | 8.63 | 18.43 |
| 2.37 | 3.45 | 4.43 | 7.55 | 6.17 | 10.79 | 22.32 | 5.43 | 7.19 | 14.16 |
| 2.53 | -11.87 | 12.96 | 20.56 | -11.97 | 16.74 | 32.85 | -12.05 | 14.35 | 27.40 |
| 2.68 | 3.32 | 5.41 | 10.02 | 5.53 | 10.36 | 20.32 | 5.12 | 7.70 | 14.92 |
| 2.84 | -1.60 | 7.84 | 15.18 | 5.28 | 10.90 | 24.08 | 4.02 | 6.87 | 13.80 |
| 3.00 | -7.78 | 8.85 | 14.72 | -21.63 | 27.66 | 60.07 | -17.97 | 20.39 | 39.17 |
| 3.16 | -2.77 | 5.25 | 11.37 | -5.68 | 13.16 | 29.53 | -4.58 | 8.32 | 18.72 |

**Table D.5. Weighing Error on Asphalt Concrete Sites.**

| Target IRI | Steer Axles | | | Tandem Axles | | | Gross Vehicle | | |
|---|---|---|---|---|---|---|---|---|---|
| (m/km) | Mean | RMS | 95% | Mean | RMS | 95% | Mean | RMS | 95% |
| 0.47 | 2.69 | 3.59 | 6.85 | 0.99 | 2.85 | 5.68 | 1.45 | 2.26 | 4.21 |
| 0.63 | 0.68 | 2.16 | 4.61 | 0.27 | 2.14 | 4.49 | 0.29 | 1.50 | 3.12 |
| 0.79 | -0.01 | 2.74 | 5.42 | 0.20 | 2.68 | 5.54 | 0.21 | 1.63 | 3.52 |
| 0.95 | -0.01 | 2.74 | 5.42 | 0.20 | 2.68 | 5.54 | 0.21 | 1.63 | 3.52 |
| 1.10 | 2.48 | 4.37 | 8.04 | 3.43 | 5.59 | 11.36 | 3.21 | 4.21 | 8.20 |
| 1.26 | 6.54 | 7.65 | 12.55 | 2.81 | 5.51 | 11.01 | 3.65 | 4.80 | 9.75 |
| 1.42 | -1.96 | 4.02 | 7.61 | -0.29 | 5.15 | 12.17 | -0.39 | 3.22 | 7.51 |
| 1.58 | 7.85 | 9.09 | 14.89 | 13.48 | 16.81 | 33.66 | 12.22 | 14.13 | 27.00 |
| 1.74 | -7.81 | 8.50 | 14.04 | -4.26 | 10.32 | 21.46 | -5.43 | 7.63 | 14.15 |
| 1.89 | -8.04 | 9.28 | 16.04 | -1.16 | 7.82 | 15.00 | -2.60 | 5.42 | 11.34 |
| 2.05 | 5.71 | 6.73 | 10.81 | 4.42 | 9.43 | 18.52 | 4.83 | 6.72 | 12.22 |
| 2.21 | 1.92 | 3.17 | 5.67 | 4.67 | 10.77 | 23.80 | 3.81 | 6.69 | 14.69 |
| 2.37 | -10.99 | 12.04 | 21.93 | -5.12 | 10.65 | 20.72 | -6.60 | 8.67 | 16.40 |
| 2.53 | 3.14 | 4.82 | 8.54 | -0.05 | 8.10 | 17.73 | 1.06 | 4.80 | 10.09 |
| 2.68 | 0.82 | 6.31 | 12.33 | 5.67 | 14.14 | 32.27 | 4.18 | 8.95 | 21.28 |
| 2.84 | -8.75 | 9.89 | 18.05 | -7.40 | 14.39 | 28.62 | -7.64 | 10.85 | 21.57 |
| 3.00 | -2.38 | 4.87 | 9.76 | -10.39 | 13.69 | 27.75 | -8.62 | 9.88 | 18.96 |
| 3.16 | 5.63 | 7.63 | 15.59 | 16.53 | 27.60 | 62.26 | 13.47 | 19.75 | 47.45 |
| 3.31 | -6.51 | 7.85 | 13.52 | -13.65 | 15.51 | 27.50 | -12.18 | 13.13 | 21.46 |
| 3.47+ | -5.09 | 8.10 | 14.67 | -0.69 | 9.39 | 19.25 | -1.78 | 6.41 | 12.38 |

## CORRELATION STANDARD

The 95th percentile error levels served as a correlation standard for testing proposed profile-based indices. Unfortunately, three sets of values exist with three separate error limits, covering steer, tandem, and total vehicle load, which complicated the analysis.

Figure D.7 compares 95th percentile error in tandem axle load with 95th percentile error in steer axle load over all 63 simulated WIM sites. A very weak statistical relationship exists between them. The figure also shows the ASTM error limits for acceptable scale performance. More than half of the sites violate the tandem axle error limit, but only two sites violate the steer axle error limit. Furthermore, no site violates the steer axle error limit without also violating the tandem axle error limit. Thus, the roughness index development described in this report did not consider steer axle load measurement error.

Figure D.8 compares error in tandem axle load with error in gross vehicle weight. A very strong relationship exists between them. This is no surprise, since all of the vehicles in this simulation study are five-axle tractor semitrailers, and a major percentage of the gross vehicle weight is carried by the tandem axles. The error values correlate with an $R^2$ value of 0.96. (This is partly dictated by the two extreme values. The $R^2$ value is 0.93 when they are excluded.) More importantly, they increase together such that the two error limits are usually violated together:

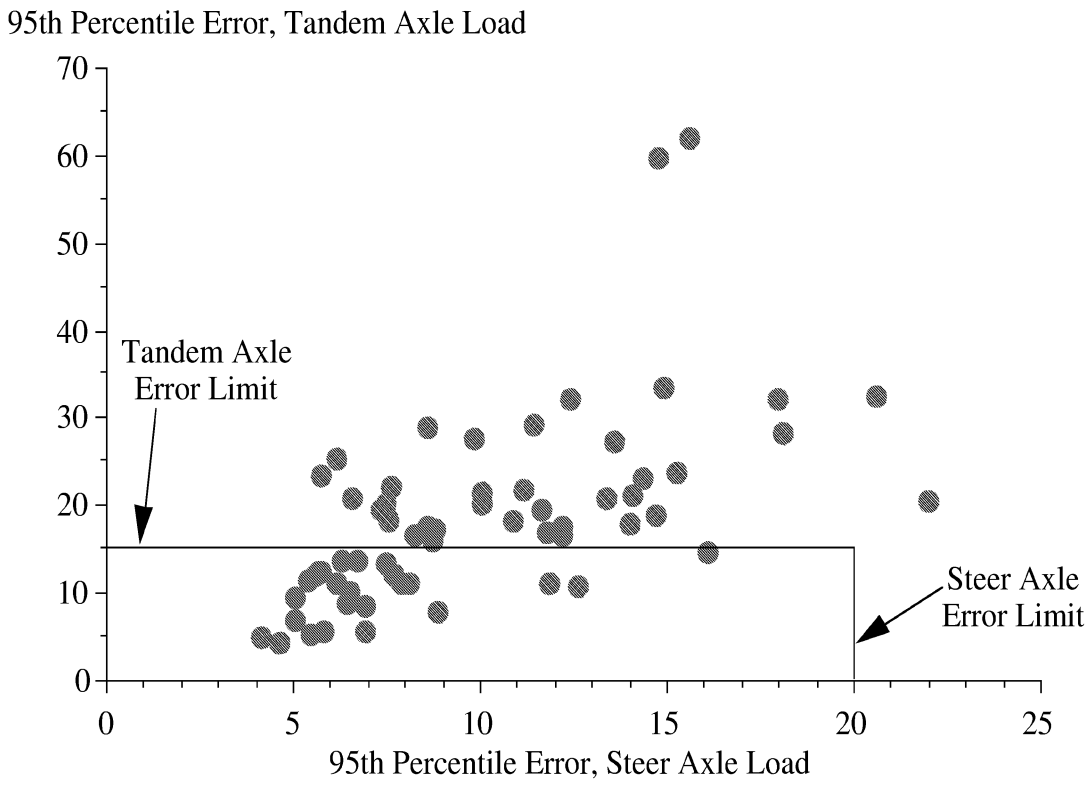


**Figure D.7. Comparison of steer axle load and tandem axle load error.**

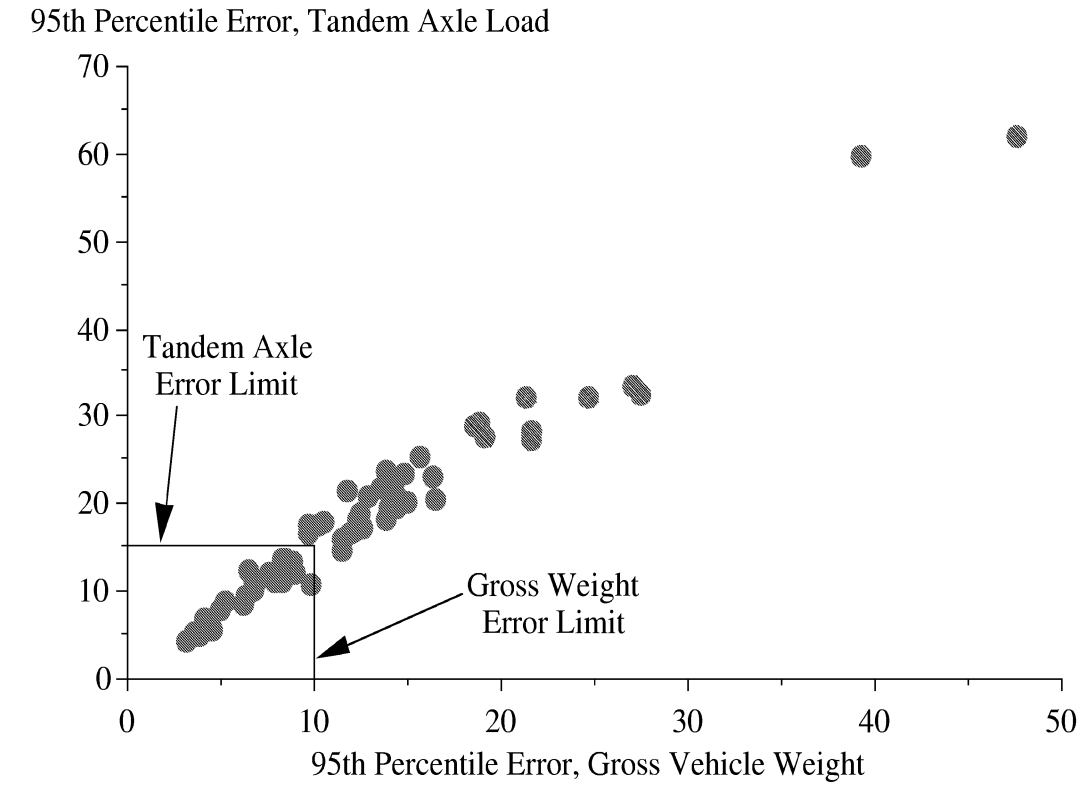


**Figure D.8. Comparison of total vehicle load and tandem axle load error.**

- 25 sites adhere to both error limits,
- 35 sites violate both error limits,
- 2 sites adhere to the gross weight error limit, but violate the tandem error limit, and
- 1 site adheres to the tandem axle weight error limit, but fails the gross weight error limit.

This makes the criteria roughly equivalent. This also means that the errors in tractor and trailer axle load measurement compensate for each other in the manner that the author of the ASTM error limits anticipated. The roughness index development described in this report considered error in both tandem axle load and gross vehicle weight.

The road profiles chosen for this study purposely covered their range of roughness uniformly. (See Appendix A.) These choices were based on overall IRI of the entire profile, which has a weak relationship to WIM scale error. Unfortunately, the distribution of 95th percentile WIM scale error was not uniform. In particular, two of the values (shown in figure D.8) are extreme compared to the others. A correlation standard for roughness index development should include a set of values that are uniformly distributed. This will prevent extreme values from imposing disproportionate influence on the level of correlation to proposed roughness indices.[††] Proposed roughness indices were correlated to error level with and without the two extreme error values to search for cases in which they changed the character of the results.

## REFERENCES


1. Cebon, D., "An Investigation of the Dynamic Interaction Between Wheeled Vehicles and Road Surfaces." Ph.D. Thesis, University of Cambridge (1985).
2. American Society of Testing and Materials, Annual Book of ASTM Standards, Volume 4.03, Road and Paving Materials; Vehicle-Pavement Systems, Philadelphia, 1999.


[††] Recall that the influence of a pair of values on the correlation between two data sets is proportional to their contribution to the variance. That means that a few extreme values can dictate a high correlation coefficient, even if no relationship between the two variables exists over the rest of the data set.

# Appendix E: Index Options

This appendix describes the indices used to estimate 95th percentile weigh-in-motion scale error. Each index was tested by correlating its value with the summary value of scale error, calculated as described in Appendix D. Millions of individual indices were attempted, covering two basic classes: (1) wave-number domain transforms, and (2) distance domain transforms. Wave-number domain transforms require calculation of the power spectral density (PSD) function. The index is then derived from the PSD. In distance domain transforms, and band-pass filter is applied and the index is accumulated from the resulting signal, which is usually stored at the same sample interval and covers the same distance as the original profile.

The details of each type of band-pass filter and the variables used to optimize their correlation with 95th percentile scale error are described here. PSD-based indices are also described, although they were mostly used in preliminary calculations to learn what spatial weighting function and frequency band held the most relevance to scale error.

## BAND-PASS FILTERS

Indices that are based on band-pass filters were calculated in the following steps:

1. Apply a band-pass filter to a profile over its entire length. The effect of this step is to apply a frequency weighting to the profile. The output of this step is another signal of equal length and sample interval.
2. Apply a spatial weighting function to the filter output. This step is included to emphasize roughness near the scale.
3. Accumulate the result into a single index.

The band-pass filters used in this study were: the Golden Car (GC) model, the Ride Number (RN) and variations on it, a general quarter-car filter, and a four-pole Butterworth band-pass filter. Each of these filters is described below. All of these filters included a pre-filter in which the profile was converted to slope via finite-difference. They can all be classified as band-pass filters, because they exclude very long and very short wavelengths. This helps avoid "abrupt" content at the boundaries of the spatial weighting function. It also prevents absolute elevation or grade from influencing index values. (Grade and absolute elevation are rarely measured accurately by inertial profilers, and have no major effect on truck vibration.)

The spatial weighting functions considered were: box, cosine taper (Hanning), and quadratic. These are illustrated in figure E.1. All of these weighting functions are defined by their shape, starting point, and ending point. When a weighting function is applied, everything outside of the boundaries is eliminated. Inside the boundaries, a signal is "weighted" when its value is multiplied by the value of the weighting function at the corresponding point.

The box function is meant to represent the same type of information provided by a roughness profile. (*1*) The Hanning window was only used in the form shown in figure E.1, where the cosine function covers the entire length of the window. (Other options exist in which the cosine function is only used to lead into and out of a weighting of unity over a large range in the center.) This type of weighting emphasizes roughness in the center, but does not exclude very rough features nearby. The quadratic weighting function is intended to cover roughness over a large range, but emphasize a small range at its center.

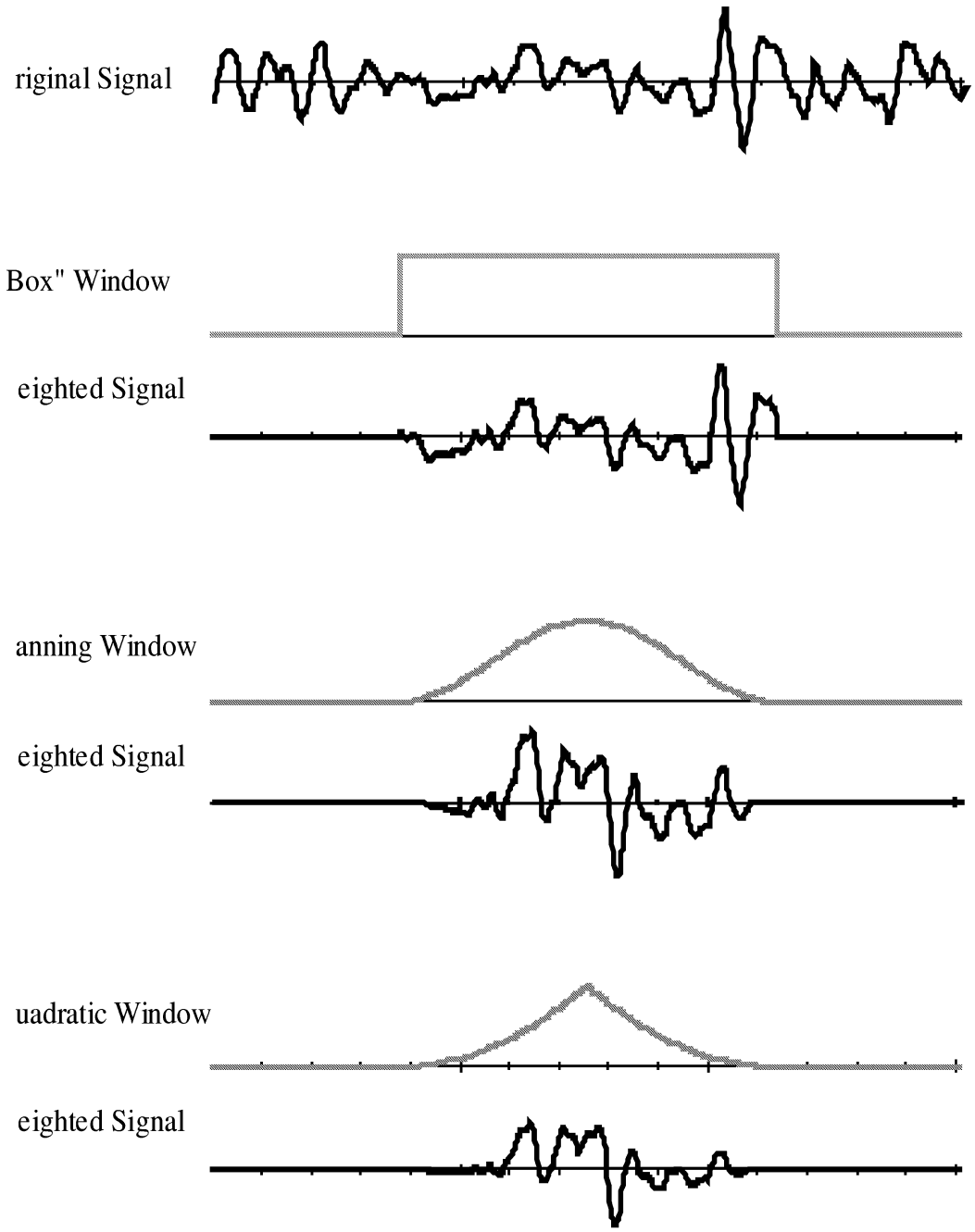


**Figure E.1. Spatial weighting functions.**

All three weighting functions have a standard shape. They are symmetrical, but do not necessarily have to be centered over the location of the weigh scale or even include the location of the weigh scale. In some instances a weighting function covered a short

segment just before, but not including, the scale. Since the shape of these functions are standard, only the starting and ending points are optimized to improve the performance of an index.

Note that the weighting functions were applied **after** the filter. That means that filter response, rather than the input profile, is weighted. As a result, rough profile features that appear just before the start of the weighting function can influence the final index value. This method was chosen to speed up the optimization process. The time savings existed because a given filter can be applied once, then thousands of weighting function endpoints could be studied. If the profile were weighted, the filter would need to be applied in every iteration. This method also allows profiles from proposed weigh-in-motion sites to be searched quickly for the best sensor location by filtering, then "sliding" the weighting function along to investigate all sensor positions. The "box" weighting function is favored because it would be the most efficient in that application.

Once each profile was filtered and weighted, the response was accumulated into a summary index. This study investigated three types of index accumulation: average-rectified (AR), RMS, and root-mean-quad (RMQ). All of these accumulation schemes use equation E-1:

$$\text{Index} = \left[ \frac{1}{N_2 - N_1 + 1} \sum_{i=N_1}^{N_2} \text{abs}(F_i \bullet W_i)^P \right]^{1/P} \qquad \text{(E-1)}$$

Where "F" is the filtered profile, "$N_1$" and "$N_2$" are the sample numbers of the spatial weighting function boundaries, "W" is the weighting function, and "P" is the accumulator exponent. The exponent value is set at 1 for AR, 2 for RMS, and 4 for RMQ.

Each of the index options described below were optimized to correlate with 95th percentile scale error over 61 sites. This was usually a matter of finding the best filtering parameters to improve the level of correlation. This search was performed with every combination of index type, weighting function, and accumulator. As such, the list of variables to optimize included a few filter coefficients, the weighting function type, weighting function boundaries, and accumulator type.

## Golden Car

The Golden Car filter is a quarter-car model that uses the standard set of vehicle parameter values from the IRI. (*2*) This filter is applied in three steps: (1) conversion of the profile to slope via finite difference, (2) smoothing by a moving average, and (3) application of the quarter-car model with Golden Car parameters. The operation and effect of all of these steps are well documented. (*3*) Figure E.2 shows the collective gain of these filters to profile slope. The output of these filters represent the spatial derivative of the suspension stroke. (*4*) This is expressed in units of slope. The IRI is the average rectified value calculated over a given length (i.e. a box weighting function). Variations from the IRI were studied by applying the weighting functions described above, and accumulating RMS and RMQ response in addition to AR response.

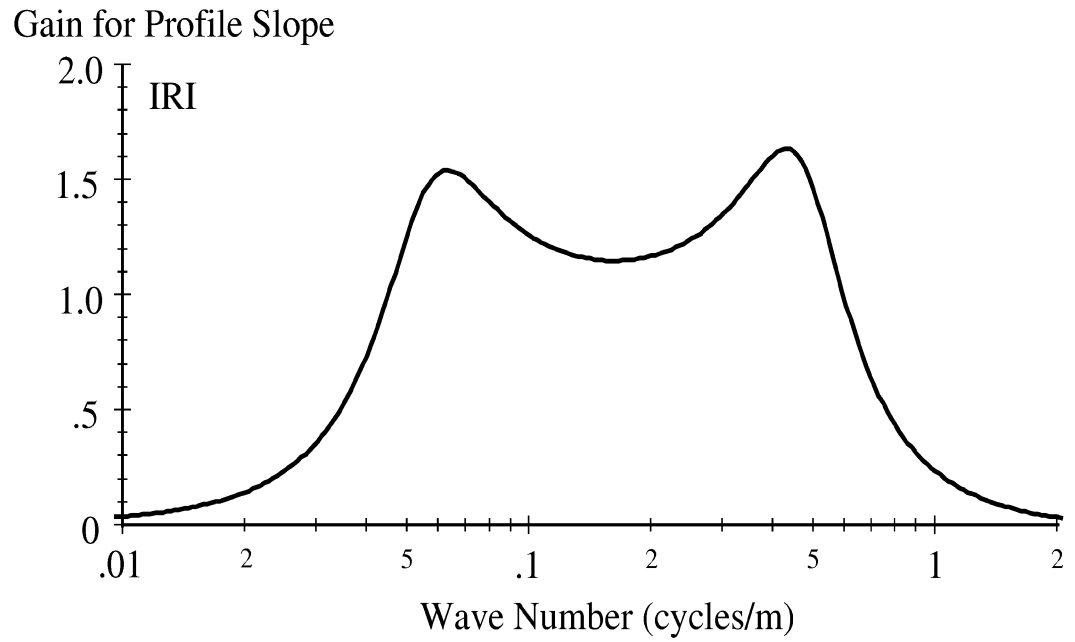


**Figure E.2. IRI filter gain.**

Two variations in the vehicle response were also investigated. First, the derivative of suspension stroke was replaced by tire deflection as the output variable. (A state variable was added to the model for this purpose.) Since the model is linear, tire deflection is proportional to tire load. It was thought that this would relate more closely to truck wheel loads. The sensitivity of the filter to wave number is shown in figure E.3. It is not very different than the gain for IRI, and is really just another band-pass filter that covers a similar range in the wave-number domain. Second, sprung mass spatial acceleration was investigated. The sensitivity of this filter to wave number is shown in figure E.4. This filtering option emphasizes the long-wavelength portion of the response.

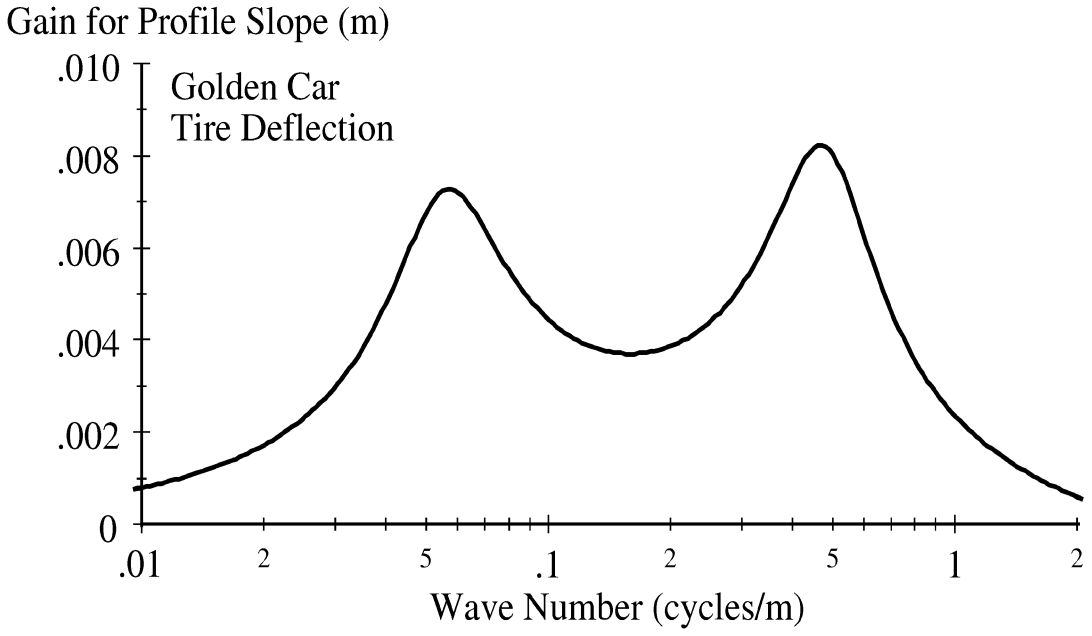


**Figure E.3. Golden Car filter gain, tire deflection.**

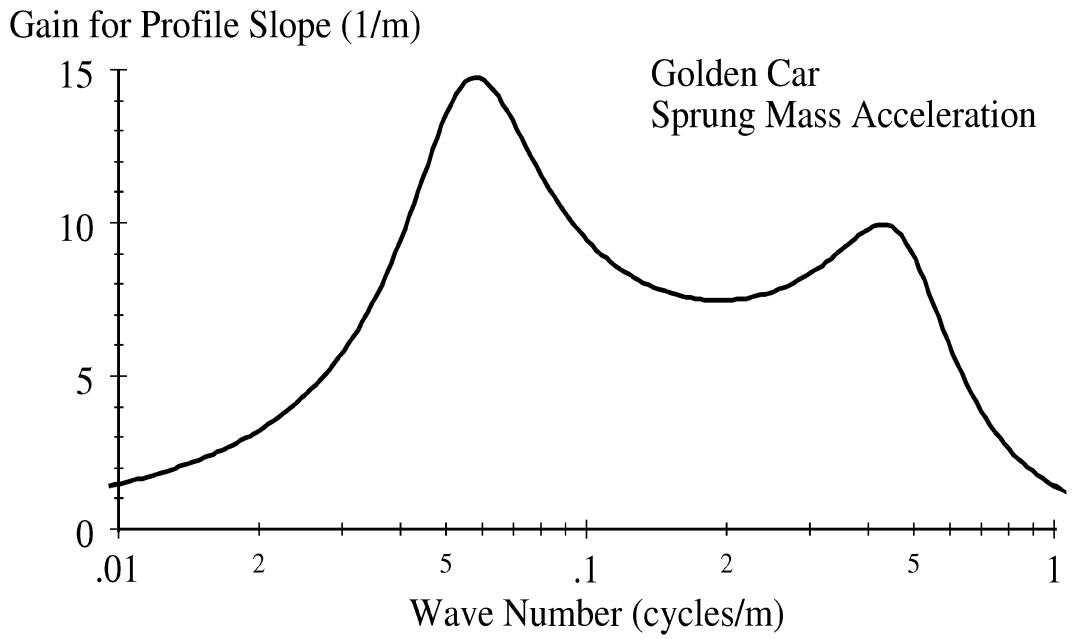


**Figure E.4. Golden Car filter gain, sprung mass acceleration.**

### IRI Hot Spot

A variation on the "box" spatial weighting function was investigated to study the relationship between weighing error and localized concentration of IRI preceding the scale. This index is equal to the IRI of the roughest segment of a given (short) length ahead of the scale. It is found by calculating the IRI of all possible short segments in the profile, then searching for the largest value over some range. Two variables were optimized in this calculation: (1) the segment length, and (2) the distance ahead of the scale to search for the maximum. This type of index is likely to succeed if a large portion of truck dynamic loading is caused by very rough localized distresses.

This type of search was performed with the IRI, and variations on the IRI using the RMS and RMQ filter response. (If this procedure had yielded much improvement in scale error prediction, it would have been applied to the other index options.)

### General Quarter-Car

A general quarter-car model was also investigated to search for a set of filter parameters that increased the correlation to weigh scale error the most. The filter parameters represent the vehicle properties: suspension stiffness, unsprung mass, tire stiffness, and suspension damping. (Sprung mass is not included because only four parameters are needed to define the filter. The other four parameters are normalized by sprung mass.)

A complete search of the possible values for these filter parameters was not performed. Rather, a "seed" set of properties were perturbed in a search for better correlation. In this process, minor changes in each parameter are tested. If a change increased correlation, the parameter was replaced with the new value. This was done thousands of times until a local maxima within the solution space was found. The optimization was seeded with parameter sets from the literature: (1) Golden Car parameters, (2) filter parameters from the Ride

Number algorithm, (3) three sets of values considered by DePont for use as a truck loading index. (*5*) Only the box weighting function was used with this option.

### Ride Number

Ride Number (RN) was also considered. It was found that the exponential transform used to cast the Ride Number onto a 0-to-5 scale was not helpful in relating to scale error. Thus, the "pre-transform" version of RN was used instead (PTRN). This is the RMS of the output of the quarter-car filter with the parameter values for the RN. (*6*) Variations of the PTRN were studied by calculating AR and RMQ filter output.

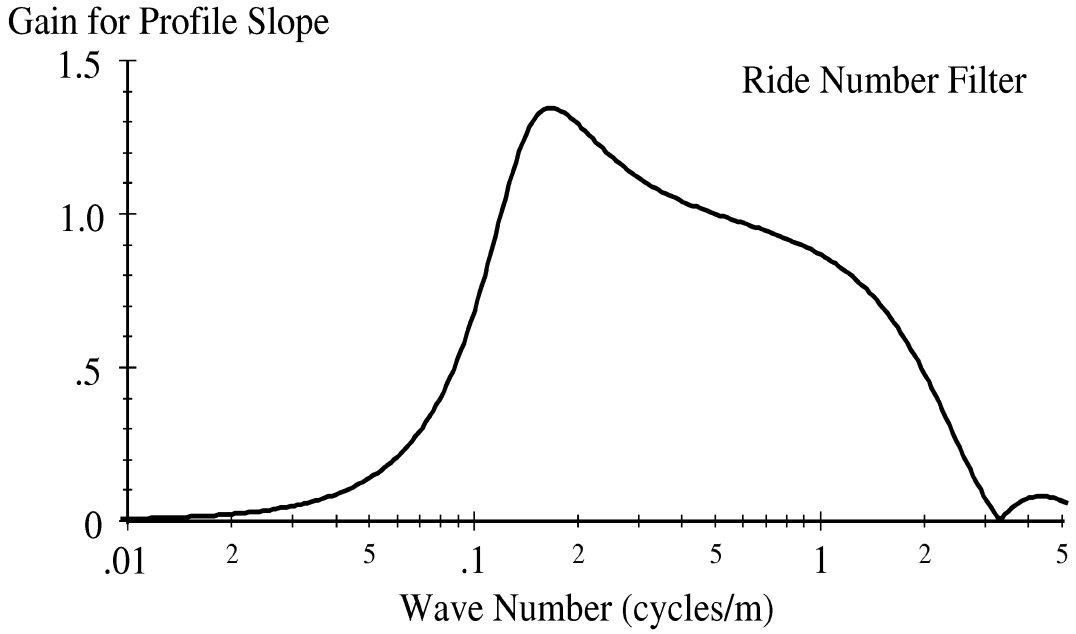


**Figure E.5. Ride Number filter gain.**

### Butterworth Filter

Indices based on a four-pole Butterworth filter were also investigated. Like the filters listed above, the profile is pre-filtered by converting it to slope. The slope profile is then filtered by a combination of a two-pole high-pass and two-pole low-pass Butterworth filter. Figure E.6 shows the gain response of the filter. The wave number sensitivity of this filter is defined by a long-wavelength cutoff and a short wavelength cutoff. These cutoff values correspond to the wave number values where the gain passes below 0.707. The properties and implementation of this filter are described in detail elsewhere. (*3*)

This filter does not have as much freedom to manipulate the shape of the filter gain as do the quarter-car options listed above, but it allows much more direct manipulation of the waveband. The two parameters, long- and short-wavelength cutoff, directly define the range of sensitivity. Optimization of the combination of long-wavelength cutoff, short-wavelength cutoff, weighting function (type and boundaries), and accumulator involved a huge search over the space of possibilities. To help reign in the scope of this task, cutoff

values were only considered in integer multiples of $2^{(1/6)}$. Thus, each pair of cutoff values really represents a range of 1/6th octave bands.

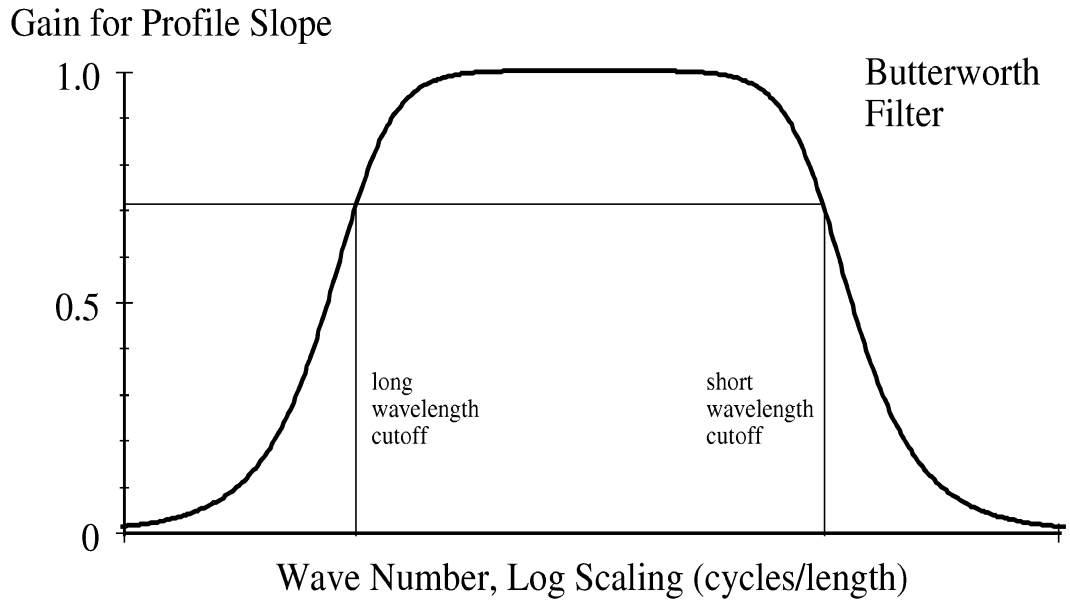


**Figure E.6. Butterworth filter gain.**

## POWER SPECTRAL DENSITY

PSD functions were not directly considered as potential options for an index. They were, however, used extensively to learn what spatial weight function boundaries and wave number sensitivity were most likely to work in the distance domain. When a promising waveband was identified using PSD analysis, a band-pass filter with similar sensitivity was developed into a candidate index. The steps used in computing a PSD-based index for this purpose were as follows:

1. The elevation profile is replaced with a slope profile, obtained point-by-point by subtracting adjacent elevation values and dividing by the sample interval. This is done to obtain a signal with content that is more uniform over the range of wave numbers of interest.
2. Apply a spatial weighting function to the slope profile, as described above. Extract a new signal that only covers the non-zero range of the weighting function.
3. Subtract the mean value from the signal. This is done so that the output of the next step represents variance, rather than RMS.
4. Perform a Fourier transform on the signal.
5. Correct the Fourier coefficients to account for the influence of the spatial weighting function. This is not needed for the "box" function. This procedure is used to maintain the interpretation of the final PSD as providing the distribution of variance. This procedure is described for a Hanning window by Bendat. (*7*)

6. Calculate the PSD coefficients in 1/6th octave bands. In this step, the Fourier coefficients that fall within each band are combined by summing their contribution to the mean square of each band. Note that some of the Fourier coefficients influence more than one band. In this case, their influence is split based on the PSD coefficient boundaries and the wave number that corresponds to the Fourier coefficient. This procedure is described by Sayers. (*8*)
7. Apply a frequency weighting to the PSD function.
8. Integrate the resulting weighted PSD.

This procedure amounts to calculating weighted RMS slope. The reason for studying RMS slope, rather than RMS elevation is illustrated in figure E.7, which compares the RMS slope and elevation in one-third octave bands for a sample section. Figure E.7 shows that the RMS elevation associated with the smallest wave number in a band is numerically much larger than the amplitude associated with the highest wave number. The range spans three orders of magnitude. The large difference in amplitude can complicate statistical analyses because side effects of the numerically large values mask the significance of the smaller values. In contrast, the RMS slope is fairly uniform over the entire range of wave numbers, covering just one order of magnitude. This will prevent the long-wavelength content from dominating broad-banded index options.

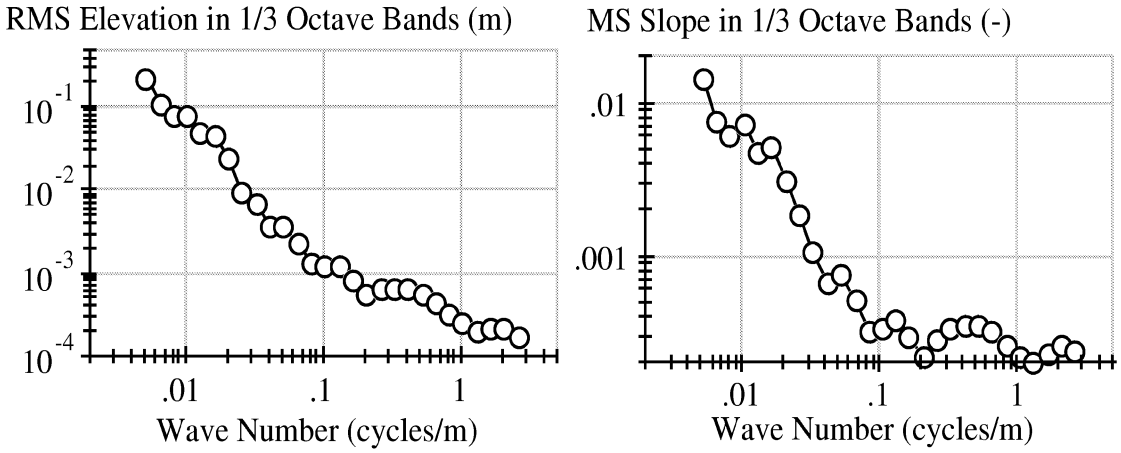


**Figure E.7. Sample RMS slope and elevation in one-third octave bands.**

Only RMS indices are possible with this procedure. On the other hand, much more freedom exists when using a PSD-based index in that complicated frequency weightings can be studied. Once the PSD is calculated the spatial weighting is fixed, but an unlimited number of frequency weighting functions can be investigated quickly without a new Fourier transform by applying only steps 7 and 8, above.

## REFERENCES

1. Sayers, M.W., "Profiles of Roughness." Transportation Research Record 1260, (1990) pp. 106-111.

2. Gillespie, T.D., et al., *Calibration of Response-Type Road Roughness Measuring Systems.* National Cooperative Highway Research Program Report 228, (1980) 81 p.

3. Sayers, M.W. and S.M. Karamihas, " Interpretation of Road Roughness Profile Data." University of Michigan Transportation Research Institute Report UMTRI-96-101, (1996) 177 p.

4. Sayers, M.W., "On the Calculation of IRI from Longitudinal Road Profile." Transportation Research Record 1501, (1996) pp. 1-12.

5. DePont, J., "Road Profile Characterisation." Transit New Zealand Research Report No. 29 (1994) 45 p.

6. Sayers, M. and S.M. Karamihas, "Evaluation of Rideability by Analyzing Longitudinal Road Profile." Transportation Research Record 1536, (1996) pp. 110-116.

7. Bendat, J.S. and A.G. Piersol, "Random Data: Analysis and Measurement Procedures." Wiley-Interscience, New York, (1971).

8. Sayers, M.W. "Dynamic Terrain Inputs to Predict Structural Integrity of Ground Vehicles." University of Michigan Transportation Research Institute Report UMTRI-88-16, (1988) 114 p.

# Appendix F: Index Development

This appendix reports some of the results from a search for the profile-based indices that correlate best to simulated weigh-in-motion error over 61 simulated sites. Several types of band-pass filter were examined. They are described in Appendix E. For each type of index, an optimal set of parameters was sought for every combination of weighting function shape and index accumulation under consideration. The parameter list included some filter parameters, which defined their wave-number response. For example, the long- and short-wavelength cutoff values were varied when using the Butterworth filter. Some filters, like the Golden Car, have only standard filter parameters, so they were held fixed. For all filter types, the range covered by the spatial-weighting function was also optimized in a search for the highest correlation.

Optimal forms of several types of index are listed here. Although less than one hundred options are listed in this Appendix, they derive from testing millions of variations. Throughout this Appendix, optimal versions of many of the potential indices are listed for every combination of box, Hanning, and quadratic weighting function with average rectified (AR), root-mean-square (RMS), and root-mean-quad (RMQ) accumulation. In some cases, more than one index is listed, because it represents a local maxima in the solution space.

With the exception of the recommended index, all of the correlation levels listed in this Appendix apply to tandem axle weighing error.

## INDIVIDUAL INDICES

### Golden Car

Three versions of the Golden Car filter were tested, as described in Appendix E. They were all optimized with twelve combinations of spatial weighting function and accumulator. For each combination, this was a search for the range of pavement near the scale that resulted in the highest level of correlation, defined by weighting function starting and ending locations.

Table F.1 lists the results for the Golden Car filter using suspension stroke as the filter output. The listed correlation level for each index type is the Pearson product moment correlation coefficient for a linear fit. The first entry in the table is the IRI. The IRI value from 22.1 meters (72.5 feet) ahead of the scale to 2.4 meters (8 feet) beyond the scale was found to correlate to scale error best, but the correlation is not very high. The rest of the options listed in the table are similar to the IRI, with variations in the spatial weighting function and accumulator. Several other types of accumulator were investigated, covering values of "P" in eq. E.1 up to 10, but none stood out as superior to those listed here. The highest correlation was found for a version of the IRI altered to report RMS filter output from 7.3 meters (24 feet) ahead of the scale to 0.6 meters (2 feet) past the scale. This range is short, and may represent wheel load variations caused by axle vibration and localized

roughness that excites body motion transient response, but it probably excludes much of the influence of body motion.

Table F.2 lists the results for the Golden Car filter using tire deflection as the filter output. It was expected that using tire deflection would improve the relationship to scale error, because it is proportional to tire load. (The filter is linear.) This was not the case. Use of sprung mass acceleration as filter output was not successful either. Those results are listed in table F.3.

The correlation is not very high for any of the Golden Car options. (The correlation level is listed as R, rather than $R^2$, so few of them account for even two thirds of the variation in scale error level over the list of sites.) These tables do provide some idea of the range of pavement around the scale that is of greatest interest, but some of the spatial weighting function endpoints are difficult to explain. The diversity in endpoints may suggest the need for a composite index to cover localized roughness near the scale and overall roughness of the site.

**Table F.1. Golden Car Index Best Options.**

| Weighting Function | | | Accumulator | Pearson's R |
|---|---|---|---|---|
| Type | Start (m) | End (m) | | |
| Box | -22.1 | 2.4 | AR | 0.788 |
| Box | -7.3 | 0.6 | RMS | 0.813 |
| Box | -7.3 | 0.5 | RMQ | 0.812 |
| Hanning | -3.4 | 2.4 | AR | 0.802 |
| Hanning | -24.7 | 15.5 | RMS | 0.785 |
| Hanning | -25.0 | 15.8 | RMQ | 0.775 |
| Quadratic | -3.5 | 3.2 | AR | 0.806 |
| Quadratic | -5.5 | 5.2 | RMS | 0.790 |
| Quadratic | -35.8 | 25.5 | RMQ | 0.774 |

**Table F.2. Golden Car "Tire Load" Index Best Options.**

| Weighting Function | | | Accumulator | Pearson's R |
|---|---|---|---|---|
| Type | Start (m) | End (m) | | |
| Box | -25.8 | 2.0 | AR | 0.786 |
| Box | -25.9 | 2.0 | RMS | 0.785 |
| Box | -11.1 | 2.9 | RMQ | 0.762 |
| Hanning | -22.4 | 12.0 | AR | 0.775 |
| Hanning | -25.3 | 15.5 | RMS | 0.776 |
| Hanning | -24.5 | 15.7 | RMQ | 0.755 |
| Quadratic | -28.8 | 17.2 | AR | 0.776 |
| Quadratic | -34.9 | 23.3 | RMS | 0.775 |
| Quadratic | -39.3 | 27.4 | RMQ | 0.753 |

## Hot Spots

An alternative windowing strategy was applied to investigate the relationship between localized rough features and scale error. This was done by choosing a short segment length and setting the index to the value of the roughest segment of that length found upstream of the scale. The two variables optimized in this search were (1) segment length, and (2) the

distance ahead of the scale to search. A very extensive search for an optimal index of this type revealed no options that correlated better to scale error significantly than those with fixed endpoints.

**Table F.3. Golden Car "Sprung Mass Acceleration" Index Best Options.**

| Weighting Function | | | Accumulator | Pearson's R |
|---|---|---|---|---|
| Type | Start (m) | End (m) | | |
| Box | -27.6 | 3.0 | AR | 0.796 |
| Box | -12.8 | 3.0 | RMS | 0.777 |
| Box | -25.8 | 1.5 | RMQ | 0.722 |
| Hanning | -27.0 | 13.3 | AR | 0.785 |
| Hanning | -30.3 | 16.9 | RMS | 0.764 |
| Hanning | -0.9 | 0.6 | RMQ | 0.750 |
| Quadratic | -2.9 | 2.0 | AR | 0.806 |
| Quadratic | -34.4 | 25.0 | RMS | 0.763 |
| Quadratic | -40.1 | 27.3 | RMQ | 0.712 |

## Ride Number

Table F.4 lists the results for Ride Number, and variations on it. (The only entry in table F.4 that truly represents Ride Number is the second row.) Note that pre-transform Ride Number was correlated, rather than the value from the 0-to-5 scale. As was the case for Golden Car indices, the only variables to optimize were weighting function starting and ending point. This is because all of the filter parameters in the Ride Number are standard. Overall, correlation was not high. The most promising option was an average rectified accumulation of roughness with a short quadratic weighting function centered near the scale.

**Table F.4. Pre-Transform Ride Number, Best Options.**

| Weighting Function | | | Accumulator | Pearson's R |
|---|---|---|---|---|
| Type | Start (m) | End (m) | | |
| Box | -11.7 | 9.5 | AR | 0.784 |
| Box | -11.7 | 11.5 | RMS | 0.753 |
| Box | -25.9 | 11.5 | RMQ | 0.688 |
| Hanning | -7.6 | 16.0 | AR | 0.774 |
| Hanning | -35.7 | 61.0 | RMS | 0.734 |
| Hanning | -48.2 | 90.0 | RMQ | 0.667 |
| Quadratic | -2.4 | 5.0 | AR | 0.801 |
| Quadratic | -36.7 | 88.5 | RMQ | 0.732 |

## Butterworth Filter

The Butterworth filter is a common filtering technique, but its response has no explicit relationship to vehicle response. Nevertheless, it was very useful in the application called for by this study, because it provides a way to directly manipulate the boundaries of the wave-number response. It is also an attractive option for a profile-based index precisely because it is not based on a vehicle model. This type of index helps the research community avoid treating it as having a sacred pedigree as a direct predictor of vehicle motion. The

choices listed here are, in fact, simply band-pass filters that correlate well to a data set of interest, as are most profile-based indices. Heavy vehicles are very diverse in their frequency response. That means that careful tuning of the gain characteristics for a specific vehicle or set of vehicles is often an exercise in de-tuning it for the rest of the population. The most mature engineering approach for this study is to simply treat the indices as band-pass filters and adjust their response to cover the range that is most relevant to vehicles. (In this type of study the fine details of the wavelength sensitivity often have more to do with the experimental design than the true engineering goals of the research.)

The Butterworth filter was optimized with twelve combinations of spatial weighting function and accumulator. For each combination, this was a search for the wavelength cutoff values and spatial weighting function endpoints that resulted in the highest level of correlation. Table F.5 lists the results. Two values are listed for some of the combinations, because they represent local maxima in the solution space. The table lists the long- and short-wavelength cutoff values for each entry. Keep in mind that the filter is usually defined using the inverse of these values (i.e., the wave-number). These are also not absolute cutoff values. Rather, they are the wavelengths corresponding to a reduction in gain of about 30 percent. (See Appendix E.)

**Table F.5. Butterworth Filter, Best Options.**

| Weighting Function | | | Accum. | Wavelength Cutoff | | Pearson's R |
|---|---|---|---|---|---|---|
| Type | Start (m) | End (m) | | Short (m) | Long (m) | |
| Box | -23.6 | 7.8 | AR | 0.9 | 47.6 | 0.814 |
| Box | -25.9 | 7.8 | AR | 0.9 | 19.8 | 0.814 |
| **Box** | **-2.7** | **0.5** | **AR** | **1.6** | **16.5** | **0.826** |
| **Box** | **-25.8** | **3.2** | **AR** | **1.1** | **11.4** | **0.818** |
| Box | -2.7 | 0.5 | RMS | 1.7 | 15.0 | 0.821 |
| Box | -23.6 | 7.8 | RMS | 1.1 | 57.3 | 0.801 |
| Box | -25.9 | 3.0 | RMS | 1.2 | 12.5 | 0.803 |
| Box | -7.3 | 0.5 | RMQ | 2.0 | 15.7 | 0.820 |
| Hanning | -29.7 | 14.8 | AR | 0.9 | 43.4 | 0.802 |
| Hanning | -23.9 | 14.8 | RMS | 1.5 | 13.1 | 0.800 |
| Hanning | -27.4 | 16.2 | RMQ | 2.1 | 11.4 | 0.778 |
| Quadratic | -4.0 | 3.4 | AR | 1.6 | 9.4 | 0.831 |
| Quadratic | -19.1 | 15.7 | RMS | 1.2 | 12.5 | 0.815 |
| Quadratic | -14.5 | 11.4 | RMQ | 1.4 | 9.4 | 0.815 |
| Quadratic | -32.9 | 22.4 | RMS | 1.3 | 43.4 | 0.797 |
| Quadratic | -31.9 | 21.8 | RMQ | 1.8 | 36.1 | 0.783 |

The correlation levels listed for the Butterworth filter are somewhat higher than those listed for Golden Car and Ride Number options. This is because the waveband of the filter could be adjusted, which provided a few extra "tuning" variables. These results provide some insight into the roughness that affects weight scale error most:

- The highest correlation was found by emphasizing roughness from about 3.1 meters (10 feet) ahead of the scale to about a meter beyond it. This range produced the two highest R values. It probably represents localized roughness and features that excite axle vibration.

- A relevant range of pavement also appears to start about 24.4 meters (80 feet) ahead of the scale and end about 7.6 meters (25 feet) beyond the scale. Longer ranges appear for the Hanning and quadratic weighting functions because they taper off their weighting near the edges.
- The wavelength range of interest falls roughly into two categories: (1) about 1.5 meters (5 feet) to about 13.7 meters (45 feet), and (2) about 0.9 meters (3 feet) to about 45.7 meters (150 feet). All of the options listed have short wavelength cutoff values between 0.8 meters (2.5 feet) and 2.0 meters (6.5 feet). The long-wavelength cutoff values are more diverse. This is partly because so much intercorrelation exists between roughness in a given waveband and roughness in adjacent ranges.
- Average rectified accumulation appeared to produce the highest correlation levels, but not by a broad margin. Average rectified accumulation probably best represents the scale error because scale error statistics were summarized as linear percentage error.

Although the options listed in table F.5 appear to cover diverse spatial and wave-number ranges, they all relate to each other quite closely. In fact, no pair of them raised the R value above 0.85 in multiple regression. Multiple regression using all of them together only raised the R value to 0.906. This relationship between the options is due in part to the interrelation between roughness over the wavelength range of interest, and partly due to the fact that most of the profiles chosen for this study have uniform roughness over the distance preceding the scale.

Table F.6 lists some index options that emerged when the optimization was performed over the jointed plain concrete sites only. These are listed to help ensure that the choice of index performs well on jointed concrete. No optimization was needed for the jointed reinforced sites, because all of the index options listed in table F.5 exhibited very high correlation on them. (In most cases, it was well over 0.9.) The index options listed in table F.6 usually emphasize wavelengths shorter than 15 meters (about 50 feet), and shorter wavelength overall than the options listed for all the sites. They also cover a smaller range of pavement ahead of the scale, and often ignore roughness in the last few meters ahead of the scale. This may be because most of these profiles include periodic roughness related to slab length, and no special effort was made to manipulate the location of the scale relative to joints. The ranges listed in the table may simply include the nearest joint upstream of the scale within most of the profiles used in this study.

### General Quarter-Car

A generalized version of the quarter-car filter was investigated by treating the four vehicle parameters as filter coefficients and optimizing their value for correlation to scale error. The optimal parameters yielded by this exercise must not be interpreted as having any direct physical meaning. In other words, the coefficients do not represent the amalgamated properties of the simulated vehicle fleet. Rather, they simply determine the wave-number range for the filter.

**Table F.6. Butterworth Filter, Best Options.**

| Weighting Function | | | Accum. | Wavelength Cutoff | | Pearson's R |
|---|---|---|---|---|---|---|
| Type | Start (m) | End (m) | | Short (m) | Long (m) | |
| Box | -7.2 | -3.5 | AR | 1.09 | 20.06 | 0.814 |
| Box | -8.1 | -4.6 | AR | 0.30 | 14.51 | 0.840 |
| Box | -5.6 | -4.1 | AR | 0.95 | 6.03 | 0.835 |
| Box | -7.9 | -4.6 | RMS | 0.36 | 12.07 | 0.832 |
| Box | -7.6 | -3.7 | RMQ | 0.72 | 15.20 | 0.871 |
| Hanning | -9.4 | -3.0 | AR | 0.30 | 14.51 | 0.807 |
| Hanning | -6.7 | -3.0 | RMS | 0.87 | 8.34 | 0.837 |
| Hanning | -10.5 | -0.8 | RMQ | 0.75 | 14.51 | 0.831 |
| Quadratic | -6.9 | -2.6 | AR | 1.00 | 6.32 | 0.831 |
| Quadratic | -12.6 | -0.8 | RMS | 0.41 | 11.00 | 0.801 |
| Quadratic | -11.7 | 1.4 | RMQ | 0.70 | 12.07 | 0.822 |

Table F.7 lists some sets of filter coefficients and spatial weighting function limits that correlated well with scale error. These combinations were sought by starting with parameter sets from the IRI, RN, and other sets that have been mentioned in the literature as having the potential to correlate to truck loads. The solution space near each parameter set was then searched for local maxima. Several of the searches concluded with the same parameter sets. This search was only documented for a box-type weighting function, because the other searches listed above showed that the Hanning and quadratic functions did not provide significant improvement.

Since the quarter-car filter provided more freedom to customize its wave-number weighting characteristics than the Butterworth filter, the maximum correlation was somewhat higher. (Think of the quarter-car as having four tuning knobs, compared to two for the Butterworth filter.) The list appears to have several options, but they really fall into three groups:

1. Short lead-in: Very high correlation was found for a filter with sensitivity in the range of wavelengths from about 1.6 meters (5.4 feet) to 16.5 meters (54 feet), a range from 2.6 meters (8.5 feet) ahead of the scale to 0.5 meters (1.5 feet) behind it, and average rectified accumulation. This is the first entry in table F.7. Several of the other entries in the table cover the same range of pavement, and are considered equivalent. This option is very similar to the third entry in table F.5 for the Butterworth filter.

2. Intermediate lead-in: High correlation was also found for a filter with sensitivity in the range of wavelengths from about 0.8 meters (2.75 feet) to 12.5 meters (41 feet), a range from 13.4 meters (44 feet) ahead of the scale to 3.0 meters (10 feet) behind it, and average rectified accumulation. More than half of the entries in the table are basically equivalent to it, and all correlate to each other very closely.

3. Long lead-in: Only one option was found with a long lead-in. This is sensitive to wavelengths from about 1.1 meters (3.6 feet) to 11.0 meters (36 feet), a range from 22.3 meters (73 feet) ahead of the scale to 3.4 meters (11 feet) behind it, and uses average rectified accumulation. Note that this filter has a sharp peak in its wavelength sensitivity at 0.13 cycles/meter (0.04 cycles/foot), which corresponds to a

7.6-meter (25-foot) wavelength. When the filter defined by the first entry in the table was altered to cover the range from 22.3 meters (73 feet) preceding the scale to 3.4 meters (11 feet) beyond it, the correlation was still 0.815.

**Table F.7. Quarter-Car Filter, Best Options.**

| Accum. | Weight Function | | Filter Coefficient Values | | | | Pearson's |
|---|---|---|---|---|---|---|---|
| | Start (m) | End (m) | K1 | K2 | C | Mu | R |
| **AR** | **-2.6** | **0.5** | **640.2** | **131.7** | **7.03** | **0.141** | **0.871** |
| **AR** | **-13.4** | **3.0** | **1470.7** | **290.8** | **9.65** | **0.083** | **0.846** |
| AR | -11.6 | 3.4 | 909.4 | 490.2 | 5.77 | 0.131 | 0.846 |
| AR | -2.7 | 0.5 | 874.1 | 490.2 | 5.88 | 0.116 | 0.834 |
| AR | -7.5 | 0.3 | 891.6 | 480.6 | 5.77 | 0.121 | 0.834 |
| AR | -7.5 | 0.3 | 1009.5 | 142.6 | 8.92 | 0.109 | 0.832 |
| AR | -7.5 | 0.3 | 1441.6 | 131.2 | 11.67 | 0.093 | 0.831 |
| **AR** | **-22.3** | **3.4** | **891.6** | **500.0** | **5.88** | **0.144** | **0.815** |
| RMS | -2.6 | 0.5 | 603.3 | 137.0 | 6.24 | 0.176 | 0.874 |
| RMS | -11.6 | 3.4 | 823.7 | 530.6 | 6.12 | 0.147 | 0.853 |
| RMS | -7.3 | 0.3 | 828.0 | 126.1 | 9.02 | 0.088 | 0.839 |
| RMS | -13.3 | 3.2 | 1136.7 | 353.2 | 9.39 | 0.150 | 0.837 |
| RMS | -2.7 | 0.5 | 791.7 | 530.6 | 6.00 | 0.126 | 0.824 |
| RMS | -7.5 | 0.3 | 840.1 | 510.0 | 6.00 | 0.121 | 0.822 |
| RMQ | -2.3 | 0.5 | 615.3 | 129.1 | 5.54 | 0.214 | 0.865 |
| RMQ | -13.1 | 3.2 | 717.1 | 585.8 | 6.76 | 0.162 | 0.835 |
| RMQ | -7.2 | 0.5 | 861.6 | 86.9 | 10.04 | 0.237 | 0.828 |

## Composite Index

None of the best options listed for the Butterworth or quarter-car filters does a perfect job of predicting simulated scale error. The results above suggest that two indices are needed, one to screen for roughness very close to the scale and another to screen for high "background" roughness leading up to the scale. Used in tandem, the two indices should do a proper job of weeding out sites with unacceptable roughness. A weak argument could be made that they will represent axle and body motion, respectively. In reality, roughness that contributes to both types of index will affect both types of vehicle vibration.

This pair of indices can be based on either the quarter-car filter or the Butterworth filter. All of the quarter-car filtering options include narrow peaks in their wavelength sensitivity characteristics. These nuances were helpful in driving up the correlation level compared to the Butterworth filter. However, it is not clear whether the added agreement was caused by increased relevance to vehicle motion or is an artifact of the specific parameters used in this simulation study. The Butterworth filter was chosen to maintain the generality of the criteria and avoid users of the indices and future researchers from interpreting the filter coefficients as vehicle properties.

The two filters selected are shown in bold in table F.5:

- The "short range" index will cover 2.7 meters (9 feet) of pavement preceding the scale and 0.5 meters (1.5 feet) after the scale. It will have a long-wavelength cutoff of 16.5 meters (54 feet) and a short-wavelength cutoff of 1.6 meters (5.1 feet).

- The “long range” index will cover 25.8 meters (84.5 feet) of pavement preceding the scale and 3.2 meters (10.5 feet) after the scale. It will have a long-wavelength cutoff of 11.4 meters (37.3 feet) and a short-wavelength cutoff of 1.1 meters (3.5 feet).

For both filters, the summary index will be accumulated by taking the average rectified value over the intended range.

Table F.8 lists the correlation of each index for the four surface types. They do most poorly on the sites with an overlay. This is partly because their roughness covers such a small range.

**Table F.8. Correlation by Surface Type.**

| Surface Type | Short Range Index | Long Range Index |
|---|---|---|
| All | 0.826 | 0.818 |
| Asphalt Concrete | 0.881 | 0.870 |
| Jointed Plain Concrete | 0.782 | 0.702 |
| Jointed Reinforced Concrete | 0.865 | 0.910 |
| Asphalt Overlay | 0.678 | 0.586 |

Figures F.1 and F.2 compare the index values to scale error for tandem axles. Each figure shows a trend line that was constructed using a least-squares linear fit, with a zero intercept required. When the Short Range Index is expressed in units of m/km, the trend line has a slope of 12.42. That means that multiplying the index by 12.42 is a rough predictor of 95$^{th}$ percentile scale error for tandem axles. Using this relationship, a limit could be set for the index of about 1.18 m/km (75 in/mi). This would yield an error level near 15 percent. Unfortunately, the scatter is so high that the limit must be set more conservatively. A limit value of 1.18 m/km (75 in/mi) would allow nine sites to pass that demonstrated an error level over 15 percent. No individual surface type accounted for a high share of these nine cases.

When the Long Range Index is expressed in units of m/km, the trend line has a slope of 11.78. That means that multiplying the index by 11.78 is a rough predictor of 95$^{th}$ percentile scale error for tandem axles. Using the relationship, a limit could by set for this index of about 1.18 m/km (75 in/mi) also. This would yield an error level near 15 percent. Unfortunately, a limit value of 1.18 m/km (75 in/mi) would allow six sites to pass that demonstrated an error level over 15 percent. Five of these caused the same problem for the Short Range Index. To account for the scatter, a more conservative limit of 0.789 m/km (50 in/mi) is recommended for both indices. Using this limit, no sites pass the long range criterion with an unacceptable error level and only one site passes the short range criterion.

Consideration of the 10 percent limit for total vehicle weighing error yielded the same conclusions, illustrated in figures F.3 and F.4. That is, the limit values for the Short Range Index and Long Range Index should both be set at 1.18 m/km (75 in/mi). The same group of sites that were problematic for tandem axle weight were also problematic for total vehicle weight.

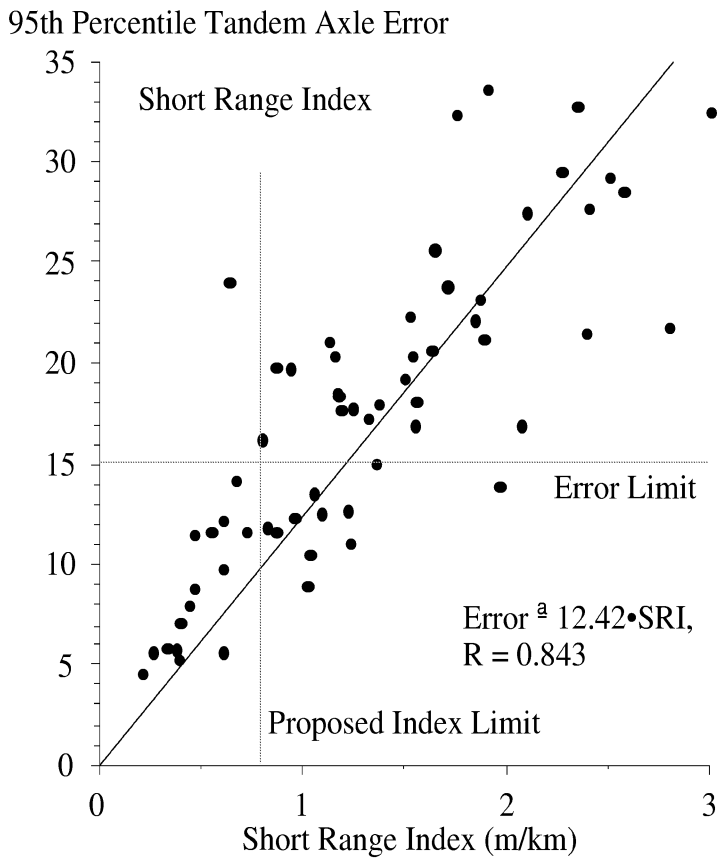


**Figure F.1. Short range WIM error index vs. tandem weighing error.**

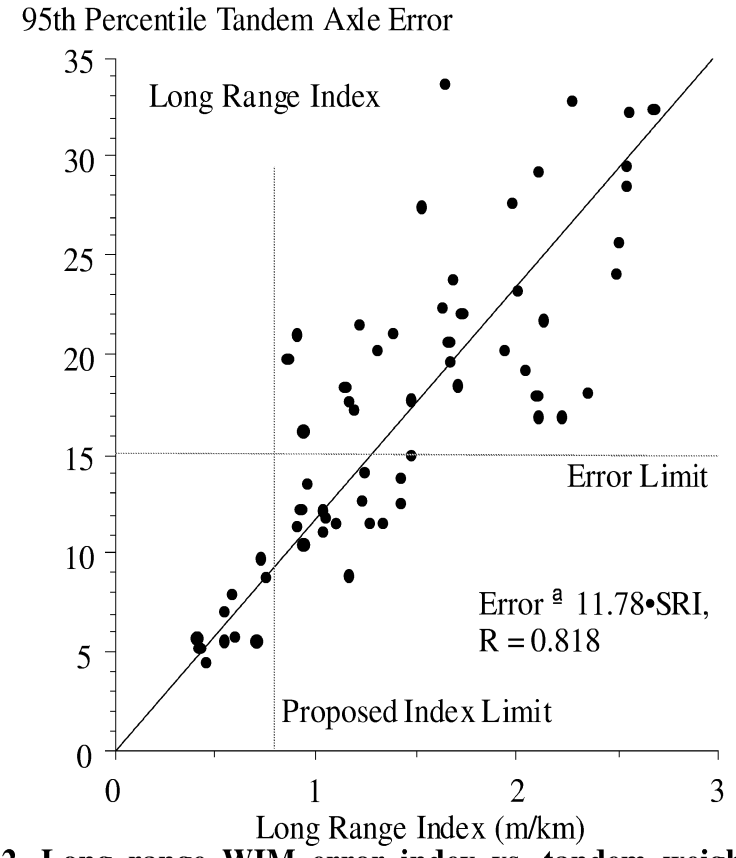


**Figure F.2. Long range WIM error index vs. tandem weighing error.**

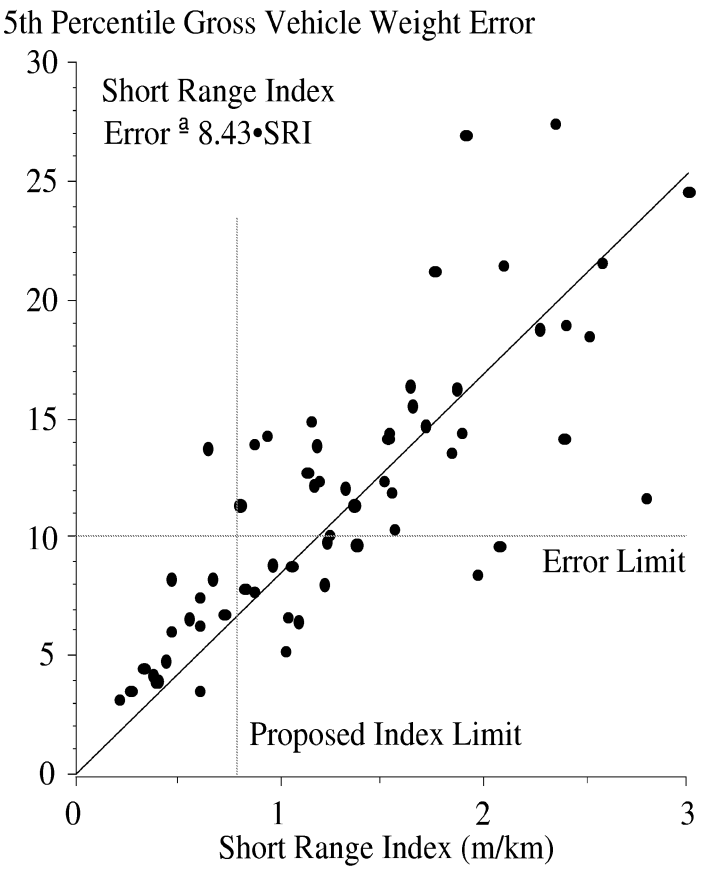


**Figure F.3. Short range WIM error index vs. gross weighing error.**

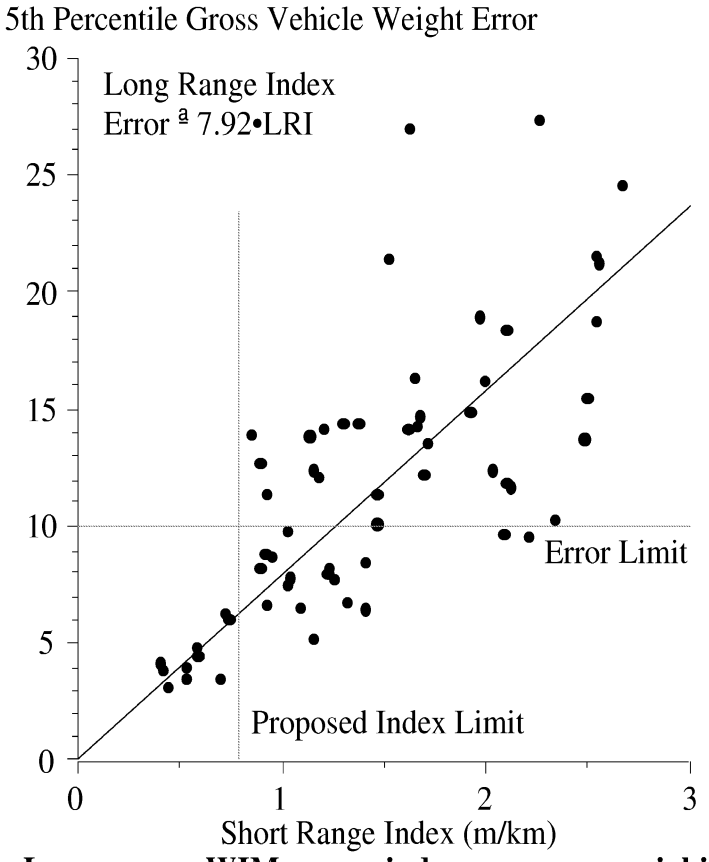


**Figure F.4. Long range WIM error index vs. gross weighing error.**

# Appendix G: Source Code

This appendix provides source code needed to implement the WIM site error criteria that are recommended in this report. The listings include a subroutine called "BUTTER", which must be called twice, and all of the subroutines needed to support it. Three of the routines which are needed to invert a matrix were copied from "Numerical Recipes."

The filter has the following properties:

- The filter is initialized using state variables that are calculated from a segment of the profile at the start. The length of that segment is adjustable.
- The profile is converted to slope.
- The profile is smoothed with a moving average filter with an adjustable base length.
- The smoothed profile is Butterworth filtered with adjustable short and long wavelength cutoffs.
- The simulated response is accumulated over the desired length by calculating the average rectified value.

## Long Range Index

The Butterworth filter is implemented for the Long Range Index by calling subroutine BUTTER as follows:

```
      CALL BUTTER(PROF1, NSAMP, DX, 0.30, 1000., PI, 5., 1.,
     &            11.37, 1.077)
```

Where PROF1 is an array containing the profile, NSAMP is the number of samples in the profile, DX is the sample interval, and PI is a summary index for the entire profile (ignore it). PROF1 and DX must have units of meters. The value 0.30 is a baselength for the moving average filter in meters. It should be set to zero if a comparable anti-aliasing filter has already been applied to the profile, which is the case for all Level E data from the Long-Term Pavement Performance Study database.

This routine modifies the array PROF1 by filtering it. After filtering, PROF1 will have units of m/km. After calling BUTTER, the Long Range Index is calculated by taking the absolute value of each point in PROF1, then averaging the values in the range from 25.8 meters (84.5 feet) ahead of the scale location to 3.20 meters (10.5 feet) behind the scale.

## Short Range Index

The Butterworth filter is implemented for the Short Range Index by calling subroutine BUTTER as follows:

```
      CALL BUTTER(PROF2, NSAMP, DX, 0.30, 1000., PI, 5., 1.,
     &            16.45, 1.559)
```

Where PROF2 is an array containing the profile, NSAMP is the number of sample in the profile, DX is the sample interval, and PI is a summary index for the entire profile (ignore it). PROF2 and DX must have units of meters. The value 0.30 is a baselength for the moving average filter in meters. It should be set to zero if a comparable anti-aliasing filter has already been applied to the profile, which is the case for all Level E data from the Long-Term Pavement Performance Study database.

This routine modifies the array PROF2 by filtering it. After filtering, PROF2 will have units of m/km. After calling BUTTER, the Long Range Index is calculated by taking the absolute value of each point in PROF2, then averaging the values in the range from 2.74 meters (9 feet) ahead of the scale location to 0.46 meters (1.5 feet) behind the scale.

**Table G.1. Code to apply the Butterworth filter.**

```
C=======================================================================
      SUBROUTINE BUTTER(PROF, NSAMP, DX, BASE, UNITSC, PI, XLEAD, XEXP,
     &                  LP1, LP2)
C=======================================================================
C Butterworth filter a longitudinal road profile and calculate PI.
C
C <-> PROF   Real     On input, an array of profile height values.
C                     On output, an array of filtered PI profile values.
C <-> NSAMP  Integer  Number of data samples in array PROF. The filtered
C                     profile has fewer points than the original.
C --> DX     Real     Distance step between profile points (m).
C --> BASE   Real     Distance covered by moving average (m).
C                     Use 0.30 for unfiltered profile input, and 0.0
C                     for pre-smoothed profiles (e.g. K.J. Law data).
C --> UNITSC Real     Product of two scale factors: (1) meters per unit
C                     of profile height, and (2) PI units of slope.
C                     Ex: height is inches, slope will be in/mi.
C                         UNITSC = (.0254 m/in)*(63360 in/mi) = 1069.34
C <-- PI     Real     The average PI for the entire profile.
C <-- XLEAD  Real     Initialization base length.
C <-- XEXP   Real     Accumulator exponent (1. = ARS, 2. = RMS).
C <-- LP1    Real     Filter long wavelength cutoff (m).
C <-- LP2    Real     Filter short wavelength cutoff (m).
      INTEGER   I, IBASE, ILEAD, NSAMP
      REAL      AMAT, BASE, BMAT, CMAT, DX, FP1, FP2, FP3, PI, PR
      REAL      PROF, SFPI, ST, UNITSC, V, XEXP, XIN, XLEAD, LP1, LP2
      REAL      TWOPI
      PARAMETER (FP3 = .70711, TWOPI = 6.283185307)
      DIMENSION AMAT(4, 4), BMAT(4), CMAT(4), PR(4), PROF(NSAMP),
     &          ST(4,4), XIN(4)
      FP1 = TWOPI/LP1
      FP2 = TWOPI/LP2
C  Set parameters and arrays.
      CALL BWABC(FP1, FP2, FP3, FP3, AMAT, BMAT, CMAT)
      CALL SETSTM(DX, AMAT, BMAT, ST, PR)
      IBASE = MAX(NINT(BASE/DX), 1)
      SFPI = UNITSC/(DX*IBASE)
C  Initialize simulation variables based on profile start.
      ILEAD = MIN(NINT(XLEAD/DX), NSAMP)
      XIN(1) = 0.0
      XIN(2) = 0.0
      XIN(3) = -FP2**2.*(PROF(ILEAD) - PROF(1))/(DX*ILEAD)
      XIN(4) = -2.*FP3*(FP1 + FP2)*XIN(3)
C  Convert to averaged slope profile, with PI units.
      NSAMP = NSAMP - IBASE
      DO 10 I = 1, NSAMP
   10   PROF(I) = SFPI*(PROF(I + IBASE) - PROF(I))
C  Filter profile.
      CALL STFILT(PROF, NSAMP, ST, PR, CMAT, XIN)
C  Compute PI from filtered profile.
      PI = 0.0
      DO 20 I = 1, NSAMP
   20   PI = PI + ABS(PROF(I))**XEXP
      PI = (PI/NSAMP)**(1./XEXP)
      RETURN
      END
```

**Table G.2. Code to set matrices for the Butterworth filter.**

```
C=======================================================================
      SUBROUTINE BWABC(FP1, FP2, FP3, FP4, A, B, C)
C=======================================================================
C
C  This routine sets the A, B and C matrix for Butterworth PI.
C
C  <-- A   Real   The 4x4 A matrix.
C  <-- B   Real   The 4x1 B matrix.
C  <-- C   Real   The 4x1 C matrix.
C  Last modified 10/17/94.

      IMPLICIT NONE
      INTEGER       I, J
      REAL          A, B, C, FP1, FP2, FP3, FP4
      DIMENSION     A(4, 4), B(4), C(4)

C  Initialize A and B matrix.
      DO 10 J = 1, 4
        B(J) = 0
        C(J) = 0
        DO 10 I = 1, 4
   10     A(I, J) = 0

C  Put filter parameters into the A Matrix.
      A(1,2) = 1.
      A(2,3) = 1.
      A(3,4) = 1.
      A(4,4) = -2.*FP3*(FP1 + FP2)
      A(4,3) = -(FP1**2. + FP2**2. + 4.*FP3*FP4*FP1*FP2)
      A(4,2) = -2.*FP3*FP1*FP2*(FP1 + FP2)
      A(4,1) = -FP1**2.*FP2**2.

C  Put filter parameters into the B matrix.
      B(2) = FP2**2.
      B(3) = A(4,4)*B(2)
      B(4) = A(4,3)*B(2) + A(4,4)*B(3)

C  Set the C matrix.
      C(1) = 1
      RETURN
      END
```

**Table G.3. Code to set the coefficients in a state transition matrix.**

```
C=======================================================================
      SUBROUTINE SETSTM(DT, A, B, ST, PR)
C=======================================================================
C Compute ST and PR arrays. This requires INVERT for matrix inversion.
C
C -->  DT    REAL   Time step (sec)
C -->  A     REAL   The 4x4 A matrix.
C -->  B     REAL   The 4x1 B matrix.
C <--  ST    REAL   4x4 state transition matrix.
C <--  PR    REAL   4x1 partial response vector.

      INTEGER   I, ITER, J, K
      LOGICAL   MORE
      REAL      A, A1, A2, B, DT, PR, ST, TEMP
      DIMENSION A(4, 4), A1(4, 4), A2(4, 4), B(4), PR(4), ST(4, 4),
     &          TEMP(4, 4)

      DO 20 J = 1, 4
        DO 10 I = 1, 4
          A1(I, J) = 0
   10     ST(I, J) = 0
        A1(J, J) = 1.
   20   ST(J, J) = 1.

C  Calculate the state transition matrix ST = exp(dt*A) with a Taylor
C  series. A1 is the previous term in the series, A2 is the next one.
      ITER = 0
   30 ITER = ITER + 1
      MORE = .FALSE.
      DO 40 J = 1, 4
        DO 40 I = 1, 4
          A2(I, J) = 0
          DO 40 K = 1, 4
   40       A2(I, J) = A2(I, J) + A1(I, K)*A(K, J)
      DO 50 J = 1, 4
        DO 50 I = 1, 4
          A1(I, J) = A2(I, J)*DT/ITER
          IF (ST(I, J) + A1(I, J) .NE. ST(I, J)) MORE = .TRUE.
   50     ST(I, J) = ST(I, J) + A1(I, J)
      IF (MORE) GO TO 30

C  Calculate particular response matrix: PR = A**-1*(ST-I)*B
      CALL INVERT(A, 4)
      DO 60 I = 1, 4
        PR(I) = 0.0
        DO 60 K = 1, 4
   60     PR(I) = PR(I) - A(I, K)*B(K)
      DO 90 J = 1, 4
        DO 70 I = 1, 4
          TEMP(J, I) = 0.0
          DO 70 K = 1, 4
   70       TEMP(J, I) = TEMP(J, I) + A(J, K)*ST(K, I)
        DO 80 K = 1, 4
   80     PR(J) = PR(J) + TEMP(J, K)*B(K)
   90   CONTINUE
      RETURN
      END
```

**Table G.4. Code to filter the profile.**

```
C=====================================================================
      SUBROUTINE STFILT(PROF, NSAMP, ST, PR, C, XIN)
C=====================================================================
C Filter profile using matrices ST, PR, and C.
C
C <->  PROF   REAL      Input profile. Replaced by the output.
C -->  NSAMP  INTEGER   Number of data values in array PROF.
C -->  ST     REAL      4x4 state transition matrix.
C -->  PR     REAL      4x1 partial response vector.
C -->  C      REAL      4x1 output definition vector.
C -->  XIN    REAL      4x1 vector of initial values of state variables.

      INTEGER   I, J, K, NSAMP
      REAL      C, PR, PROF, ST, X, XIN, XN
      DIMENSION C(4), PR(4), PROF(NSAMP), ST(4, 4), X(4), XIN(4), XN(4)

C  Initialize simulation variables.
      DO 10 I = 1, 4
   10   X(I) = XIN(I)

C  Filter profile using the state transition algorithm.
      DO 40 I = 1, NSAMP
        DO 20 J = 1, 4
          XN(J) = PR(J)*PROF(I)
          DO 20 K = 1, 4
   20       XN(J) = XN(J) + X(K)*ST(J, K)
        DO 30 J = 1, 4
   30     X(J) = XN(J)
        PROF(I) = X(1)*C(1) + X(2)*C(2) + X(3)*C(3) + X(4)*C(4)
   40   CONTINUE
      RETURN
      END
```

**Table G.5. Code to invert a matrix.**

```
C=======================================================================
      SUBROUTINE INVERT(Y1, N)
C=======================================================================
C  This routine will store the inverse of NxN matrix Y1 in matrix YINV.
C  It was copied from "Numerical Recipes."
C
C  Y1   --> Real     The matrix to be inverted.
C  YINV --> Real     The inverse of matrix Y1.
C
      INTEGER      N, INDX, I, J
      REAL*4       Y1, YINV, D, A
      DIMENSION    Y1(N, N), YINV(4, 4), INDX(4), A(4, 4)

      DO 8 I = 1, N
        DO 9 J = 1, N
    9     A(I, J) = Y1(I, J)
    8   CONTINUE
      DO 10 I = 1, N
        DO 20 J = 1, N
   20     YINV(I, J) = 0.0
        YINV(I, I) = 1.0
   10   CONTINUE
      CALL LUDCMP(A, INDX, D)
      DO 30 J = 1, N
   30   CALL LUBKSB(A, INDX, YINV(1, J))
      DO 40 I = 1, N
        DO 50 J = 1, N
   50     Y1(I ,J) = YINV(I, J)
   40   CONTINUE
      RETURN
      END
```

**Table G.6. Supporting code (LUDCMP) to invert a matrix.**

```
C=====================================================================
      SUBROUTINE LUDCMP(A, INDX, D)
C=====================================================================
C  This routine was copied from "Numerical Recipes" for matrix
C  inversion.
C
      INTEGER      N, INDX, NMAX, I, J, IMAX
      REAL*4       A, TINY, VV, D, AAMAX, SUM, DUM
      PARAMETER    (NMAX = 100, TINY = 1.0E-20, N = 4)
      DIMENSION    A(N, N), INDX(N), VV(NMAX)

      D = 1.0
      DO 10 I = 1, N
        AAMAX = 0.0
        DO 20 J = 1, N
   20     IF(ABS(A(I,J)).GT.AAMAX) AAMAX=ABS(A(I,J))
        IF(AAMAX.EQ.0.0) PAUSE 'Singular matrix'
        VV(I) = 1.0/AAMAX
   10   CONTINUE
      DO 30 J = 1, N
        DO 40 I = 1, J-1
          SUM = A(I, J)
          DO 50 K = 1, I-1
   50       SUM = SUM - A(I, K)*A(K, J)
          A(I, J) = SUM
   40     CONTINUE
        AAMAX = 0.0
        DO 60 I = J, N
          SUM = A(I, J)
          DO 70 K = 1, J-1
   70       SUM = SUM - A(I, K)*A(K, J)
          A(I, J) = SUM
          DUM = VV(I)*ABS(SUM)
          IF(DUM.GE.AAMAX)THEN
            IMAX = I
            AAMAX = DUM
          ENDIF
   60     CONTINUE
        IF(J.NE.IMAX)THEN
          DO 80 K = 1, N
            DUM = A(IMAX, K)
            A(IMAX, K) = A(J, K)
            A(J, K) = DUM
   80       CONTINUE
          D = -D
          VV(IMAX) = VV(J)
        ENDIF
        INDX(J) = IMAX
        IF(A(J, J).EQ.0.0) A(J, J) = TINY
        IF(J.NE.N)THEN
          DUM = 1.0/A(J, J)
          DO 90 I = J+1, N
   90       A(I, J) = A(I, J)*DUM
        ENDIF
   30   CONTINUE
      RETURN
      END
```

**Table G.7. Supporting code (LUBKSB) to invert a matrix.**

```
C=======================================================================
      SUBROUTINE LUBKSB(A, INDX, B)
C=======================================================================
C  This routine was copied from "Numerical Recipes" for matrix
C  inversion.

      INTEGER      N, INDX, I, II, LL
      REAL*4       A, B, SUM
      PARAMETER    (N = 4)
      DIMENSION    A(N, N), INDX(N), B(N)

      II = 0
      DO 10 I = 1, N
        LL = INDX(I)
        SUM = B(LL)
        B(LL) = B(I)
        IF(II.NE.0)THEN
          DO 20 J = II, I-1
   20       SUM = SUM - A(I, J)*B(J)
        ELSEIF(SUM.NE.0)THEN
          II = I
        ENDIF
        B(I) = SUM
   10   CONTINUE
      DO 30 I = N, 1, -1
        SUM = B(I)
        IF(I.LT.N)THEN
          DO 40 J = I+1, N
   40       SUM = SUM - A(I, J)*B(J)
        ENDIF
        B(I) = SUM/A(I, I)
   30   CONTINUE
      RETURN
      END
```